Online Issn : 2249-4626
Print Issn : 0975-5896

Global Journal of Science Frontier Research : A
Physics and Space Science

DISCOVERING THOUGHTS AND INVENTING FUTURE

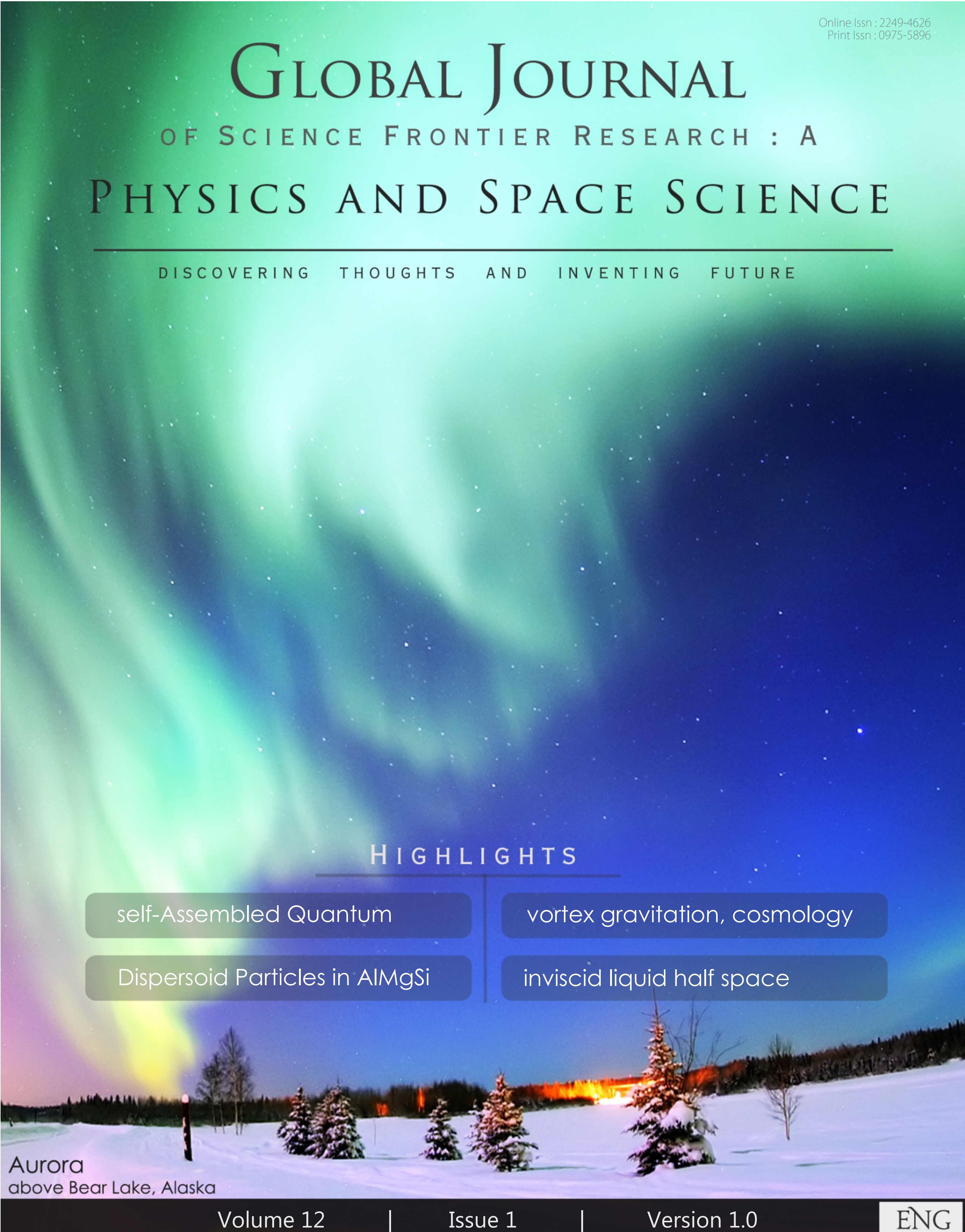

Highlights

- self-Assembled Quantum
- vortex gravitation, cosmology
- Dispersoid Particles in AlMgSi
- inviscid liquid half space

Aurora
above Bear Lake, Alaska

Volume 12 | Issue 1 | Version 1.0

ENG

Global Journal of Science Frontier Research: A
Physics & Space Science

Global Journal of Science Frontier Research: A

Physics & Space Science

Volume 12 Issue 1 (Ver. 1.0)

Open Association of Research Society

Incorporation No.: 0423089
License No.: 42125/022010/1186
Registration No.: 430374
Import-Export Code: 1109007027
Employer Identification Number (EIN):
USA Tax ID: 98-0673427

Global Journals Inc.

*(A Delaware USA Incorporation with "Good Standing"; **Reg. Number: 0423089**)*

Sponsors: *Open Association of Research Society*
Open Scientific Standards

Publisher's Headquarters office

Global Journals Inc., Headquarters Corporate Office, Cambridge Office Center, II Canal Park, Floor No. 5th, ***Cambridge (Massachusetts)***, Pin: MA 02141 United States

USA Toll Free: +001-888-839-7392
USA Toll Free Fax: +001-888-839-7392

Offset Typesetting

Open Association of Research Society, Marsh Road, Rainham, Essex, London RM13 8EU
United Kingdom.

Packaging & Continental Dispatching

Global Journals, India

Find a correspondence nodal officer near you

To find nodal officer of your country, please email us at *local@globaljournals.org*

eContacts

Press Inquiries: *press@globaljournals.org*
Investor Inquiries: *investers@globaljournals.org*
Technical Support: *technology@globaljournals.org*
Media & Releases: *media@globaljournals.org*

Pricing (Including by Air Parcel Charges):

For Authors:
22 USD (B/W) & 50 USD (Color)
Yearly Subscription (Personal & Institutional):
200 USD (B/W) & 250 USD (Color)

Editorial Board Members (HON.)

Dr. Bart Lambrecht
Director of Research in Accounting and FinanceProfessor of Finance
Lancaster University Management School
BA (Antwerp); MPhil, MA, PhD (Cambridge)

Dr. Carlos García Pont
Associate Professor of Marketing
IESE Business School, University of Navarra
Doctor of Philosophy (Management), Massachusetts Institute of Technology (MIT)
Master in Business Administration, IESE, University of Navarra
Degree in Industrial Engineering, Universitat Politècnica de Catalunya

Dr. Fotini Labropulu
Mathematics - Luther College
University of ReginaPh.D., M.Sc. in Mathematics
B.A. (Honors) in Mathematics
University of Windso

Dr. Lynn Lim
Reader in Business and Marketing
Roehampton University, London
BCom, PGDip, MBA (Distinction), PhD, FHEA

Dr. Mihaly Mezei
ASSOCIATE PROFESSOR
Department of Structural and Chemical Biology, Mount Sinai School of Medical Center
Ph.D., Etvs Lornd University
Postdoctoral Training,
New York University

Dr. Söhnke M. Bartram
Department of Accounting and FinanceLancaster University Management SchoolPh.D. (WHU Koblenz)
MBA/BBA (University of Saarbrücken)

Dr. Miguel Angel Ariño
Professor of Decision Sciences
IESE Business School
Barcelona, Spain (Universidad de Navarra)
CEIBS (China Europe International Business School).
Beijing, Shanghai and Shenzhen
Ph.D. in Mathematics
University of Barcelona
BA in Mathematics (Licenciatura)
University of Barcelona

Philip G. Moscoso
Technology and Operations Management
IESE Business School, University of Navarra
Ph.D in Industrial Engineering and Management, ETH Zurich
M.Sc. in Chemical Engineering, ETH Zurich

Dr. Sanjay Dixit, M.D.
Director, EP Laboratories, Philadelphia VA Medical Center
Cardiovascular Medicine - Cardiac Arrhythmia
Univ of Penn School of Medicine

Dr. Han-Xiang Deng
MD., Ph.D
Associate Professor and Research Department Division of Neuromuscular Medicine
Davee Department of Neurology and Clinical NeuroscienceNorthwestern University Feinberg School of Medicine

Contents of the Volume

Global Journal of Science Frontier Research
Physics & Space Science
Volume 12 Issue 1 Version 1.0 January 2012
Type : Double Blind Peer Reviewed International Research Journal
Publisher: Global Journals Inc. (USA)
Online ISSN: 2249-4626 & Print ISSN: 0975-5896

X-Ray window simulation; the use of COMSOL 3.4 Multiphysics software

By Dikedi P.N
King's College, London

Abstract - Ways are sought after, to prevent overlying target material on membrane from breaking or melting, by simulating structures (using COMSOL 3.4 Multiphysics software) of various materials. Results of these simulations and graphs (using Origin 7.5 software) are presented. The implications conferred by these graphs on the report are discussed. Power densities, of impinging electrons, thermal conductivities and thickness of membrane are considered as key parameters for optimal performance.

GJSFR-A Classification: FOR Code: 029999

X-RAY WINDOW SIMULATIONTHE USE OF COMSOL 3.4 MULTIPHYSICS SOFTWARE

X-Ray window simulation; the use of COMSOL 3.4 Multiphysics software

Dikedi P.N.

Abstract - Ways are sought after, to prevent overlying target material on membrane from breaking or melting, by simulating structures (using COMSOL 3.4 Multiphysics software) of various materials. Results of these simulations and graphs (using Origin 7.5 software) are presented. The implications conferred by these graphs on the report are discussed. Power densities, of impinging electrons, thermal conductivities and thickness of membrane are considered as key parameters for optimal performance.

I. Introduction

A simulation of the deformed structure (using COMSOL 3.4 multiphysics software) and graphs from results of various simulations (using Origin 7.5 software) are presented.

It is assumed that membrane breakage is caused by both the pressure differential between the top (Ti or Cr) and bottom layer (Si_3N_4) and the maximum temperature at the 1µm spot, (provided that maximum temperature exceeds the melting point of the membrane); hence simulations of Ti or Cr/ Si_3N_4 structures are presented based on temperature and stress/strain distribution within this structure. Using the heat transfer module of COMSOL 3.4 multiphysics software, the present simulations are somewhat modified compared to the previous ones. Simulations of a quarter of the full structure are considered for simplicity; Figure 1 is a 3 d view which showed that the focused electron beam impinged on an area of a quarter of a circle of radius 0.5µm.

II. Simulations of Various Structures

Further modelling of Ti/Si_3N_4 structure was performed (using COMSOL 3.4 multiphysics software) so as to reduce as much as possible the maximum temperature conferred on the hot spot. Although the heat flux/power density is a key parameter upon which the maximum temperature depends, however ways are sought for to avoid reducing the heat flux; a reduction implies that X-ray photon flux would reduce which in turn implies that exposure time of irradiated biological samples would increase.

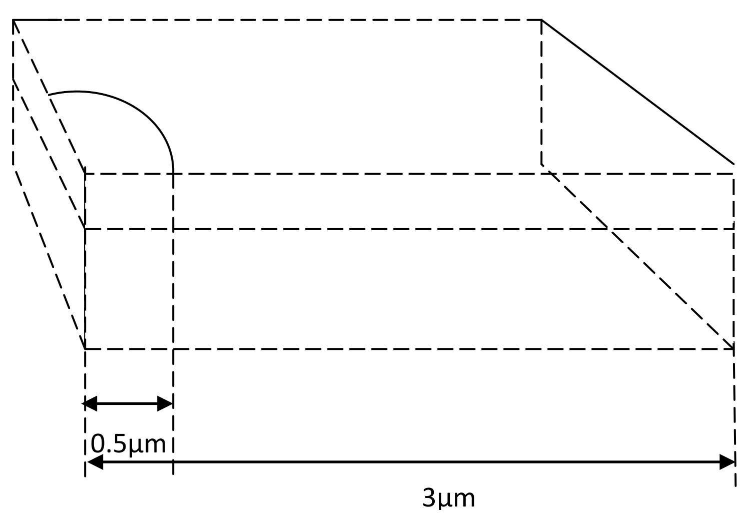

Figure 1 : A 3d view of the Cr/ Si_3N_4 (or Ti/ Si_3N_4) structure showing the hot spot represented by the quarter of a circle of radius 0.5µm.

Figure 2 is a deformed structure of chromium coated silicon nitride membrane whose deformation is due to pressure differential between the top and bottom of the structure describing both temperature and stress distribution within the structure. The deformation occurred the most at the 1 µm hot spot due to heat flux impartation. This region has a maximum temperature and stress of 2122K and 1.109x109 Pa respectively; amazingly, stress has insignificant effect on the maximum temperature of the structure. Figure 3 describes the boundary conditions applied to titanium/silicon nitride structure; boundaries between

Author : *Physics Department, King's College, London*
E-mail : pdikedi@yahoo.co.uk

Global Journal of Science Frontier Research (A) Volume XII Issue I Version I January 2012

layers are set as ‘continuity’ meaning that heat flows continuously across layers of dissimilar materials. The outer boundaries are set as ‘temperature’ meaning that the surrounding is assumed to be have room temperature. The 1μm hot spot is set as ‘heat flux’ with the description $\{(s1>0.45)*(s1<0.55)*1e^{10}\}$ meaning that 0.45 to 0.55 describes the hot spot where the maximum temperature must be deposited where $1e^{10}$ denotes the value of the power density i.e.$10^{10}W/m^2$. Figure 4(a) is a Simulated structure of 1μm of silicon nitride membrane overlain with 2μm of beryllium and 200nm of titanium.

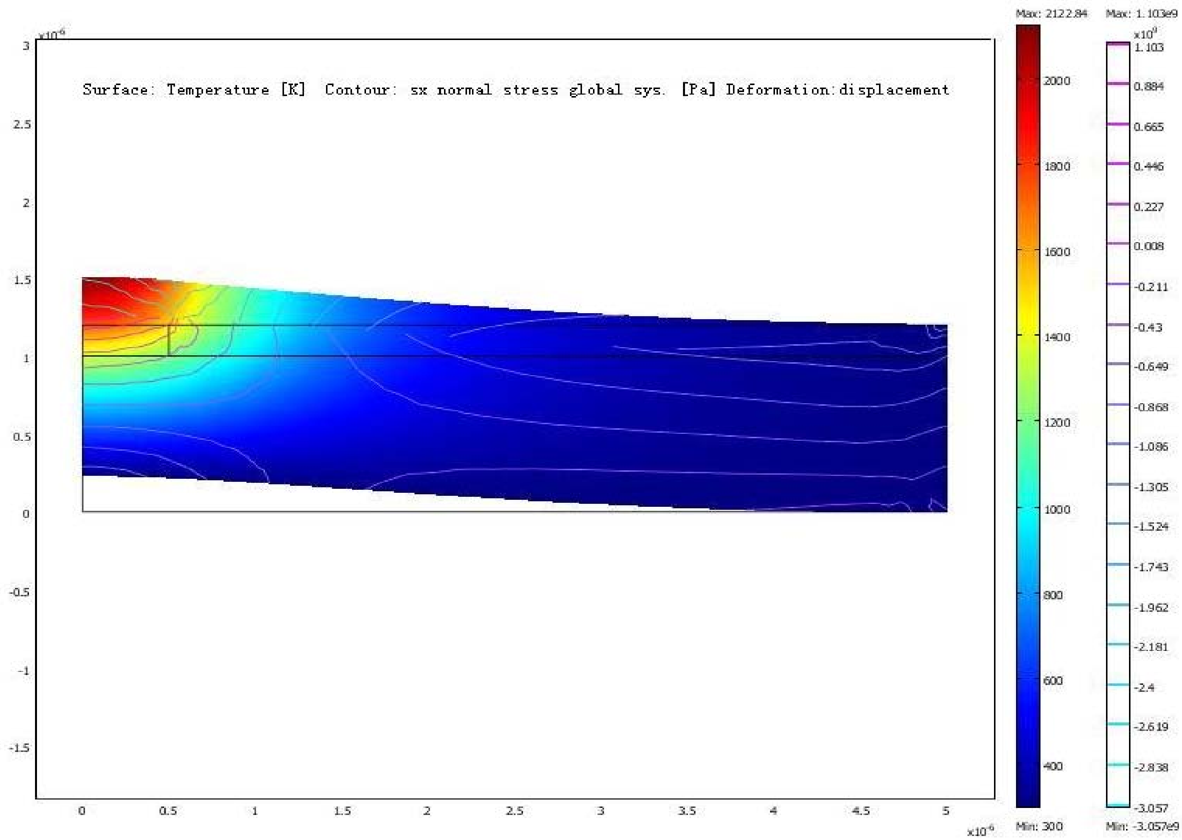

Figure 2 : A deformed structure of Chromium/Silicon nitride showing both temperature and stress distribution.

The maximum temperature achieved at the Titanium surface (upper layer) was 420.926K and the minimum temperature reached at the Silicon nitride surface (lower layer) was 273.15K. The result of the modelling is favourable because the maximum temperature of 420.926K is much less than the melting point of titanium. Maximum temperature at the hot spot varies directly with power density of the focused beam for both chromium and titanium of 100nm thickness. Figure 4(b) is a simulated structure of 1μm silicon nitride membrane overlain with 5μm of beryllium and 200nm of chromium; maximum temperature attained is 2184.549K and minimum is 273.15K. Figure 4(c) is a percentage heat flux distribution across five layers of an arbitrary material describing 40%, 30%, 15 %, 10 % and 5% of the total heat flux distributed through first, second, third, fourth and fifth layer.

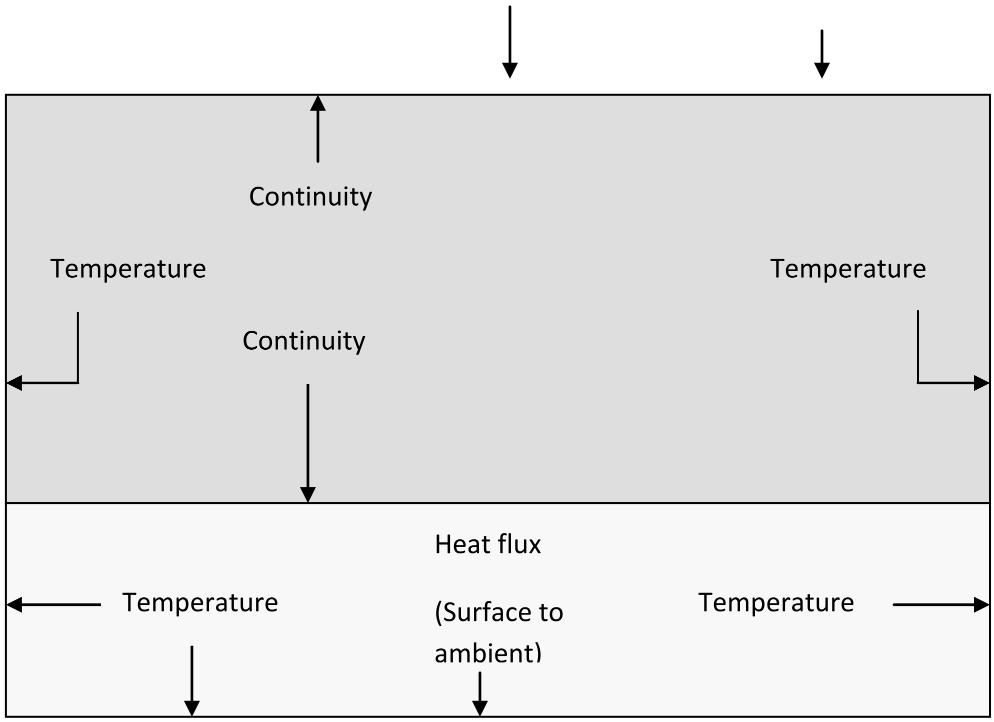

Figure 3.3 : Titanium/Beryllium /Silicon nitride Silicon nitride structure made of $2\mu m$ Beryllium layer overlain with a $200nm$ Titanium layer and underlain with $1\mu m$ Silicon nitride layer

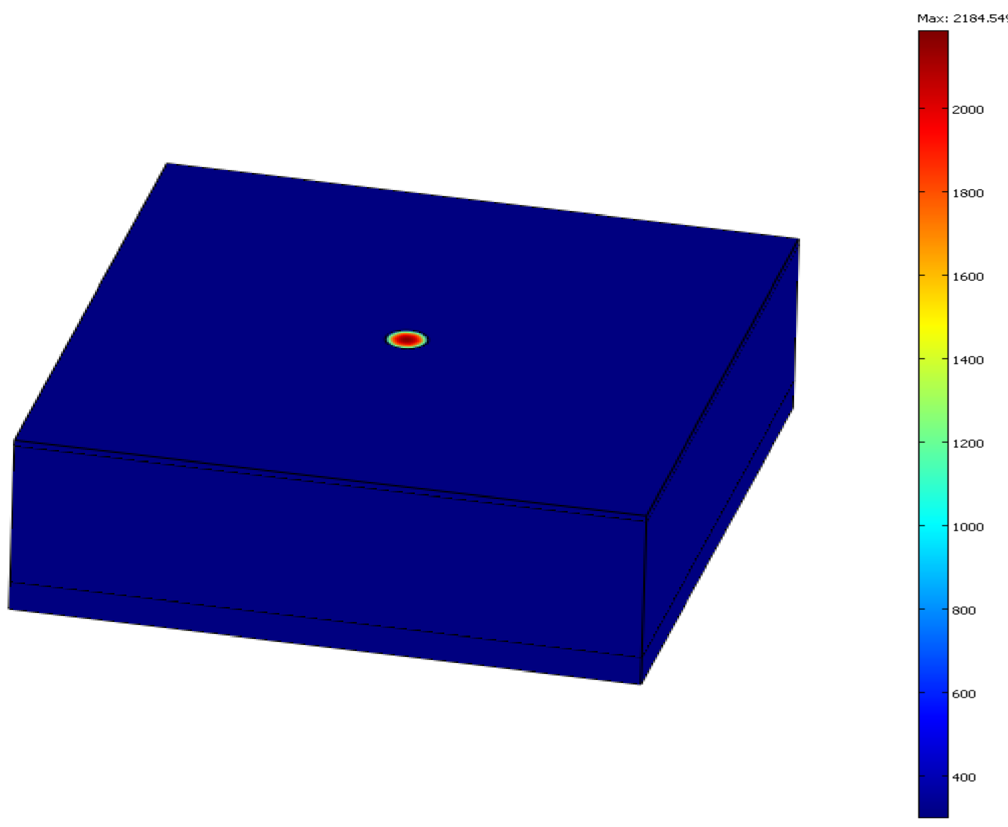

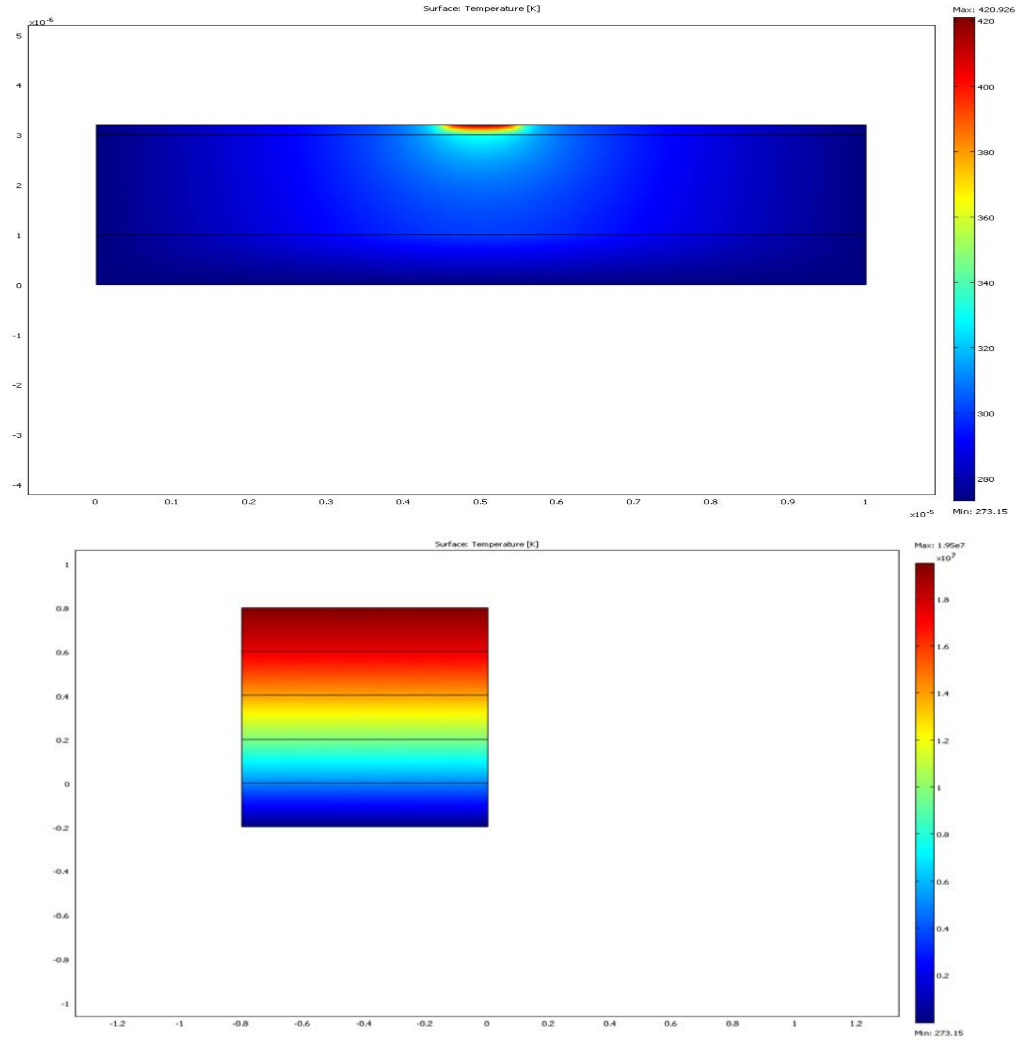

Figure 4(a) simulated structure of 1μm of silicon nitride membrane overlain with 2μm of beryllium and 200nm of titanium. Figure 4(b) Simulated structure of 1μm silicon nitride membrane overlain with 5μm of beryllium and 200nm of chromium. Figure 4(c) Percentage heat flux distribution across five layers of an arbitrary material

The relationship between the maximum temperature and the power density or heat flux is well established by the homogeneous hyperbolic heat equation [1] given by

$$q''(x,t)) + \tau \frac{\partial q''}{\partial t}(x,t) \cong -k\partial \frac{\partial T}{\partial x}(x,t), \qquad (3.1)$$

Where q'' is the dissipated heat flux; and T and k are the temperature and thermal conductivity of the medium. Compared to chromium, a higher maximum temperature is achieved in titanium when both samples are exposed to the same power density- Figure 5 shows this with more steepness from chromium

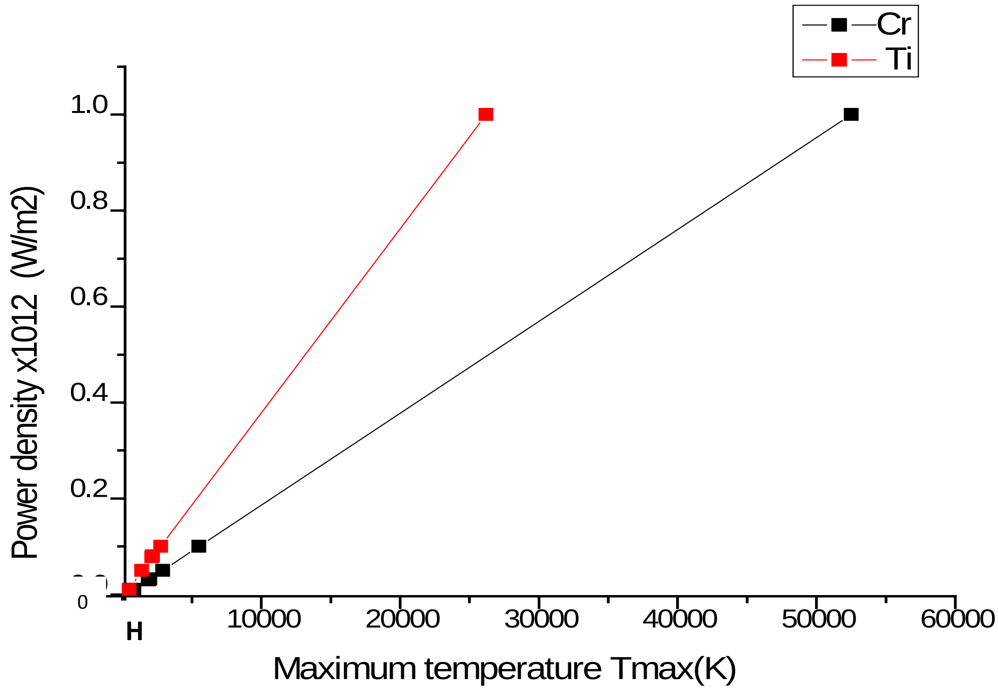

Figure 5 : A graph of power density of focused beam as a function of maximum temperature of the 1 μm spot.

III. THICKNESS OF THE WINDOW AS A FUNCTION OF MAXIMUM TEMPERATURE

The results from simulations also show that maximum temperature at the hot spot changes with thickness of both chromium and titanium. Maximum temperature increases with increasing thickness of chromium; maximum temperature also increases but with decreasing thickness of titanium. From previous simulations, it is well established that for arbitrary top and bottom layers, provided that the top layer material has a higher thermal conductivity, maximum temperature of the top layer will increase with increasing thickness. However, provided that the top layer has a lower thermal conductivity, maximum temperature of the top layer will increase with decreasing thickness. Figure 6 illustrates that at optimised power density of $\leq 0.078 W/m^2$ and $0.03\ W/m^2$ for chromium and titanium respectively, each of 200nm thickness; the maximum temperature attained are unable to cause breakage.

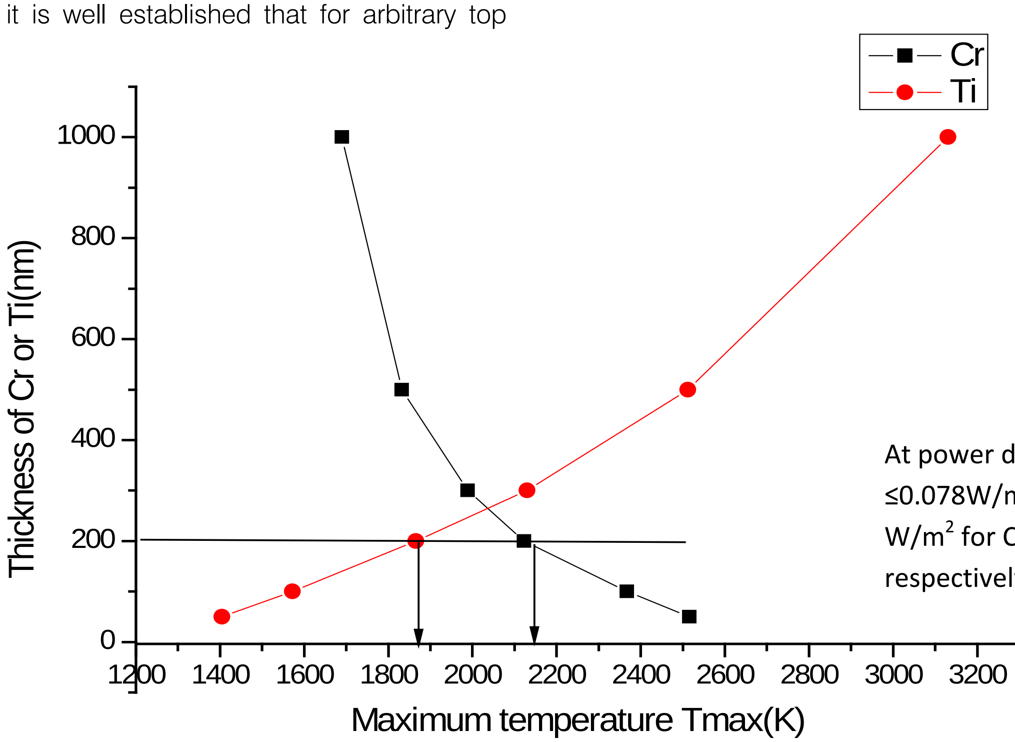

Figure 6 : A graph of thickness of chromium and titanium as a function of maximum temperature.

IV. Optimised Power Density as a Function of Window Thickness

Results from simulations show how optimised power densities of focused electron beam vary with thickness of titanium and chromium as illustrated in figure 7 Chromium is able to withstand more heat flux than titanium. Increasing the thickness of chromium makes it more able to withstand heat flux; however increasing the thickness of titanium makes it less able to withstand heat flux. 230nm thickness each of chromium and titanium can withstand power density of $0.081 W/m^2$ and $0.029 W/m^2$ respectively. It implies that time spent for irradiation is less if the membrane is made of chromium (more X-ray photon flux). Care must be taken when considering various membrane thicknesses, to ensure optical transparency. The more robust membranes show a decline in optical transparency.

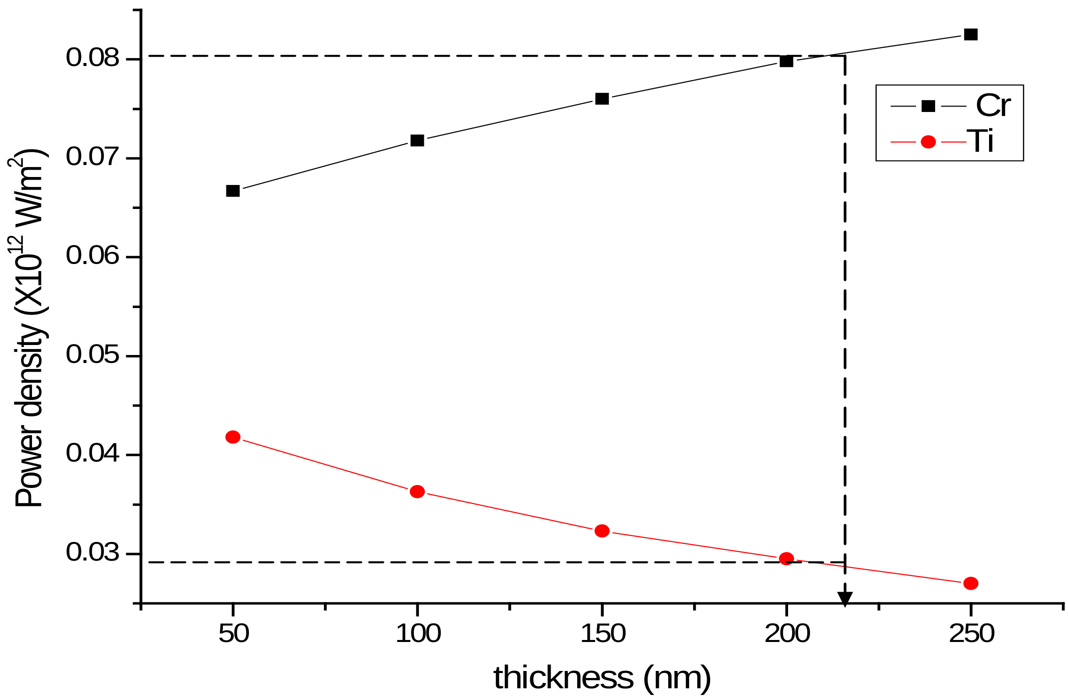

Figure 7 : A graph of power density of focused beam as a function of thickness of chromium and titanium.

V. The Effect of Stress

By varying the pressure at the bottom layer while keeping the pressure at the top layer constant the maximum temperature at the hot spot remained the same, hence work was discontinued on this

VI. Conclusion

Power density is directly related to maximum temperature; maximum temperature increases or decreases with it which agrees perfectly well with the homogenous heat equation. The thickness of membrane material is a function of maximum temperature on it; provided that the top layer material has a higher thermal conductivity, maximum temperature of the top layer will increase with increasing thickness. However, provided that the top layer has a lower thermal conductivity, maximum temperature of the top layer will increase with decreasing thickness.

Though there are some ambiguities in presented results of the simulation, chromium is preferred to titanium as a target material due to its higher thermal conductivity and melting point of 90.3W/mk and 2180K respectively, meaning that it can withstand more heat flux with less maximum temperature passed to it. This implies that chromium will emit more X-ray photon flux, thus reducing the time spent in irradiating cells-more cells can be irradiated. Pressure differential has an insignificant effect on the maximum temperature of the hot spot.

Future work will be directed towards creating more simulations by varying the temperature of helium gas, to check how it affects the maximum temperature of the membrane as well as finding more parameters which may affect the temperature of the hot spot.

References Références Referencias

1. Vladimir VK, Vasily BN (2002). "The relationship between the local temperature and the local heat flux within a one –dimensional semi-infinite domain of heat wave propagation" Mathematical Problems in Engineering **2003** (2003), Issue 4, Pp 173-179
2. Comsol 3.4 multiphysics software kit

Appendix

Basic Thermal Properties of materials considered in the simulation (From CRC handbook)

Titanium

Thermal conductivity k = 0.219 W/ (cm. K) = 21.9 W/ (m. K) at 300K
Density r = 4500 kg/m3
Heat capacity Cp = 0.125cal/ (g. K) = 523 J/ (kg. K)

Silicon nitride

Thermal conductivity k = 0.072 cal.cm-1.s-1.k-1 = 30.1 W/ (m. K) @300K
Density r = 3180 kg/m3
Heat capacity Cp = 0.17 cal/ (g. K) = 712 J/(kg. K)

Aluminium

Thermal conductivity k = 2.37 W/ (cm. K) = 237 W/ (m. K) at 300K
Density r = 2700 kg/m3
Heat capacity Cp = 0.215 cal/ (g. K) = 900 J/ (kg. K)

Chromium

Thermal conductivity k = 0.903 W/ (cm. K) = 90.3 W/ (m. K) at 300K
Density r = 7190 kg/m3
Heat capacity Cp = 0.107 cal/ (g. K) = 448 J/ (kg. K)

This page is intentionally left blank

Global Journal of Science Frontier Research
Physics & Space Science
Volume 12 Issue 1 Version 1.0 January 2012
Type : Double Blind Peer Reviewed International Research Journal
Publisher: Global Journals Inc. (USA)
Online ISSN: 2249-4626 & Print ISSN: 0975-5896

Dynamic Characterization of InAs/AlGaAs Broadband self-Assembled Quantum Dot Lasers

By D. Ghodsi Nahri, H. Arabshahi
Mashhad Branch, Islamic Azad University, Mashhad, Iran

Abstract - In this research we have solved the rate equations for InAs/AlGaAs broadband self-assembled quantum dot (QD) laser with considering the homogeneous broadening (HB) and inhomogeneous broadening (IHB) of the linear optical gain using fourth order Runge-Kutta method. We show that enhancing the injected current results in improving the dynamic characteristics, and increasing the steady-state photons, and show that with increase of the full width at half maximum (FWHM) of HB, the threshold current, turn-on delay and steady-state photons increase. Our calculation results also show that the simulated broadband self-assembled QD laser does not reach the complete steady-state when HB is near or equal to IHB.

Keywords : InAs/AlGaAs Broadband Self-assembled quantum dot laser; Dynamic Characterization; Optical gain theory .

GJSFR-A Classification : FOR Code : 020604

DYNAMIC CHARACTERIZATION OF INASALGAAS BROADBAND SELF-ASSEMBLED QUANTUM DOT LASERS

Strictly as per the compliance and regulations of :

Dynamic Characterization of InAs/AlGaAs Broadband self-Assembled Quantum Dot Lasers

D. Ghodsi Nahri[α], H. Arabshahi[Ω]

Abstract - In this research we have solved the rate equations for **InAs/AlGaAs** broadband self-assembled quantum dot **(QD)** laser with considering the homogeneous broadening **(HB)** and inhomogeneous broadening **(IHB)** of the linear optical gain using fourth order Runge-Kutta method. We show that enhancing the injected current results in improving the dynamic characteristics, and increasing the steady-state photons, and show that with increase of the full width at half maximum **(FWHM)** of **HB**, the threshold current, turn-on delay and steady-state photons increase. Our calculation results also show that the simulated broadband self-assembled **QD** laser does not reach the complete steady-state when HB is near or equal to **IHB**.

Keywords : InAs/AlGaAs Broadband Self-assembled quantum dot laser; Dynamic Characterization; Optical gain theory;

I. Introduction

Broadband light-emitting devices, such as super luminescent diodes (SLDs) and external cavity tunable lasers are ideal optical sources for applications in many areas. For example, SLDs can be used in the fields of optical coherence tomography (OCT), fiber-optic gyroscope (FOG) and wavelength-division-multiplexing (WDM) system; while external cavity tunable lasers are used in the fields of optical spectroscopy, biomedical, metrology and dense wavelength division multiplexing (DWDM). It was proposed that the characteristic of size inhomogeneity naturally occurred in self-assembled quantum dots (QDs) grown by Stranski-Krastanow (SK) mode is beneficial to broadening the material gain spectra and therefore, to broadening the lasing emission spectra (Sun et al., 1999). Broadband emitting QD-SLDs and broadband external cavity tunable QD lasers with QD gain medium have been studied (Liu et al., 2005; Lv et al., 2008; Zhang et al., 2004; Zhang et al., 2008). Here, we present simulated results in broadband emitting QD lasers. These InAs/AlGaAs QDs exhibit a broad photoluminescence (PL) full width at half maximum (FWHM) of 80 meV, which is much wider than that grown on GaAs substrate (Lv et al., 2008; Tan et al., 2007; Tan et al., 2008).

The short migration length of indium atoms on AlGaAs surface increases the size dispersion of InAs QDs, resulting in the broadening of optical gain spectrum. By optimizing the GaAs spacer thickness of multi-stacked InAs/AlGaAs QDs, over 250 μm PL FWHM is achieved. In this paper, considering the homogeneous broadening (HB) and inhomogeneous broadening (IHB) of the optical gain, we have solved the rate equations numerically using fourth order Runge-Kutta method and analyze the dynamics characteristics of InAs/AlGaAs self-assembled QD laser diodes (SAQD-LDs).

II. Linear Optical Gain

Based on the density-matrix theory, the linear optical gain of QD active region is given as

$$g^{(1)}(E)=\frac{2\pi e^{2}\hbar N_{D}}{cn_{r}e_{0}m_{0}^{2}}.\frac{\left|p_{cv}^{\sigma}\right|^{2}(f_{c}-f_{v})}{E_{cv}}B_{cv}(E-E_{cv}) \tag{1}$$

where n_r is the refractive index, N_D is the volume density of QDs, $\left|P_{cv}^{s}\right|^{2}$ is the transition matrix element, f_c is the electron occupation function of the conduction-band discrete state, f_v is that of the valence-band discrete state, and E_{cv} is the interband transition energy. The linear optical gain shows the homogeneous broadening of a Lorentz shape as

$$B_{cv}(E-E_{cv})=\frac{\hbar\gamma_{cv}/\pi}{(E-E_{cv})^{2}+(\hbar\gamma_{cv})^{2}} \tag{2}$$

where FWHM is given as $2\hbar\gamma_{cv}$ with polarization dephasing or scattering rate γ_{cv}. Neglecting the optical-field polarization dependence, the transition matrix element is given as

$$\left|P_{cv}^{\sigma}\right|^{2}=\left|I_{cv}\right|^{2}M^{2} \tag{3}$$

where I_{cv} represents the overlap integral between the envelope functions of an electron and a hole, and

$$M^{2}=\frac{m_{0}^{2}}{12m_{e}^{*}}.\frac{E_{g}(E_{g}+D)}{E_{g}+2D/3} \tag{4}$$

as derived by the first-order k.p is the interaction between the conduction band and valence band. Here,

Author [α] : Department of Physics, Mashhad Branch, Islamic Azad University, Mashhad, Iran.
Author [Ω] : Department of Physics, Payame Noor University, PO Box 19395-3697, Tehran, Iran . E-mail : arabshahi@um.ac.ir

E_g is the band gap, m_e^* is the electron effective mass, D is the spin-orbit interaction energy of the QD material. Equation 3 holds as long as we consider QDs with a nearly symmetrical shape (Sugawara, 1999; Sugawara et al., 2000). In actual SAQD-LDs, we should rewrite the linear optical gain formula of equation 1 by taking into account inhomogeneous broadening due to the QD size and composition fluctuation in terms of a convolution integral as

$$g^{(1)}(E) = \frac{2\pi e^2 \hbar N_D}{cn_r e_0 m_0^2} \int_{-\infty}^{\infty} \frac{\left|p_{cv}^{\sigma}\right|^2}{E_{cv}} (f_c(E') - f_v(E')) \times$$
$$B_{cv}(E - E')G(E' - E_{cv})dE' \qquad (5)$$

where E_{cv} is the center of the energy distribution function of each interband transition, $f_c(E')$ is the electron occupation function of the conduction-band discrete state of the QDs with the interband transition energy of E', and $f_v(E')$ is that of the valence band discrete state. The energy fluctuation of QDs are represented by $G(E' - E_{cv})$ that takes a Gaussian distribution function as

$$G(E' - E_{cv}) = \frac{1}{\sqrt{2\pi}\xi_0} \exp(-(E' - E_{cv})^2 / 2\xi_0^2) \qquad (6)$$

Whose FWHM is given by $G_0 = 2.35x_0$. The width G_0 usually depends on the band index c and (Sugawara, 1999; Sugawara et al., 2000).

III. Rate Equations

The most popular and useful way to deal with carrier and photon dynamics in lasers is to solve rate equations for carrier and photons (Markus et al., 2003; Sugawara, 1999; Sugawara et al., 2000; Tan et al., 2007; Tan et al., 2008). In our model, we consider an electron and a hole as an exciton, thus, the relaxation means the process that both an electron and a hole relax into the ground state simultaneously to form an exciton. We assume that the charge neutrality always holds in each QD.

In order to describe the interaction between the QDs with different resonant energies through photons, we divide the QD ensemble into j=1, 2,... 2M+1 groups, depending on their resonant energies for the interband transition over the longitudinal cavity photon modes. $j = M$ corresponds to the group and the mode with the central transition energy E_{cv}. We take the energy width of each group equal to the mode separation of the longitudinal cavity photon modes which equals to

$$D_E = ch / 2n_r L_{ca} \qquad (7)$$

where L_{ca} is the cavity length. The energy of the jth QD group is represented by

$$E_j = E_{cv} - (M - j)D_E \qquad (8)$$

where $j = 1, 2, ..., 2M + 1$. The QD density jth QD group is given as

$$N_D G_j = N_D G(E_j - E_{cv})D_E \qquad (9)$$

Let N_j be the carrier number in jth QD group, According to Pauli's exclusion principle, the occupation probability in the ground state of the jth QD group is defined as

$$P_j = N_j / 2N_D V_a G_j \qquad (10)$$

where V_a is the active region volume. The rate equations are as follows (Grundmann, 2002; Sugawara, 1995; Sugawara et al., 1997; Sugawara et al., 2000; Sugawara et al., 2005; Tan et al., 2008)

$$\frac{dN_s}{dt} = \frac{I}{e} - \frac{N_s}{\tau_s} - \frac{N_s}{\tau_{sr}} + \frac{N_w}{\tau_{we}}$$

$$\frac{d\ _w}{dt} = \frac{NN_s}{\tau_s} + \sum_j \frac{N_j}{\tau_e D_g} - \frac{N_w}{\tau_{wr}} - \frac{N_w}{\tau_{we}} - \frac{N_w}{\overline{\tau}_d}$$

$$\frac{dNj}{dt} = \frac{N_w G_j}{\tau_{dj}} - \frac{N_j}{\tau_r} - \frac{N_j}{\tau_e D_g} - \frac{c\Gamma}{n_r}.g^{(1)}(E)S_m$$

$$\frac{dS_m}{dt} = \frac{\beta N_j}{\tau_r} + \frac{c\Gamma}{n_r}.g^{(1)}(E)S_m - S_m / \tau_p \qquad (11)$$

where N_s, N_w, and N_j are the carrier numbers in separate confinement heterostructure (SCH) layer, wetting layer (WL) and jth QD group, respectively, S_m is the photon number of mth mode, where m=1,2…2M+1, I is the injected current, G_j is the fraction of the jth QD group type within an ensemble of different dot size population, e is the electron charge, D_g is the degeneracy of the QD ground state without spin, b is the spontaneous-emission coupling efficiency to the lasing mode. $g_{mj}^{(1)}$ is the linear optical gain which the jth QD group gives to the mth mode photons where is represented by

$$g_{mj}^{(1)}(E) = \frac{2\pi e^2 \hbar N_D}{cn_r \varepsilon_0 m_0^2} \cdot \frac{\left|p_{cv}^{\sigma}\right|^2}{E_{cv}} (2p_j - 1).$$
$$G_j B_{cv}(E_m - E_j) \qquad (12)$$

the related time constants are as τ_s, diffusion in the SCH region, τ_{sr}, carrier recombination in the SCH region, τ_{we}, carrier reexcitation from the WL to the SCH region, τ_{wr}, carrier recombination in the WL, τ_{dj}, carrier relaxation into the jth QD group, τ_r, carrier recombination in the QDs, τ_p, photon lifetime in the cavity, The average carrier relaxation lifetime, $\overline{\tau}_d$, is given as

$$\tau_d^{-1} = \sum_j \tau_{dj}^{-1} G_j = \tau_{d0}^{-1}(1 - P_j)G_j \qquad (13)$$

where τ_{do} is the initial carrier relaxation lifetime. The photon lifetime in the cavity is

$$\tau_p^{-1} = (c / n_r)[\alpha_i + \ln(1/R_1R_2)/2L_{ca}] \qquad (14)$$

where R_1 and R_2 are the cavity mirror reflectivities, and a_i is the internal loss. The laser output power of the m th mode from one cavity mirror is given a

$$I_m = \hbar\omega_m cS_m \ln(1/R)/(2L_{ca}n_r) \qquad (15)$$

where w_m is the emitted photon frequency, and R is R_1 or R_2. We solved the rate equations numerically using fourth order Runge-Kutta method to obtain the carrier and photon characteristics by supplying the step-like current at the time of $t = 0$. The system reaches the steady-state after finishing the relaxation oscillation.

IV. Simulation Results And Discussion

We have solved the rate equations 11 using numeric method of Runge-Kutta and simulated the carrier and photon characteristics. Figure 1 shows the simulated results of carrier characteristics at the FWHM of IHB 80 meV for different injected currents I=1.5, 2, 2.5, 5, and 10 mA and at the FWHM of HB $2\hbar\gamma_{cv=}$ 80 meV.

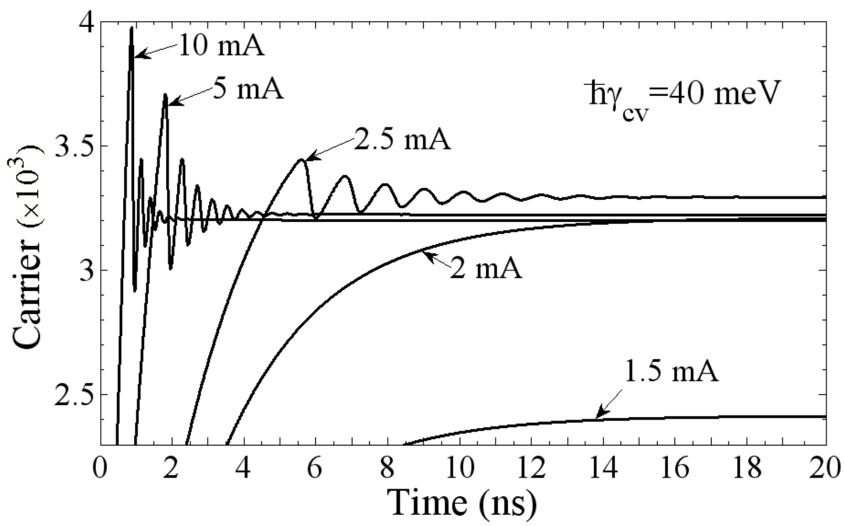

Fig. 1 : Simulated results of carrier characteristics at the FWHM of IHB 80 meV for different injected currents of 1.5, 2, 2.5, 5, and 10 mA and at the FWHM of HB 20 meV.

As shown in figure 1, with increasing the injected current, maximum of the relaxation oscillation magnitude and relaxation oscillation frequency increase.

Figure 2 shows the simulated results of photon characteristics at the FWHM of IHB 80 meV for different injected currents I=2, 2 .5, 5 and 10 m A and at the FWHM of HB 24, 40, 56, and 80 meV.

As shown in figure 2, the steady-state photons increase as the injected current is increased. This is because, as the injected current increases, the QD carriers increase that it results in increasing the cavity lasing photons, these increased photons that we call “early photons” lead to enhancing the stimulated emission rate, as a result, the QD carriers decrease (Figure 1) and the lasing photons increase at the new steady-state. With increasing the injected current, turn on delay decreases, this occurs because the required carriers for beginning of the relaxation oscillation are supplied earlier. Relaxation oscillation frequency and maximum of the relaxation oscillation magnitude also enhance as the current elevates. Further increase of early photons leads to further enhancement of the relaxation oscillation frequency and maximum of the relaxation oscillation magnitude. Because, further increase of the stimulated emission rate leads to the quicker light amplification and decreasing the cavity photon lifetime as a result the relaxation oscillation frequency increases and the laser reaches the steady-state earlier. As the FWHM of HB increases from a to d, turn on delay and the threshold current increase, because density of states (DOS) of the central group increase as a result the required carrier number for beginning of lasing emission increases and are supplied later. Steady-state photons except to figure 2a at the current I=2.5 m A increase due to increasing the QDs lying within the HB of the central mode.

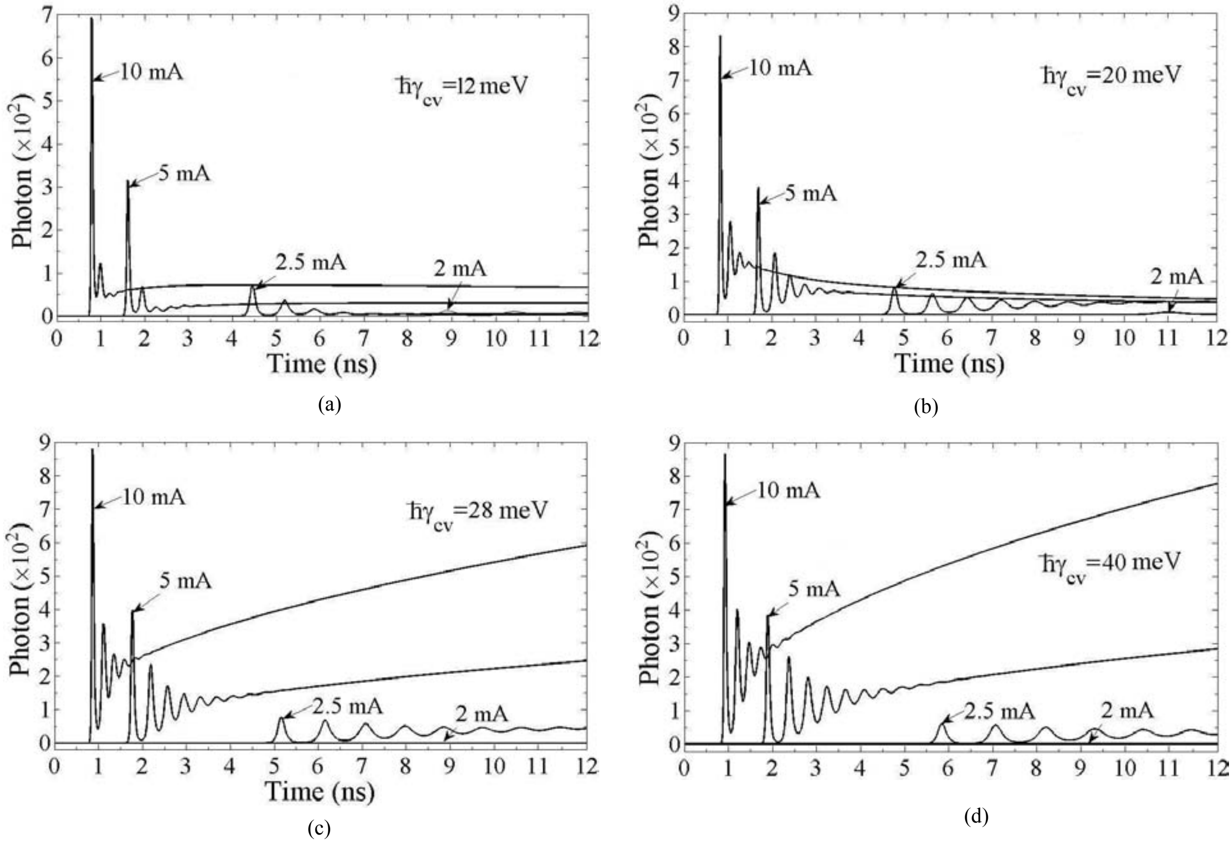

Fig. 2 : Simulated results of photon characteristics at the FWHM of IHB 80 meV for different injected currents I=2, 2.5, 5, and 10 mA when the FWHM of HB is 24, 40, 56 and 80 meV.

Enhancing of the HB up to a special value for a specific current (for example, in figure 2a, up to $\hbar\gamma_{cv} = 12 meV$ for I=2 mA) leads to increasing of maximum of the relaxation oscillation magnitude and the steady-state photons, because the central group DOS and thus the central group carriers enhance. Further elevating of the HB results in heightening of the empty DOS at the central group (decreasing of the population inversion) and decreasing of maximum of the relaxation oscillation magnitude and the steady-state photons (see Figure 3). As shown in Figure 3, at the injected current I=2 mA, with increasing of the FWHM of HB from 24 meV, the steady-state photons decreases as the population inversion is provided at a higher current at HB more than 56 meV and as a result, the threshold current elevates.

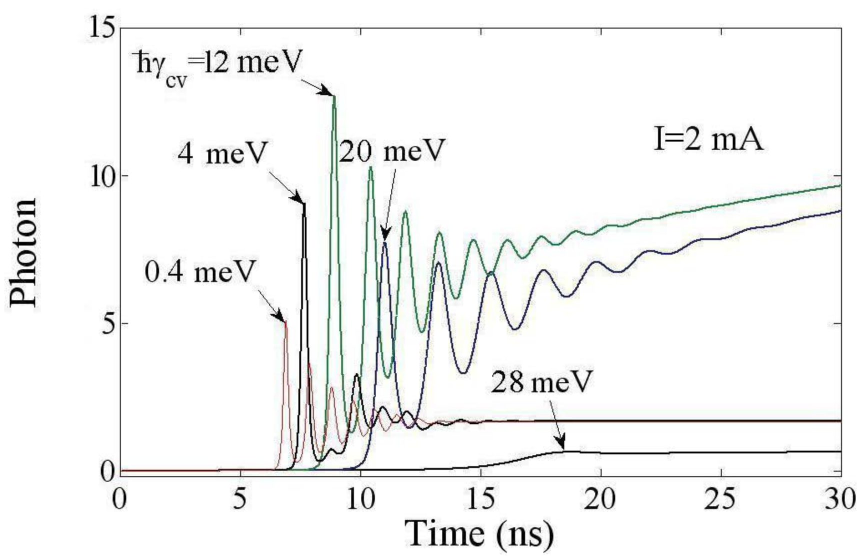

(a)

Fig. 3 : Photon-characteristics at the FWHM of IHB 80 meV for I=2 mA and at $\hbar\gamma_{cv=}$ 0.4, 4, 12, 20, and 28 meV.

Figure 4 shows other illustration from photon-characteristics at the FWHM of IHB 80 meV for different injected currents I=2, 2 .5, 5 , and 10 m A at a longer calculating time and at (a) $\hbar\gamma_{cv} = 12 meV$, (b) $20 meV$, (c) $28 meV$, and (d) $40 meV$.

As shown in figure 4a, the steady-state photons at I=2.5 m A are lesser than that of I=2 m A. Lasing photons at I=5 and 10 m A reach the complete steady state after 100 ns and 60 ns, respectively. As it is shown in figure 4b, the lasing photons at I=5 and 10 m A decrease as the time increases and they become lesser than that of I=2 m A after 45 ns, they do not reach the complete steady-state even after 100 ns. Lasing photons at 10 m A become lesser than that of 5 m A after 30 ns. Lasing photons at I=2.5 m A increase as the time enhances, and they do not reach the complete steady-state after 100 ns. As it is shown in figure 4c, the lasing photons at I=2.5 mA reach the complete steady-state after 80 ns, but, the lasing photons at I=5 and 10 mA do not reach the complete steady-state and they elevate as the time increases. As it is shown in figure 4d, the lasing photons at I=5 and 10 mA do not reach the steady-state after 300 ns. These non steady-states are due to not considering the gain saturation effect.

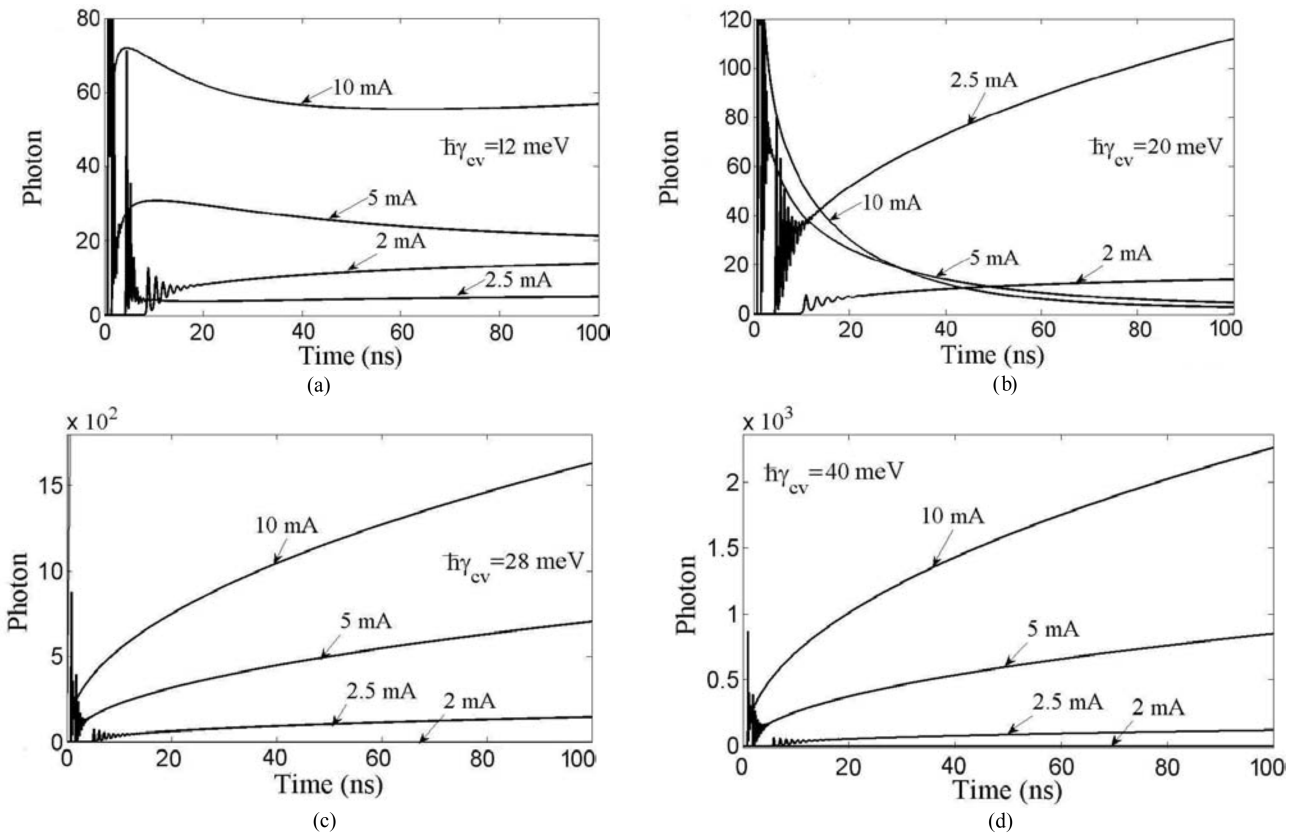

Fig. 4 : Other illustration from photon-characteristics for different injected currents I=2, 2.5, 5, and 10 mA at 100 ns and at (a) $\hbar\gamma_{cv} = 12\ meV$ (b) $20\ meV$, (c) $28\ meV$ and (d) $40 meV$.

V. Conclusion

InAs/AlGaAs self-assembled QD lasers with broadband emitting spectra have been studied. Considering the HB and IHB of the linear optical gain, we have solved the rate equations numerically using fourth order Runge-Kutta method and analyzed the dynamic characteristics of InAs/AlGaAs broadband SAQD-LDs. Dynamic characteristics and steady-state photons improve as the current increases. Turn-on delay, the threshold current and steady-state photons increase as the HB enhances. In addition, the SAQD-LD does not reach the complete steady-state when HB is near or equal to IHB.

References Références Referencias

1. Grundmann M (2002). Nano Optoelectronics. Springer, New York.
2. Liu N, Jin P and Wang Z (2005). InAs/GaAs quantum-dot super luminescent diodes with 110 nm bandwidth. Electron. *Lett.*, 41: 1400-1402.
3. Lv,X Q, Liu N, Jin P and Wang Z (2008). Broadband emitting super luminescent diodes with InAs quantum dots in AlGaAs matrix. IEEE *Photon. Technol. Lett.*, 20: 1742-1744.
4. Markus A, Chen J, Gauthier-Lafaye O and Fiore A (2003). Impact of Intraband relaxation on the performance of a quantum-dot laser. IEEE J. Sel. Top Quantum electron., 9: 1308-1314.

5. Sugawara M (1995). Theory of spontaneous-emission lifetime of Wannier in mesoscopic semiconductor quantum disks. Phys. Rev. B Condens. Matter., 51: 10743-10754.
6. Sugawara M, Mukai K and Shoji H (1997). Effect of phonon bottleneck on quantum-dot laser performance. Applied Phys. Lett., 71: 2791-2793.
7. Sugawara M (1999). Self -Assembled InGaAs/GaAs Quantum Dots. Academic Press 60.
8. Sugawara M, Mukai K and Ishikawa H (2000). Effect of homogeneous broadening of optical gain on lasing spectra in self-assembled InxGa1ÀxAsÕGaAs quantum dot lasers. Phys. Rev. B, 61: 7595-7603.
9. Sugawara M and Ishida M (2005). Modeling room-temperature lasing spectra of 1.3-μm self-assembled InAs/GaAs quantum-dot lasers: Homogeneous broadening of optical gain under current injection. Applied Phys., 97: 043523-043530.
10. Sun Z, Ding D, Gong Q, Zhou W and Wang Z (1999). Quantum-dot superluminescent diode: A proposal for an ultra-wide output spectrum. Opt. Quantum Electron., 31: 1235-1246.
11. Tan C, Wang Y and Ooi B (2007). Role of optical gain broadening in the broadband semiconductor quantum-dot laser. Applied Phys. Lett., 91: 061117-061119.
12. Tan C, Wang Y and Ooi B (2008). The role of optical gain broadening in the ultrabroadband InGaAs/GaAs interband quantum-dot laser. Comput. Matter. Sci., 44: 167-173.
13. Zhang Z, Wang Z and Liu F (2004). High performance Quantum - dot superluminescent diodes. IEEE Photon. Technol. Lett., 16: 27-29.
14. Zang Z and Wang Z Q (2008). High-power quantum-dot superluminescent LED with broadband drive current insensitive emission spectra using tapered active region. IEEE Photon. Technol. Lett., 20: 782-784.

Global Journal of Science Frontier Research
Physics & Space Science
Volume 12 Issue 1 Version 1.0 January 2012
Type : Double Blind Peer Reviewed International Research Journal
Publisher: Global Journals Inc. (USA)
Online ISSN: 2249-4626 & Print ISSN: 0975-5896

Foundation of vortex gravitation, cosmology and cosmogony

By Sergey Orlov
Petrozavodsk State University Petrozavodsk, Russia

Abstract - A hypothesis is proposed concerning the cause of the origin of universal gravitation. This cause consists in a system of the ether vortex rotations. Physical and mathematical grounds are described and the formula for the determination of the space gravitation forces is deduced. On the basis of the vortex gravitation, the principles of creation and existence of the celestial bodies are shown. Methods of the use of the vortex gravitation properties for the space flight projection are proposed.

Keywords : Ether Theory, Vortex Gravitation, Cosmology and Cosmogony.

GJSFR-A Classification : FOR Code: 020103

FOUNDATION OF VORTEX GRAVITATION, COSMOLOGY AND COSMOGONY

Strictly as per the compliance and regulations of :

Foundation of vortex gravitation, cosmology and cosmogony

Sergey Orlov

Abstract - A hypothesis is proposed concerning the cause of the origin of universal gravitation. This cause consists in a system of the ether vortex rotations. Physical and mathematical grounds are described and the formula for the determination of the space gravitation forces is deduced. On the basis of the vortex gravitation, the principles of creation and existence of the celestial bodies are shown. Methods of the use of the vortex gravitation properties for the space flight projection are proposed.

PACS : 98.80.Bp

Keywords : Ether Theory, Vortex Gravitation, Cosmology and Cosmogony.

" In the Universe there is nothing except an ether and its whirlwinds."

"René Descartes"

I. Introduction

The proposed model of gravitation, cosmology and cosmogony is based on an assumption that the initial cause of rotations of all the celestial objects or their systems in the Universe is the vortex rotation (in corresponding space regions) of a gaseous cosmic-space medium, viz. the ether.

The ether rotation occurs according to the same law as the rotation of a celestial body. In the solar system (torsion), the vortex-type ether rotation has the torsion character and corresponds to the circulation of the planets around the Sun (the Kepler 3-rd law).

The torsion-like vortex ether rotation creates an ether pressure change inside the torsion in accordance with the aerodynamics laws. The pressure gradient in the space medium creates the expulsive force acting onto the bodies located in this medium, and this force is directed toward the center of the torsion.

II. The Expulsive Force is Just The Gravity Force

Calculations of the expulsive (gravity) forces is carried out on the basis of mechanics of continua and (or) aerodynamics with the use of the Navier-Stokes equations. In the present work, an algebraic formula for the gravitation forces is obtained, which does not contain reduce coefficients, likewise the gravitation constant in the Newton formula.

In the article, some conclusions and foundations are proposed , as well as novel methods for investigation of the numerous properties of the celestial bodies of the cosmic substance, such as:

1. Universal vortex gravitation has a discoid configuration, which is confirmed by some astronomy facts, e.g., by ellipsoidal planet orbits. If one takes into account this property of gravitation, this allows an explanation of the inaccuracy of the commonly-accepted Universe Gravity (Newtonian attraction) Equation. Also, this allows obtaining of a correction for the two-dimensional Newton's formula. On the basis of the obtained three-dimensional formula for the determination of the gravitation forces, a possibility appears to plan cosmic flights with a significant decrease of the energy consumption.
2. Based on the principle of vortex gravitation, physical models are developed in the article, in which different properties of the cosmic objects, as well as the principles of creation of the universal substance and celestial objects, Black Holes, the character of their motion, masses, age, evolution of stars, planets, and the Universe in the whole, are presented.
3. Foundations of the distance increase between the galaxies are proposed, and these foundations are in fact the confirmations of the Universe contraction. With the help of the physical model of vortex gravitation, the causes of ebbs and flows in the oceans are explained.
4. On the basis of the model of vortex gravitation, analytical explanations of the numerous scientific paradoxes has been suggested:

- Paradox of Seliger, the Earth rotation velocity decrease, existence of "dark matter", etc.

Advantages of the proposed model of gravitation as compared with the Newtonian formula consist in the fact that it determines the gravity forces using the commonly-recognized basic physical properties and laws. Meanwhile, the Newton's law is based only on the experimental, observable facts. Therefore, on the basis of the vortex gravitation model, a possibility appears to account for the nature of the gravitation and to work out technological methods for an affect onto the gravity forces.

A huge number of thinkers pointed out the main role of the cosmic vortexes in the process of the world substance creation. In the Ancient World they were Empedocles, Leucippus, Democritus, Aristotle and

Author : Petrozavodsk State University, 185001, s. Severnaya 11, 6, c. Petrozavodsk, Russia. E-mail : ion@sampo.ru

some others. In the Renascence this idea was developed by R. Descartes, J. MacCullagh, J. J. Thomson, and W. Thomson (Lord Kelvin).

It should be noted that that times there was no a developed science concerning continua. Mathematics and physics were not enriched yet with the works by Bernoulli, Euler, Navier, Stoks, etc. Therefore, the above mentioned scientists could not formulate their ideas in a physical and mathematical form and their findings were formulated rather in form of philosophical speculations. In 20th century, the substance "ether" was groundlessly removed from the scientific consideration as if it was being «pseudo-scientific», which stopped the development of the theory of the space ether vortexes for long years. In the present article, we present numerous evidences of the existence of vortex gravitation, sufficient to consider it as a working hypothesis or a theory. The evidences are proposed for consideration all over the text below.

a) Model of the Origin of the Universal Gravitation Force

In this section, a model of appearance of the gravitation attraction force is considered from the viewpoint of aerodynamics. Namely, the two - dimensional model (Fig.1) is considered on the basis of the following initial postulates. These postulates will be expanded and defined more exactly below.

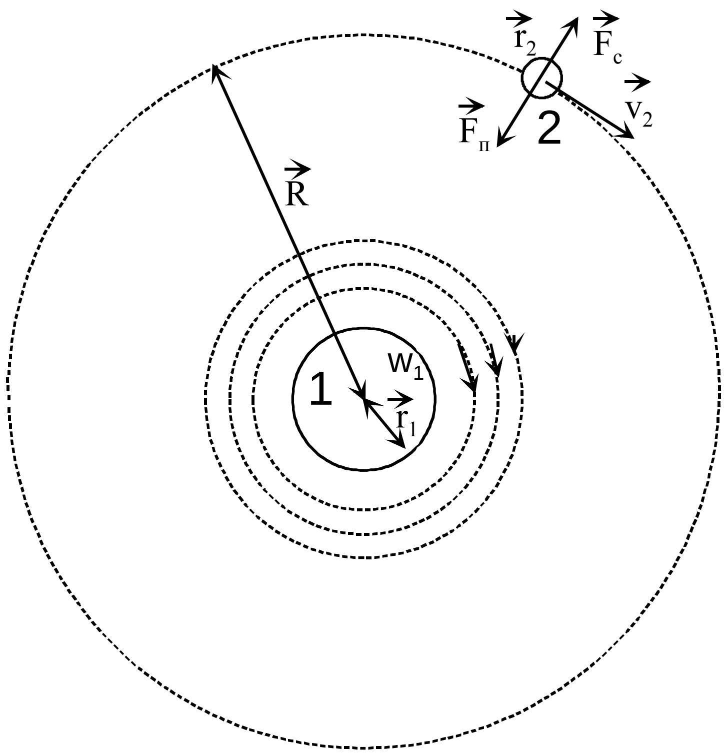

Fig.1 : Two-dimensional model of gravitational interaction of two bodies. The forces are shown acting on body 2: F_c – the centrifugal force, $F_п$ – the force of attraction of body 2 from body 1; v_2 – linear velocity of body 2 at the orbit, R – the radius of the orbit, r_1 – the radius of body 1, r_2 – the radius of body 2, w_1 – angular velocity of ether rotation at the surface of body 1, and m_2 are the mass of body 2.

1. There exists an ether vortex around any physical object.
2. The ether motion in the vortex has laminar nature and obeys the laws of hydro - or aero-dynamics; the ether viscosity is low.
3. The pressure gradient, arising during the vortex motion of the ether gas, is the reason for an attractive force from body 1 to body 2 (see Fig.1).
4. The direction of the force $\mathbf{F_п}$ does not depend on the direction of the ether angular velocity, which is necessary for the attractive force between the bodies, irrespective of their relative position. This implies the absence of the Magnus force – the force of interaction between the two vortexes which appears in the classical aerodynamics. Such an assumption can take place at a weak interaction between the two ether flows, as if they would move one through another, not affecting mutual motion.
5. The appearing attraction force must describe the experimentally obtained law of gravity :

$$F_п = G \cdot \frac{m_1 \cdot m_2}{r^2} \tag{1}$$

where m_1, m_2 are the masses of bodies 1 and 2, respectively, $G=6.672 \cdot 10^{-11}$ $N \cdot m^2/kg^2$ – the gravitation constant, and r – the distance between the bodies.

Next we consider the appearance of the attraction force in more detail and derive a formula describing it. As was said above, a pressure gradient arises as the result of the vortex motion. Let's find the radial distribution of the pressure and the ether velocity.

For this purpose, we write the Navier-Stokes equation for the motion of a viscous liquid (gas).

$$\rho\left[\frac{\partial}{\partial t}+\vec{v}\cdot\mathrm{grad}\right]\vec{v}=\vec{F}-\mathrm{grad}\,P+\eta\Delta\vec{v} \quad (2)$$

where ρ is the ether density, $\vec{V}$ and P are, respectively, its velocity and pressure, and η - the ether viscosity. In cylindrical coordinates, taking into account the radial symmetry $v_r=v_z=0$, $v_\varphi=v(r)$, $P=P(r)$, the equation can be written as the system:

$$\begin{cases} -\dfrac{v(r)^2}{r}=-\dfrac{1}{\rho}\dfrac{dP}{dr} \\ \eta\cdot\left(\dfrac{\partial^2 v(r)}{\partial r^2}+\dfrac{\partial v(r)}{r\partial r}-\dfrac{v(r)}{r^2}\right)=0 \end{cases} \quad (3)$$

In case of a compressible substance (ether), there will be a function $\rho=f(P)$ (instead of ρ).

From the first equation of system (3), one can find $P(r)$ provided that the dependence $v(r)$ is known. The latter, in turn, should be found from the second equation of that same system (one of the solution of which is the function $v(r)\sim 1/r$). At zero viscosity, the system permits any dependence $v(r)$ [2].

The force affecting the body can be estimated from the formula

$$\vec{F}_{п}=-V\bullet\mathrm{grad}\,P(r) \quad (4)$$

where V is the volume of body 2.

In cylindrical coordinates the modulus of $\vec{F}_{\Pi}$ is

$$F_{п}=V\cdot\frac{\partial P}{\partial r} \quad (5)$$

Then, comparing equations (3) and (5), for the incompressible ether (ρ=const) we find that

$$F_{п}=V\cdot\rho\cdot\frac{v(r)^2}{r}. \quad (6)$$

For the correspondence of the ether rotation to the planet motion law (according to Kepler 3-rd law) in one cosmic (e.g., S olar) system, $v(r)$ must obey the dependence $v(r)\sim\dfrac{1}{\sqrt{r}}$, and not the $v(r)\sim\dfrac{1}{r}$.

Taking into account the edge condition $v(r_1)=w_1\cdot r_1$,

$$v(r)=\frac{w_1\cdot r_1^{\frac{3}{2}}}{\sqrt{r}} \quad (7)$$

Thus

$$F_{п}=V\cdot\rho\cdot\frac{w_1^2\cdot r_1^3}{r^2} \quad (8)$$

Here we make one more supposition (№ 6) – Ether penetrates through all the space, including the physical bodies. The volume V in formula (8) is an effective volume, i.e. the volume of elementary particles, which the body is composed of. All the bodies are composed of electrons, protons, and neutrons. The radius of an electron is much smaller than that of a proton and neutron. The radii of the latter are approximately equal to each other, $r_n\sim 1.2\cdot10^{-15}$ m. The same is true as to the masses: $m_n\sim1.67\cdot10^{-27}$ kg (r_n and m_n are the radius and the mass of a nucleon). Therefore, the volume in formula (8) is:

$$V=\frac{m_2}{m_n}\cdot\frac{4\pi}{3}\cdot r_n^3 \quad (9)$$

Taking into account the formula (9), Eq.(8) can be rewritten as

$$F_{п}=\frac{4\cdot\pi\cdot r_n^3\cdot\rho}{3\cdot m_n}\cdot\frac{w_1^2\cdot r_1^3\cdot m_2}{r^2} \quad (10)$$

Supposing further (supposition № 7) that

$$w_1^2\cdot r_1^3=A\cdot m_1 \quad (11)$$

where A is a constant, Eq.(10) takes the form

$$F_{п}=\frac{4\cdot\pi\cdot r_n^3\cdot\rho}{3\cdot m_n}\cdot A\cdot\frac{m_1\cdot m_2}{r^2} \quad (12)$$

Comparing equations (12) and (1), one can find that $A=1.739\cdot10^{18}$ $m^3/s^2\cdot kg$. The data on the parameters of free ether used for calculations were taken from Ref.[1].

The supposition № 7 is reasonable, since w_1 and r_1 are the parameters of body 1. If we divide both the left- and right-hand sides of Eq.(11) by r_1^3, we will obtain that the square of the ether angular velocity on the surface is proportional to the body's density. Let's find, e.g., the angular ether velocity on the surface of the Sun:

$$w_1=\sqrt{A\cdot\frac{m_1}{r_1^3}} \quad (13)$$

The mass of the Sun is $m_1=1.99\cdot10^{30}$ kg, $r_1=6.96\cdot10^8$ m, and $w_1=1.022\cdot10^{11}$ c^{-1}.

The ether linear velocity on the surface is $v(r_1)=w_1\cdot r_1=7.113\cdot10^{19}$ m/s. This velocity is lower than the average speed ether ($6.6\cdot10^{21}$ m/s [1]) by two orders of magnitude. Thus, the obtained value of the ether wind linear velocity appears to be quite reasonable. For Earth, $m_1=5.98\cdot10^{24}$ kg, $r_1=6.38\cdot10^6$ m, and $w_1=2.001\cdot10^{11}$ s^{-1}, $v(r_1)=1.277\cdot10^{18}$ m/s.

On the basis of vortex gravitation, the value of w_1 in any celestial torsion is determined from the condition of the equality of the centrifugal forces and the gravitation forces for a celestial body.

Taking into account the compressibility of ether, e.g. in the isothermal case (T=const), i.e. when

$$\rho = f(P) = \frac{P}{R \cdot T} \qquad (14)$$

where R is the specific gas constant $R = \frac{R_0}{\mu} = \frac{R_0}{m_0 \cdot Na} = 1.972 \cdot 10^{93}$ $J \cdot kg^{-1} \cdot K^{-1}$ ($R_0 = 8.314$ $J \cdot mol^{-1} \cdot K^{-1}$ – the absolute gas constant, μ - the ether molecular weight, $m_0 = 7 \cdot 10^{-117}$ kg – the mass of an amer [1], $Na = 6.022 \cdot 10^{23}$ mol^{-1} – the Avogadro number), after the first equation in system (3) to be solved, we have got a function of the pressure radial distribution. This function, using e.g. the values of w_1 and r_1 for the Sun, results in a very insignificant change of the density with radius enabling the ether to be considered as an incompressible substance, and thereby, enabling the above-presented formulas to be used.

Let's now find the dependence P(r) solving the first equation of system (3). Taking Eq.(7) into account, we'll find that

$$P(r) = P_0 + \rho \cdot w_1^{\,2} \cdot r_1^{\,3} \cdot \left[\frac{1}{r_1} - \frac{1}{r} \right] \qquad (15)$$

where P_0 is the ether surface pressure. Using the boundary condition $P(\infty) = P_b$, we get $P_0 = P_b - \rho \cdot w_1^{\,2} \cdot r_1^{\,2}$ with P_b being the pressure of free ether. (Fig. 2)

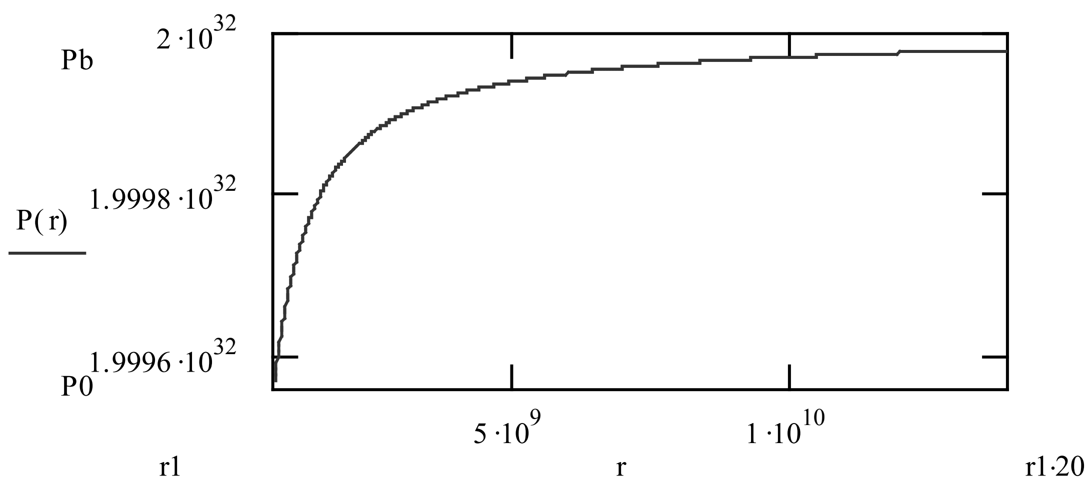

Fig.2 : Radial distribution of the ether pressure for the Sun (f.15).

From the obtained formula for vortex gravitation, it is obvious that, in the existing Newton's law of gravitation, instead of the reason of gravity (the gradient of pressure), the consequence of that (i.e. the mass) is used.

b) Spatial Model of Gravitation

In order to solve the posed problem of calculations of the forces of vortex gravitation, it is necessary to determine the space ether torsion configuration.

In view of the very small ether density, it is impossible to study the ether by means of direct methods. However, since (on the basis of the ether cosmogony – see Section 3 below) the ether creates celestial bodies and transfers to them the momentum of their movement, then it is possible to determine the character of the ether rotation and its configuration using the form of the celestial objects and the character of their movement.

Because the main vortex shape characteristics are its diameter and thickness, the main objective of the investigation of the torsion configuration is just to determine these two parameters.

The size of the torsion diameter is quite obvious and is equal to the diameter of the corresponding cosmic (solar) system. The latter is determined by the most distant orbits of the satellites of this torsion.

At the same time, the vortex-like ether rotations occur in the cosmic space as some discoid media of a negligible (very small) thickness.

This suggestion is based on commonly-known astronomy facts.

1. Because all the celestial objects have spherical or ellipsoidal shapes, for the accumulation of the cosmic matter as a sphere (under the action of the vortex gravitation), it is needed that an active axis thickness of the vortex ether flow be less than the diameter of the created body. The point is that, if the ether would rotate as a "rotor" with a significant axis thickness, then such a rotor would produce the gravitation with cylindrical configuration. In this case, the cosmic matter indrawn by this torsion would have the same cylindrical form. Since as such the cylindrical shapes of the celestial objects are not observed, then the conclusion is obvious, namely, the ether rotation has a form of a "thin" rotating disc.

Global Journal of Science Frontier Research (A) Volume XII Issue I Version I January 2012

When comparing the value of diameter of any celestial object with the diameter of the corresponding space system (solar, planetary), it is obvious that the diameter of an object is negligibly small as compared with the system diameter, and consequently a vortex "cuts up" the cosmic space by a layer with an also negligibly small thickness.

2. All the systems of celestial objects (galaxies, systems of planets and satellites) circulate around a center in a unique orbital plane with small inclination.

Such trajectories of the celestial systems are possible only in the case if the ether (in corresponding space regions) also rotates in the same planes with a negligibly small axes thickness cutting the massive ether. According to the aerodynamics laws, the pressure decreases in these planes, and all the bodies or substances from the neighboring regions are pushed out toward the central plane of this rotation and (or) are kept back in it.

Kepler recognized action of powers attraction in solar system on inverse-square law only in planes ecliptic.

As plane of ecliptic has small deviation from flat of sunny, gravitational torsion bar, that its suggestion molybdenum-put very close to offered vortical, go-symmetric gravitation.

The most pictorial visual rendition of the cosmic torsion shape one can see looking at a galaxy as an example. The spiral-like armlets of galaxies earnestly show their vortex nature. Also, it is known from astronomy that the diameter and thickness of a galaxy has a ratio 10:1. Since this dependence corresponds to point 2 of the present Section above, it is quite obvious that this configuration of celestial torsions is the most typical in cosmic space. That is, stellar (e.g., solar) and planetary (e.g., Earth) ether torsions have the same discoid form.

III. Some Conclusions

The model of the universal vortex gravitation determines absolutely new principles of the origination and existence of the universe substance.

The below-suggested calculations and results do not pretend to be complete and exact. The main purpose of Section 3 is to present evidences of the existence of vortex nature of the gravitation forces with its discoid configuration, as well as to show applied possibilities of the model of vortex gravitation for the principally new study of numerous cosmology phenomena. Any specialist can independently work out ways and methods of calculations and investigations on the basis of vortex gravitation.

a) Black Holes

In 1783 John Mitchell has presented his work where he sowed that a sufficiently massive and compact star should have such a high gravitation field that light could not get it out. Such objects are called Black Holes.

On the basis of the proposed model of vortex gravitation and obtained formula (10), and also taking into account the assumption **№6** of Section 2, one can determine the gravitation force in any point of space, including that inside celestial objects, particularly inside the Sun.

It has been established by means of calculations that vortex gravitation, corresponding by its strength to the gravitation force of a Black Hole (BH), exists in the sun torsion in a distance of 3 kilometers from the center.

This distance corresponds to schwarzschild radius, but thus it is not required condensation of material of Sun to volume of such radius.

Besides, on the basis of that same calculation, all the celestial torsions, including the planetary ones, should theoretically have a gravitation force, corresponding to that of the BH. A super-high gravitation force, caused by a corresponding pressure, creates in the centers of all celestial objects (including planets) a physical basis for the existence of thermal-nuclear reactions in these central zones.

Hence, BH is a central part of the cosmic ether torsion which, possessing gravitation, creates a new celestial object. That is, **BH is not a collapse of a celestial object, but it is a newly-formed cosmic torsion which does not possess a physical body yet.**

An outside observer can fix a Black Hole only at the moment when the center of the cosmic torsion is not still hidden by the cosmic substance which the torsion have to suck in starting from the moment of birth. After the concentration of cosmic substance in the center of the torsion in a volume sufficient to hid over-gravitation zone, this celestial object turns into a conventional celestial object – a planet, star, etc.

The super-massive BH in the center of our galaxy, rotating with a huge speed, convincingly supports the proposed concept of the nature of black holes.

b) Evolution of Stars

In modern astrophysics, the star evolution is considered according to the following scheme:

- at the initial stage, the appearance of dense clouds of gas and dust occurs, from which, under the action of the own gravitation, a compressing proto-star is formed. Then, an ordinary star is formed, and after that it turns into a red giant, and further – into a white dwarf. As the concluding phase of the star existence, modern cosmology considers the stage of BH which is accompanied by the collapse of the celestial object.

It should be noted that in this hypothesis, the reasons for the appearance of the gas-dust matter, as well as those for substance and stars from this diffusive medium, are not indicated. Besides, the proposed process of the celestial objects self-densification has very weak argumentation.

The star evolution based on the principle of vortex gravitation is quite the reverse as compared to the classical ideas; however, it is in complete conformity with the basic physical laws.

As was shown in Section 3.1, any torsion in the initial stage, in its central zone, has a form of BH. After the substance accumulation exceeding the volume of BH, the gravitation forces on the outer layers of the created star decrease inversely proportionally with square of the distance from the torsion center. In spite of this, these forces preserve their great magnitude which compels the star substance to compress up to the neutron state. Consequently, the next star stage after the BH is the neutron star which, in turn, is subdivided into several phases. The initial phase of the neutron star is the pulsar. At present, the pulsar PSRJ1748-2446 ad with the revolving speed of 716 rps has been found. Further increase of the star (pulsar) mass and corresponding slowing-down of its rotation changes the star properties to the physical state called in astronomy as the white dwarf. The white dwarf circulation period is few hours. Continuous increase of the white dwarf mass transforms it into the red giant. In the concluding stage of the neutron state, the star, accumulating a corresponding mass, decreases significantly the rotation speed, and the density of outer layers (taking into account the corresponding decrease of the surface gravitation forces) also decreases by several orders of magnitude. It is the stage of the ordinary star. This stage is divided into the initial one (hot ordinary star) and the next (cold ordinary star). Then the star increases its mass up to that of the proto-star and decreases the rotation speed.

Specific physical properties of a star – the mass, temperature, luminosity, rotation speed, density, surface gravity force – correspond to each stage of its life. As the mass and the radius of a star increase, the surface moves away from the center, and the gravitation force on the outer layers and the surface substance density correspondingly decrease. However, inside the star, the star substance remains to exist, and it possesses the properties corresponding to the previous evolution stage of this star. Particularly, inside the ordinary cold star, on a certain depth, the substance in the hot star state is reserved; deeper – the matter is in the neutron state; and finally, in the center – the BH state. In all the layers of the star substance, the gravitation force grows in accordance with the principle and the formula of the vortex gravitation.

In modern cosmology, nova outbursts are treated as the end of the evolution of these stars.

From the viewpoint of vortex cosmogony, nova and super-nova outbursts should be treated as indications of new stars because:

✓ outer layers of each star, or radio-, electromagnet, and light radiations, emitted by this star, are held back at its surface since the gravitation force at this surface exceeds the centrifugal forces acting due to the star rotation or the radiation momentum. Because the star volume and radius increase permanently, the vortex gravitation force on the surface of this star has to decrease inversely proportionally with square of the distance from the star (torsion) center. Therefore, evolution moments have to come in the life of each new star when the gravitation force on the object surface decreases down to the value incapable of holding back not only radiations, but also – outer layers of the star substance. In such cases, astronomy observations fix either the appearance of nova stars or super-nova outbursts accompanied by ejection of the star substance to the cosmic space. Further super-nova mass increase results in the rotation speed, and hence centrifugal force acting onto the outer layers, decrease. As a result, the star massive will be in a stable state, and the detachment of the outer layers into the cosmic space will over.

c) Cause of The Ellipsoidal Shape of Orbits

It is known that the planets circulate around the Sun by an ellipse with a small eccentricity.

This fact is accounted for from the viewpoint of vortex gravitation; moreover, it serves as a convincing proof of the existence of this gravitation with its discoid plane-symmetrical configuration (Section 2.2).

The cause of the planets orbit "compression" is the inclination of these orbits to the sun torsion plane. This statement is based on the following.

As is known, the planes of orbital motion of all the planets are situated with small deviations one from another. Consequently, planet orbit planes have inclinations to the plane of the sun gravitation torsion, where the highest gravitation force for this orbit acts, and the planets should intersect the sun torsion in two points during their orbital motion. As will be shown below, these intersection points coincide with the centers of perihelion and aphelion.

In the aphelion and perihelion, the sun gravitation force acts onto the planets with the highest magnitude at this orbit, and hence the orbit possesses a maximum curvature. At going out (deviation) from the sun torsion plane, the gravitation forces decrease and the planet trajectory "unbends" (Fig. 3). As such the cycle of the gravitation force and motion trajectory change repeats for each planet and for each turn around the Sun. The more the planet circulation trajectory is deviated from the central sun torsion plane, the higher is the degree of the gravitation force decrease in these regions, and hence the higher is the degree of "straightening" or "compression" of the orbit. Due to a permanent cyclic change of these forces, the orbit becomes ellipsoidal.

At significant inclinations and high speeds, the orbit of a satellite (meteorite, comet) have a hyperbola or parabola trajectory, and, correspondingly, the celestial object, once turning around the Sun, abandons the sun gravitation torsion field forever.

Determining of the sun torsion direction

On the basis of the stated above, it is obvious that the orbit trajectory eccentricity value of any planet depends on the value of inclination of this orbit to the sun torsion. Therefore, a reverse relation takes place, i.e. the lower the orbit eccentricity, the lower the inclination of the planet orbital plane to the sun torsion plane.

Since the Venus orbit has the least eccentricity, for preliminary calculations, it is permissibly to accept the following property of the sun torsion:

- ✓ the direction of the sun gravitation torsion in the World coordinates coincides with the Venus orbital plane direction to a highest degree.

Therefore, all the inclinations and latitudes of any astronomical point can be determined with regard to the orbital plane of Venus with a small correction up to 0.5 degree.

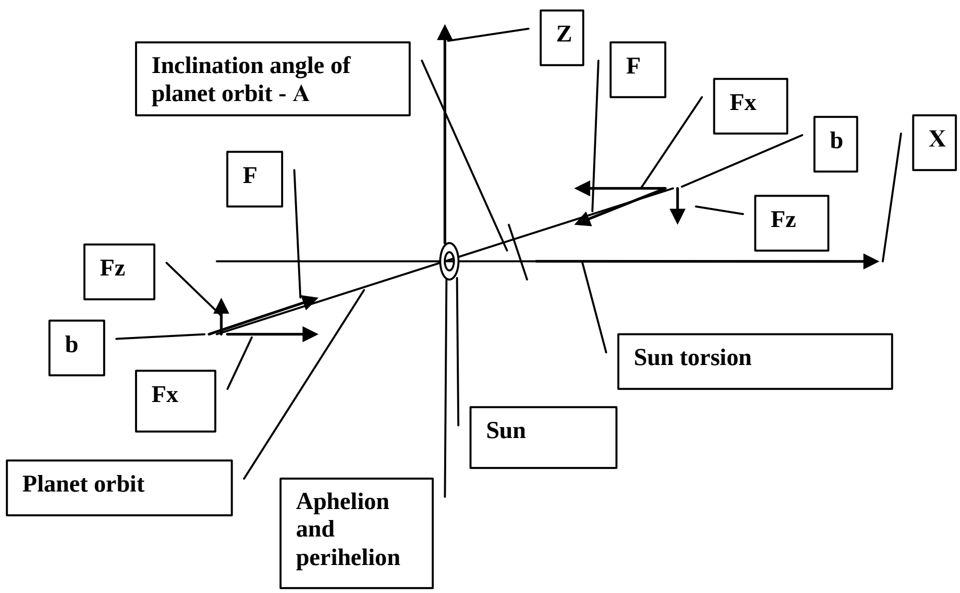

Fig. 3 : Kinematical scheme of orbital motion

Let's consider the planet circulation in more detail with the Mercury motion as an example, in accordance with its heliocentric coordinates of 1993 [5].

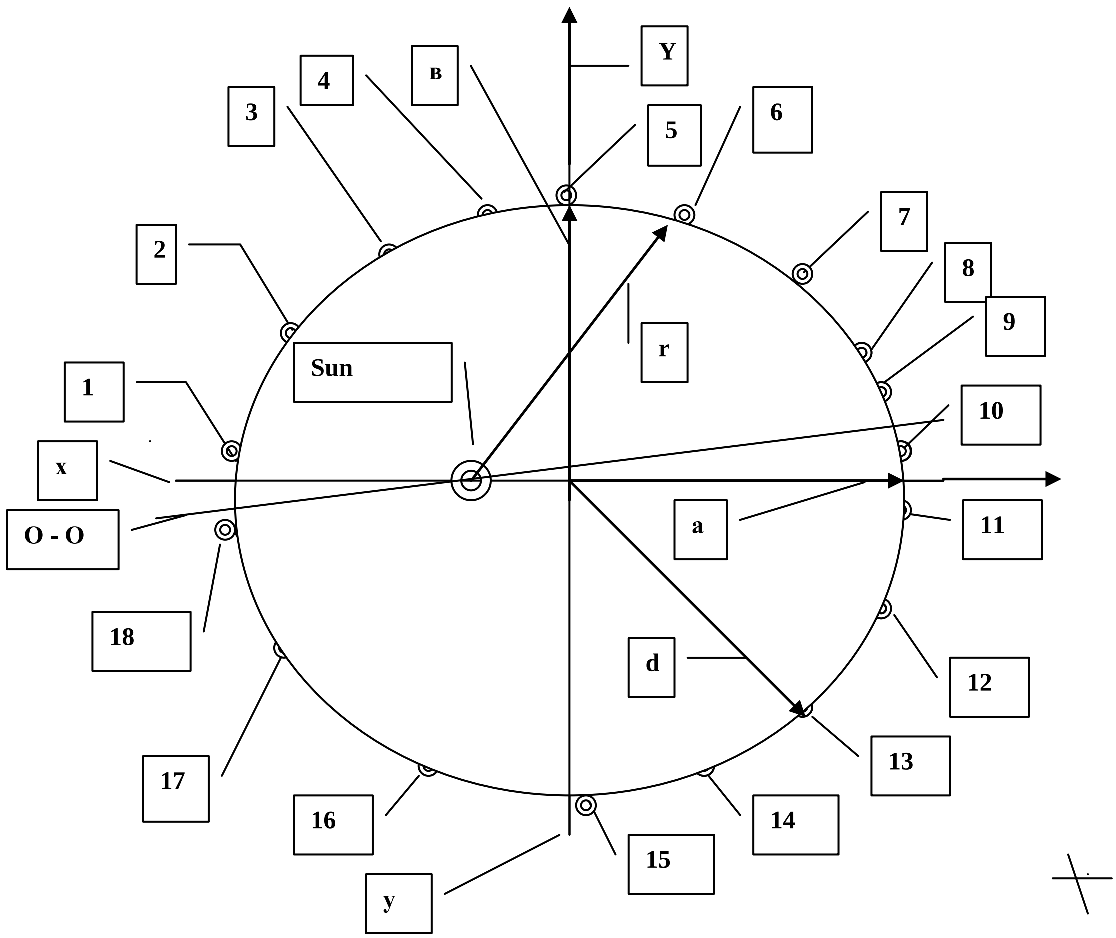

Fig. 4 : Orbit of Mercury

In Table 1 and Fig's 3 and 4, the following denotations are used:

Z – the torsion rotation axis

№ - numbers of the Mercury orbit points according to the astronomy calendar of1993

Д – the heliocentric longitude J2000.0 of these points

r – the radius-vector, in A. U.

d – the distance from the ellipse center to the point under study, in million km.

V – the orbital speed, in km/s

R – the curvature radius, in million km, $\mathbf{R = a^2\ b^2 / d^3}$ where **a, в** are the major and minor axes

Fc – the centrifugal forces

Fg – the gravitation forces.

The values of centrifugal and gravitation forces are in portions of the planet mass.

O – O – the apse line coinciding with the line of intersection of the Mercury orbital plane with sun torsion plane. The center of Mercury perihelion has the longitude of **(85.83 – 8.18)** degree regarding to the point №1 in 1993.

On the basis of comparison of latitudes from the astronomy calendar, it has been established that the Mercury traverses the Sun (Venus) torsion in the aphelion and perihelion. The same is true for the other planets. Therefore, at these parts of the planet motion, the orbit curvatures are maximum and equal to each other, and the gravitation forces correspond to their classical values, i.e. they are inversely proportional to square of the distance to the Sun or are equal to the centrifugal forces.

Thus, the exact position of the sun torsion by its latitude relatively to the ecliptic is indicated by the latitudes of the aphelion and perihelion centers of each planet and by the apse line directions of these planets.

Comparing the astronomy point latitude values with the ratio of the gravitation and centrifugal forces in these space points, one can find that the more the planet orbit is inclined to the sun torsion, the higher is the difference between the Newtonian calculated gravitation forces and the actual centrifugal forces in those same points.

We consider two points of the Mercury orbit (**№ 9 и № 10** in Fig. 3).

Table 1: Mercury orbit parameters

№	Д, degree	r	d	V	R	Fc	Fg
9	250,04	0,4657	58,11	38,41	55,46	26,60	27,32
10	263,78	0,4659	58,03	38,96	55,69	27.26	27,29

The distance between point 10 and the Sun is 0.4659 x 150 = 69.885 million km.
For point 9 it is - 0.4657 x 150 = 69.855 million km.

The distance of point 10 from the Sun is 1.0004 times longer than that for point 9. Therefore, in point 10, the Newtonian sun gravitation forces have to be 1.001 times less than those in point 9 (see Table 1). In reality, according to the calculation, the value of centrifugal forces in point 10 are 1.025 times higher as compared to point 9 which is associated with a larger orbit curvature in this point (see Table 1). Since the planet circulation centrifugal forces are reactive and always equal to the gravitation forces, it is follows from the above-said that, in this region of Mercury motion trajectory, the classical gravitation law is not fulfilled.

On the basis of the vortex gravitation model with a plane-symmetrical configuration, this paradox has a physical-mathematical ground.

The Newton's world attraction law or formula 10 in Section 2.1 can describe the action of the gravitation forces only in the plane of the gravitation torsion.

The above-presented calculation of the centrifugal forces appearing at the planet motion in the aphelion shows that the inertial circulation of the planets along an ellipsoidal trajectory in a central-symmetrical gravitation field is impossible in accordance with the classical ideas.

It should be noted that the planet orbit perihelion revolving round the Sun is also accounted for by a permanent change of the force magnitudes acting upon the planets.

d) Calculation of Gravitation In Three-Dimensional Model

The change of the dynamical properties of the planets at their inclination, discussed in Section 3.3, gives a possibility to obtain a formula describing the change of gravitation forces in the three-dimensional model.

Comparing the orbit compression coefficients for all the planets with cosine of the angle of inclination of these orbits to the sun torsion, one finds that these values are directly proportional to each other :

$$\mathbf{b/a \sim Cos\ A} \qquad (16)$$

Proofs of equation

axis X – the direction of the parent torsion central plane.
axis Z – the rotation axis of the parent torsion.
A – the inclination angle of the satellite (planet) orbit torsion.
OB – the curvature radius of the torsion-satellite revolving at the coincidence of the satellite-torsion motion trajectory with the parent torsion rotation plane, i.e. at the perihelion or aphelion, or at the apex of the orbit major semiaxis:

$$\mathbf{OB = b^2 / a} \qquad (17)$$

OD1 - the curvature radius of the torsion-satellite revolving when it moves in a region possessing the inclination of angle A from the parent torsion central plane, i.e. at the apex of the orbit minor semiaxis:

$$\mathbf{OD_1 = a^2 / b} \qquad (18)$$

We prove that the equation cos **A** = **b/a** is fulfilled at equalities **(17)** and **(18)**

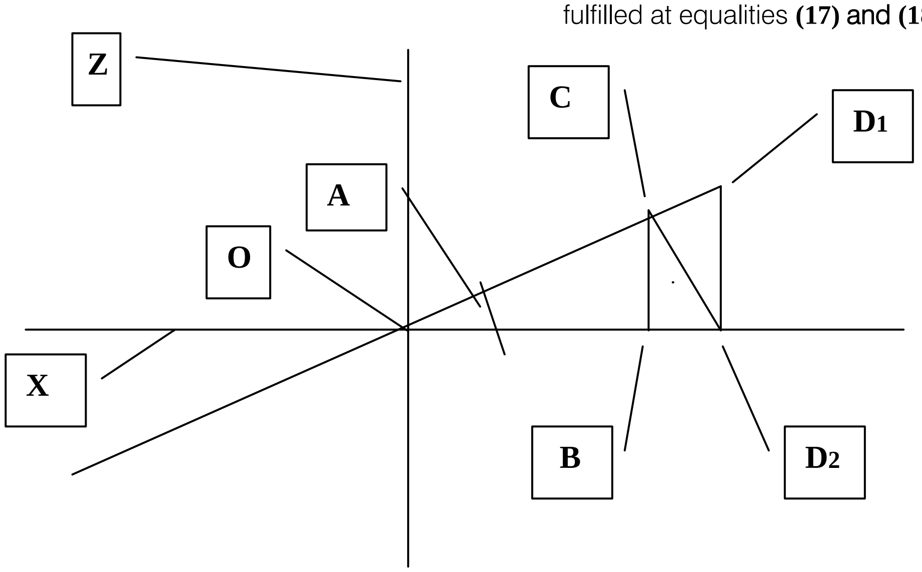

Fig.5 : Plane projections of minor and major orbital semiaxes.

Proof :

First we draw a segment **OB** on the axis **X** (fig.5) coinciding with the apses line. This segment is to be equal to the curvature radius in the major semiaxis apex and is directed along the sun torsion central plane or the apses line.

Let's now draw a line from the center **O** with the angle **A**; the direction of this line has to coincide with the minor semiaxis apex.

Since, from the problem condition, **cos A = b/a = OB/OC**, then:

$$OC = OB\ a/b = (b^2/a)\ (a/b) = b$$

Let's drop a perpendicular from point C on axis X, as the angle OCD_2 is right :

$$OC/OD_2 = \cos A = b/a, \text{ whence}$$

$$OD_2 = OC\ a/b = b\ (a/b) = a,$$

And finally we drop a perpendicular from point D2 on line OC, as the angle D_1D_2O is right:

$$OD_2 / OD_1 = \cos A = b/a, \text{ whence } OD_1 = OD_2\ (a/b) = (a^2/b)$$

Therefore, equations **(17)** and **(18)** are fulfilled provided that cos **A** = **b/a**. That is, the cosine of the planet orbit inclination angle in the minor semiaxis apex to the sun torsion plane is equal to the compression coefficient of this orbit.

Note 1 : The inclination A of an orbital point does not coincide with the angle of inclination of this point indicated in astronomy calendars, because, according to the astronomy rules, all the coordinates in the Solar system are measured heliocentrically and from the ecliptic plane.

Since the centrifugal forces are reactive and always equal to the sun attraction forces, these centrifugal forces may be considered as experimental or etalon values for the estimation of the accuracy and correctness of the results of gravitation forces calculations. Therefore, the change of the value of the planet centrifugal forces at a change of their coordinates is always equal to the change of the value of the gravitation force acting onto this planet.

Determining of the three-dimensional gravitation coefficient Kg.

Let's write the formulas to determine the orbit (ellipse) curvature radius:

- in the major semiaxis apex or in perihelion and aphelion:

$$R_{кр.a} = b^2 / a \quad (19)$$

- in the minor semiaxis apex:

$$R_{кр.в} = a^2 / b \quad (20)$$

On the basis of the 2nd Kepler law, the planets change the orbital velocity **(V)** as a function of the distance to the Sun **(R)**, in the limits of their orbits, in the following proportion:

$$Va \sim 1/Ra \qquad Vb \sim 1/Rb \quad (21)$$

where

Va – the orbital speed in the perihelion (aphelion), i.e. in the apex of the planet orbit major semiaxis,

Vb – the orbital speed in the apex of the planet orbit minor semiaxis

Ra – the distance from the Sun to the aphelion (perihelion).

Rb – the distance from the Sun to minor semiaxis apex.

The centrifugal force is determined from the formula:

$$Fc = m\ V^2 / R_{кр} \quad (22)$$

Substituting (19) – (21) into (22):

$$Fca = m\ Va^2 / R_{кр.a} \sim m\ a / Ra^2\ b \quad (23)$$

$$Fcb = m\ Vb^2 / R_{кр.b} \sim m\ b / Rb^2\ a^2 \quad (24)$$

Since the gravitation forces in the aphelion and perihelion Fa correspond to their classical values or to the centrifugal forces, then, to determine a deviation of the gravitation forces in the torsion periphery (in the minor semiaxis apex – point b), it is necessary to determine the analogous deviation of the values of the centrifugal forces as compared to those same forces in the perihelion. For this purpose, we divide formula (24) by formula (23):

$$Fcb / Fca = [b^3 / a^3]\ [Ra^2 / Rb^2]$$

Here the relative value Ra^2 / Rb^2, in accordance with formula 10 in Section 2 or with the Newton formula, determines the gravitation force change as a function of the change of the distance from the torsion center to the points under consideration.

According to the expression (16), the value **b/a** equals to the cosine of the inclination angle in the considered point. Hence, this value determines the change of the gravitation forces as a function of the inclination of the considered point to the sun torsion. Therefore, one can write:

$$b^3/a^3 = \cos^3 A = Kg \quad (25)$$

The gravitation forces in any point of the cosmic space are determined by the formula:

$$Fv = Fg \cos^3 A \quad (26)$$

where

Fg – the gravitation force in the two-dimensional model (formula 10 in Section 2 or Newton equation)

Fv – the gravitation force in the three-dimensional model

Consequently, using the gravitation coefficient Kg, one can determine the gravitation forces in any point distant from the center of a cosmic torsion.

Formula (26) shows that, when moving away from the gravitation torsion plane, parallel to the torsion axis, the gravitation force decrease inversely as the cube of the distance - $1/s^3$

Experimental Verification of the Vortex Gravitation Equation – (26)

Any theory is considered to be proved if its conclusions and formulas correspond to experimental facts. Since the gravitation forces correspond to the centrifugal (experimental) forces, then, to determine a deviation of the gravitation forces in the torsion periphery (in the minor semiaxis apex – point b), it is necessary to determine the analogous deviation of the values of the centrifugal (experimental) forces as compared to those same forces in the perihelion.

1. *Pluto*

a = 5906,375 x 10^6 km – major semiaxis, b = 5720, 32 x 10^6 km – minor semiaxis

r = 5907,963 x 10^6 km – the distance from the Sun to the Pluto orbit minor semiaxis apex

Kc – compression coefficient of the orbit

Kc = 1 - e^2 = b/a = Cos A = 0,9685

Kg – gravitation coefficient

Kg = b^3/a^3 = Cos^3 A = 0,9084

Rb – curvature radius in the Pluto orbit minor semiaxis apex

Rb = a^2/b = 6098,48 x 10^6 km

Vb = 4,581 km/c – the orbital speed in the apex of the Pluto orbit minor semiaxis

The centrifugal force in the minor semiaxis apex

Fcb = 0,00344 Mp, **Mp** – mass of the Pluto.

Newtonian gravitation forces in its point

Fgb = 0,00382 Mp (+11,1% concerning Fcb)

The vortex gravitation forces

Fvb = Fg x Kg = 0,00382 x 0,9084 = 0,00347 Mп (+ 0,87% concerning Fcb)

2. *Mercury (analogous calculation)*

a = 57,91x 10^6, в = 56,67 x 10^6, r = 58,395 x 10^6 .

e = 0,2056, Ксж = в/а = 1 - e^2 = Cos A = 0,9786, Kg = 0,9372.

Rb = 59,177, Vb = 46,4775

The centrifugal force in the minor semiaxis apex

Fcb = 36,503 Mm, Mm – mass Mercury

Newtonian gravitation forces

Fgb = 39,09 Mm, (+7,1% concerning Fcb)

The vortex gravitation forces

Fvb = 36,63 Mm (+ 0,35% concerning Fcb)

Consequently, formula (9) is really correct.

It is known that, according to the two-dimension gravitation formula (i.e. the Newton's one or formula 10 from Section 2), the gravitation (gravity) force on the pole is **Fp = 9,87m**. On the other hand, the actual gravity force determined by means of geodetic gravimetry is **Fp = 9,83m**, which is **0.43%** less than the calculated value.

This difference can be explained only on the basis of the above-indicated calculation in the frameworks of the three-dimensional gravitation model. That is, on the poles, the gravitation is created by the ether front turbulences, and the ether velocity is varied by a different law as compared to that in the longitudinal torsion direction. Hence, the gravitation force decreases differently in the longitudinal direction and in the pole direction.

The gravitation force distribution in some cosmic torsion determines the form of a cosmic object created in this torsion. The configuration of epure № 2 is especially close to the galaxy configuration. Therefore, this calculation proves additionally a plane-symmetric configuration of the attraction forces.

Also, the cosmic expedition of the automatic station to Venus in April 2006 has found the zone of small satellites revolving in one plane, and atmospheric craters have been found on the planet poles. The planet of Saturn is also surrounded by a ring of small satellites situated in one orbital plane. These facts convincingly prove the plane configuration of the planetary gravitation torsions, which is in agreement with the above calculations.

The projecting of middle- and long-distance cosmic flights with the taking into account the plane-symmetric gravitation torsion configuration will allow a significant reduction of the transport expenses.

e) Motion of Torsion - Satellites

In order to account for the motion of satellite torsions around the parent torsion center, it is sufficient to use the momentum conservation law and the property of a celestial body to increase its mass due to the own gravitation.

Let's write the angular momentum conservation law of motion:

$$\mathbf{M\ V\ R = const} \quad \text{whence} \quad \mathbf{Km\ Kv\ Kr = 1} \qquad (27),$$

where

M, V, R – the mass, orbital velocity, and the distance to the planet circulation orbit.

Kr,v,m – coefficients of the change of the celestial object orbital distance, velocity, and mass.

The plant mass increase of **1.6 x 10^{15} kg per year**, given in [1], in a cosmic scale, is an alternating value and depends on the planet distance from sun torsion center because:

- the cosmic dust density in any cosmic torsion, including the sun's one, increases from the periphery to the center. This is explained by the fact that the dust from outside, during its radial motion toward the center of the sun torsion under the action of gravitation, should remove into a lower volume, and hence it should become denser. The volume of each orbital layer with a negligibly small thickness is proportional to the area of this orbital surface (S) or to square of the distance from the orbit center:

$$\mathbf{S = 4\ \Pi\ R^2}.$$

Therefore, the cosmic dust density in any torsion increases as square of distance in direction toward the torsion center. Since the influx of cosmic dust into the planetary torsion is proportional to the density of the adjoining cosmic substance, one may arrive at a conclusion that the closer the torsion-satellite revolving orbit is to the parent torsion center, the higher the cosmic dust influx enters into the torsion of this satellite, which can be written as:

$$Kr = Km^{-2} \quad (28)$$

Substituting (28) to (27), one can find that:

$$Km = Kv \quad \text{or} \quad Kr = Kv^{-2} \quad (29)$$

Formulas **(28,29)** prove:

1. 3rd Kepler law, because formula (29) is equivalent to this law:

$$R \sim V^{-2} \quad \text{or} \quad V^{2}R = const$$

2. All the torsion-satellites move with an acceleration and by a spiral to the parent torsion center, because it follows from formulas **(27),(28)** and **(29)** that as the torsion satellite mass increases (at Km above zero), the distance to the torsion rotation center decreases, and its orbital speed increases.

It should be noted that formulas **27,28,29** describe the satellite motion only in the central plane of the gravitation torsion.

At inclination of the orbits of the celestial objects-satellites, the following motion trajectory is feasible :

- at the initial stage of the existence of the torsion-satellite, a maximum increase of its relative mass occurs. Therefore, on the basis of the present section (form. 28), a rapid decrease of the orbital motion radius of this torsion occurs. As the satellite mass increases, the relative mass growth **(Km)** decreases, because the absolute mass growth of the torsion-satellite is constant. After the accumulation of a considerable mass of the satellite substance, the relative increase of its mass should be negligible. Then the celestial objects-satellites (stars, planets, planet satellites), possessing the inclinations of their own orbits to the gravitation parent torsion disk plane, can stop the spiral approaching toward the parent torsion center and, afterwards, continue their spiral orbital motion, but toward the periphery, not to the center. This is accounted for by the fact that, during the orbital motion of the satellites in the minor semi-axis apex, i.e. in the region of a maximum deviation from the parent torsion plane, the centrifugal forces can be higher than the gravitation forces, which must cause an orbit radius increase of these satellites.

Let's consider the orbital motion of the Moon, which has the following characteristics:

- the orbit compression coefficient **Kc = 0.997**
- gravitational coefficient **Kg = Kc^3 = 0.991**
- Moon orbital speed in the minor semi-axis apex **Vb = 1.01858 km/s**
- distance from the Earth to the minor semi-axis apex **Rb = 0.38378 x 10^6 km**
- orbit curvature radius in the minor semi-axis apex **Rкр = 0.3856 x 10^6 km**

The centrifugal force acting on the Moon in the minor semi-axis apex is therefore:

Fc = 2.691 Mm, where **Mm** is the Moon mass.

According to the Newton law, the Earth gravitation force acting on the Moon in the same orbital point must be:

Fgn = 2.706 Mm (+0.55%)

In the model of vortex gravitation this force is:

Fgv = Fgn x Kc^3 = 2.706 x 0,991 = 2.682Mm (- 0.33%)

Therefore, from the Newton law, the Moon must approach to the Earth, and from the vortex gravitation model, it must move away from the Earth.

Actually, the Moon orbit indeed moves away from the Earth by 38 mm a year; this fact additionally confirms the validity of the vortex gravitation model and, correspondingly, the incorrectness of the Newton law.

Analogous calculations can be made in order to find the exact changes of the orbits of all the planets or stars.

f) Moonflight

Let's consider a problem of comparing the works expended on getting over the gravitation attraction forces (F) by a body, when traveling from point A to point C (see Fig.6) by the paths AC and ABC at two different F(r, φ) dependences.

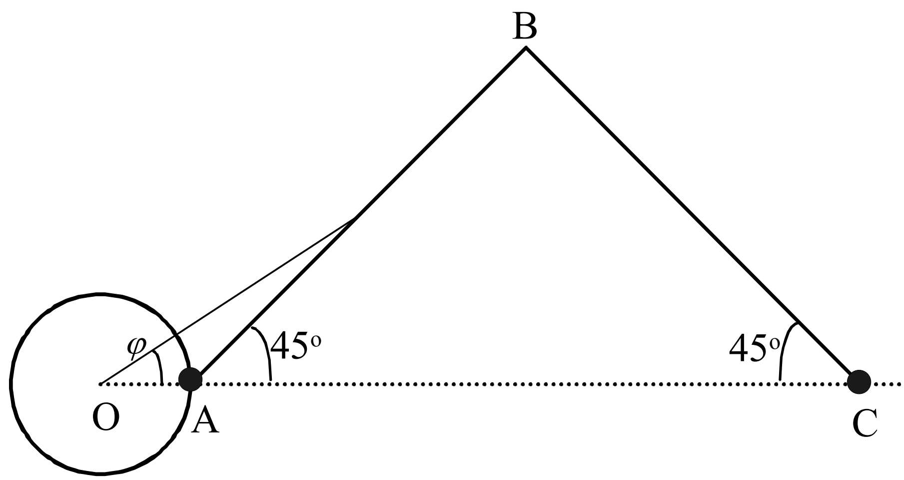

Fig. 6 : Scheme of space flight

O – centre of Earth
A – start of flight
C – Moon (finish)
AC – projection of gravitational flat

In the first case, F is independent of φ and obeys the Newton law (1)

$$F(r) = G\frac{m_1 \cdot m_2}{r^2} \quad , \qquad (30)$$

where m_1 and m_2 are the masses of bodies, G – the gravitation constant, and r – the distance between the bodies.

In the second case, F depends on φ in accordance with formula (26) of Section 3.4

$$F(r,\varphi) = G\frac{m_1 \cdot m_2}{r^2} \cdot \cos^3(\varphi), \qquad (31)$$

where φ is the angle between axis OC and the position radius-vector of the replaced body.

As is known, the work equals to the path integral

$$A = \int \vec{F} \cdot d\vec{r}\,. \qquad (32)$$

Let A_{AC} be the work expended at the transference AC for the case of the dependence (1). We determine the works A_{AB} and A_{BC}. For A'_{AC} being the work expended at the transference AC for the case of the dependence (2) we determine, respectively, the works A'_{AB} and A'_{BC}.

Now we write the integral (3) for each case

$$A_{AC} = \int_{r_1}^{r_2} G \cdot \frac{m_1 \cdot m_2}{r^2}\, dr \qquad (33)$$

$$A_{AB} = \int_0^{\varphi_{BOC}} G \cdot \frac{m_1 \cdot m_2 \cdot (\cos(\varphi) - \sin(\varphi)) \cdot \cos(\frac{3 \cdot \pi}{4} + \varphi)}{r_1 \cdot \sin(\frac{\pi}{4} - \varphi)}\, d\varphi \quad , \qquad (34)$$

$$A_{BC} = \int_0^{\varphi_{BOC}} G \cdot \frac{m_1 \cdot m_2 \cdot (\cos(\varphi) + \sin(\varphi)) \cdot \cos(\frac{\pi}{4} + \varphi)}{r_2 \cdot \cos(\frac{\pi}{4} - \varphi)}\, d\varphi \quad , \qquad (35)$$

$$A'_{AC} = A_{AC} \quad , \qquad (36)$$

$$A'_{AB} = \int_0^{\varphi_{BOC}} G\cdot \frac{m_1\cdot m_2\cdot(\cos(\varphi)-\sin(\varphi))\cdot\cos(\frac{\cdot\pi}{4}+\varphi)\cdot\cos^3(\varphi)}{r_1\cdot\sin(\frac{\pi}{4}-\varphi)}d\varphi \qquad (37)$$

$$A'_{BC} = \int_0^{\varphi_{BOC}} G\cdot \frac{m_1\cdot m_2\cdot(\cos(\varphi)+\sin(\varphi))\cdot\cos(\frac{\pi}{4}+\varphi)\cdot\cos^3(\varphi)}{r_2\cdot\cos(\frac{\pi}{4}-\varphi)}d\varphi, \qquad (38)$$

where r_1 – the distance OA, r_2 – OC, and φ_{BOC} – the angle BOC.

Formula (36) is valid because, in this direction, the forces (30) and (31) are equal to each other.

Calculating the integrals (36-38) numerically for the case of moonflight ($r_1=6400\cdot10^3$ m, r_2= 400 00000m, $m_2=6\cdot10^{24}$ kg, m_1=1 kg), one obtains $A_{AC} = 6.1554643\cdot10^7$ J, $A_{AB} = 6.1140242\cdot10^7$ J, $A_{BC} = 4.1440045\cdot10^4$ J, $A'_{AB} = 4.5279719\cdot10^7$ J, $A'_{BC} = 3.5727542\cdot10^5$ J.

One can see that $A_{AC}= A_{AB} + A_{BC}$, which just must be the case for the Newtonian forces when the work does not depend on the transference path from point A to point C.

In the case of the law (31), the work on the path ABC equals to $A'_{ABC}= A'_{AB} + A'_{BC}= 4.5636994\cdot10^7$ J. This is less than the work $A'_{AC} = A_{AC} = 6.1554643\cdot10^7$ J.

The ratio (decrease) of the works is $s=\mathbf{A'_{ABC}} / \mathbf{A_{AC}} = \mathbf{0.7414062}$. The value of s depends on the distances r_1 and r_2 and on the transference path.
Thus, the transference by the path ABC in the case of the law (2) is more energetically preferable than that directly by the path AC.

The above calculation shows that the moonflight with a detour of the Earth torsion should decrease the fuel consumption on 25%.

At present, most interplanetary cosmic apparatus get accelerations which can not be explained on the basis of cosmic calculations in the relativity theory of Einstein. Particularly, deviations have been found for the apparatus of «Galileo», «Rosetta» and «Cassini». The suggested model of vortex gravitation (formula 26) shows that, if the trajectory of the satellite flight does not coincide with the Sun gravitation torsion plane, then one should take into account the value of gravitation coefficient in the calculation of solar gravity acting onto the satellites. This coefficient (Cos3 A) reduces the value of solar gravity, which gives a certain acceleration to cosmic satellites and results in a deviation of the motion trajectory.

g) Causes of Ebbs And Flows

It is known that the appearance of the sea ebbs and flows twice in 24 hours and 50 minutes is explained by the influence of the gravitation fields of the Moon and Sun and by the centrifugal forces (Galileo, Descartes, Newton and others).

Since the Moon and Sun are in zenith under one Earth surface point only once a day (or in 24 hours 50 min.), they could not have an equal influence upon this point by means of their gravitation twice a day.

The model of vortex gravitation gives a new explanation of this phenomenon, which consists in the following.On the basis of the vortex gravitation, the form of the Earth gravitation torsion is discoid and plane-symmetrical. Its direction mainly coincides with the Moon orbit plane which is inclined to the ecliptic on 5 degrees and 9 min. Meanwhile, the Earth equator plane has the inclination to the ecliptic of 23.7 degree. The compression coefficient of the Moon orbit, or the cosine of the inclination, is 0.9985. That is, the inclination of the Moon orbit to the Earth torsion is 3 degree and 6 min (Section3.4, formula (1)). A geometrical comparison of these inclinations evidences that each Earth surface point rotates with a considerable angle as related to the Earth gravitation torsion plane. Thus, one and the same point of the Earth surface every time intersects the gravitation torsion across its direction, or it first approaches to and then moves away from the torsion. The force of the vortex Earth gravitation, acting onto this point, changes in this case correspondingly (see Fig. 7).

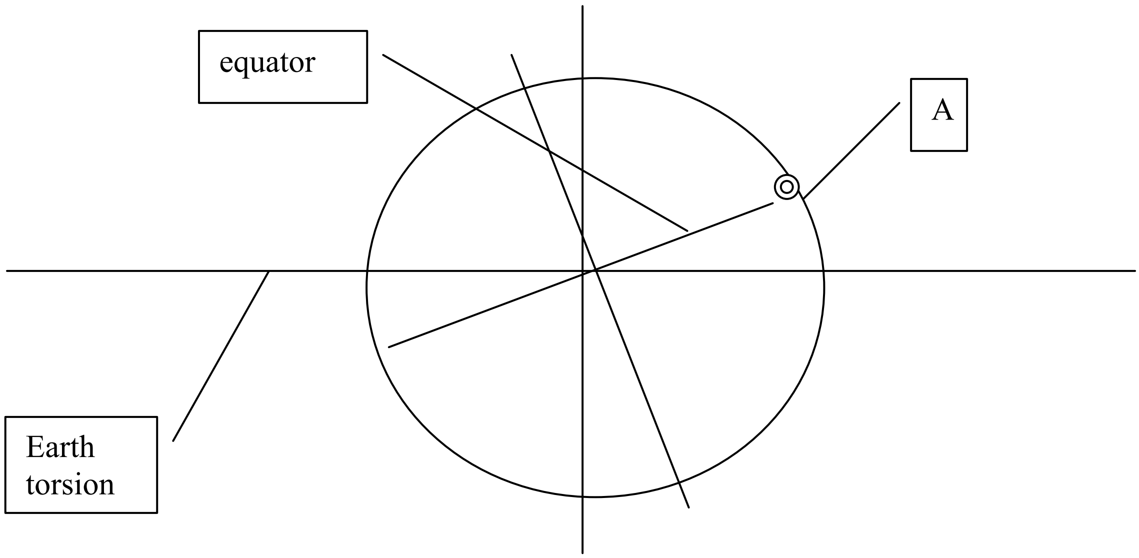

Fig.7 : Inclination of the Earth equator

Point A, at its daily motion around the Earth center, must twice intersect the Earth torsion central plane, and it must twice move away from it. Consequently, the Earth gravitation forces achieve their maximum influence on point A twice a day, and they achieve their minimum value also twice a day. This has a physical influence upon the Earth surface and the level of water in this point. This, in turn, accounts for the fact that the ebbs and flows occur in one point twice a day.

As was mentioned in Section 3.5, by geodetic gravimetry, it has been established that the Earth gravitation force on the poles has a 0.43% lower value as compared with the theoretical calculation. This confirms the above-noticed non-uniform gravitation force on the Earth surface.

As is known, the sun gravitation force on the Earth orbit is 0.06% of the gravitation force of our planet on its own surface. The Moon affects on the Earth surface with the attraction force of 0.0003% of the Earth gravitation force.

When comparing these values, it is obvious that the wave-like change of the Earth gravitation forces under the action of the own rotation occurs, at the Earth surface, with a much higher intensity than the same change of the Earth gravitation under the action of the gravitation of the Sun and Moon at their mutual rotation.

It should be noted that a permanent wave-like change of the gravitation field intensity in the Earth surface layers could be a noticeable catalyst for the tectonic motions of the earth's crust plates and seismicity increase.

Also, the cyclic change of the gravitation force in one point should be taken into account in precision investigation and productions in medicine and other areas of natural sciences, including the registration of sport records.

h) Magnetic Pole of The Earth

On the basis of the vortex gravitation, one can suppose that the magnetic field of the Earth is due to the rotation of the Earth ether torsion, and it is not due to the merely Earth rotation itself.

Because the Earth rotation axis (**$O_З$** , Fig. 7) is inclined to the Earth torsion rotation axis (**$O_О$**) on the angle of ~ 20 grades, one can arrive at a conclusion that the Earth surface intersects the Earth torsion and magnetic field axis in latitude of ~ 70 grade. Taking into account the Earth rotation, it is obvious that the Earth magnetic poles accomplish the daily revolution around the geographic poles in the same latitudes (70 degree). The attitudes of the magnetic poles depend on the time of day.

This accounts for the convergence of magnetic and geographic poles and the instability of the Earth electromagnetic orientation.

i) Tungus Meteorite

The fall of the meteorite in 1908 near the river of Tungus in Siberia has put a number of questions, and some of them are not decided so far. Particularly, neither a shell-hole nor traces of the meteorite substance have been found, which contradicts to physics laws.

The model of vortex gravitation allows an analytical explanation of this paradox.

It is supposed that the Tungus meteorite was a new-created torsion-satellite of the Earth torsion which formed almost in the center of the front (peripheral) region of the Earth torsion. This is supported by the value of the Tungus latitude (60 degree), while the Earth torsion axis latitude is 70 degree (see Section 3.9). Therefore, this torsion-satellite formed in the periphery

Global Journal of Science Frontier Research (A) Volume XII Issue I Version I January 2012

region with a deviation of ~ 10 degree from the Earth torsion rotation axis. In this region, the vortex gravitation force is considerably higher than that in the more distant periphery regions (i.e. regions farthest from the Earth torsion axis). In accordance with the predominance of the gravitation forces under the centrifugal ones, the tungus torsion (after its appearance) did not form as a perpetual satellite of the Earth, but it directed toward the Earth center. This torsion had not time to accumulate the cosmic substance and was in the state of a Black Hole or a pulsar. During collision with the Earth surface, the commonly-known colossal explosion occurred without an emission of the meteorite substance, which the tungus torsion did not contain (and even if it would contain, the quantity of this substance was negligible; and also this substance represented micro-particles like nucleons). The flow of micro-particles of such sizes could not create any visual traces on the Earth surface and hence it was not found. The damage traces in the fall place were produced only by sadden ultra-low pressure release into the atmosphere which caused a destructive air wave running few times around the Earth.

j) Expansion or Compression of the Universe?!

At present, the moving of galaxies away from each other is accounted for by the expansion of the Universe which began due to the so-called "Big Bang".
For the analysis of the galaxies' moving away, we use the following known physical properties and laws:

1. The galaxies revolve round the center of the metagalaxy making one turn per 100 trillion years [4]. 1. Therefore, the metagalaxy is a giant torsion where the laws of vortex gravitation and classical mechanics are valid (Section 3.2).
2. Because Earth increases its mass **[1],** one may assume that all the other celestial objects and their systems (galaxies) also increase the masses under the action of their own gravitation in accordance with the laws presented in Section 3.2. In this case, on the basis of the formulas of this section, it is evident that the galaxies must move by a spiral toward the metagalaxy center with an acceleration which should be inversely proportional to the distance from the metagalaxy center or to the galaxy mass increase.

The radial acceleration of the galaxies during their motion toward the metagalaxy center results in their mutual moving away from each other, which has been indicated by Hubble, and which, by now, is mistakenly treated as the expansion of the Universe.

Thus, the following conclusion can be made from the above-said :

- **The Universe does not expand, but, on the contrary, twists by a spiral or contracts**.

It is quite probably that a metagalaxy Black Hole is situated in the center of the metagalaxy, and it is impossible therefore to observe it.

At the circulation of the galaxies around the metagalaxy center on a lower orbit, the orbital motion speed of these galaxies must be higher than that of the galaxies moving on a higher orbit. In this case, the galaxies must close together in certain time mega-intervals. This explains the approaching of the galaxy **M31**.

In the initial stage of the cosmic torsion appearance, it should be in the state of BH (see Section 3.1). In this period, the increase of the cosmic torsion relative mass is maximal. Therefore, the magnitude and vector of the velocity of this torsion (BH) also possess maximum changes. That is, the character of motion of the Black Holes does not correspond to the motion of neighbor cosmic objects.

At present, the BH approaching to us has been found. The motion of this BH is explained by the above-discussed dependence.

At considerable inclinations of the celestial object orbits to the plane of the corresponding torsion, an increase of the orbit radii of these objects or their systems can occur, or the stationary value of the radius will be conserved.

One should note **the contradictions of the hypothesis of "Big Bang"**, which, by incomprehensible reasons, are not taken into account by modern science:

- according to the 2nd law of thermodynamics, a system (Universe) being left to itself (after the explosion), turns into a chaos and disorder.

In reality, the harmony and order observed in the Universe contradict this law.

- any particle of the substance exploded with a huge intensity will acquire only straight radial direction of motion.

Universal rotation of all the celestial objects and their systems in the space around the center or another object, including the metagalaxy, completely refutes the inertial nature of the motion of cosmic objects, obtained from the explosion.

- according to the existing models (model of Fridman), the cause of the Big Bang was the compression of the Universe down to the size of the solar system. As the result of this super-giant densification of the cosmic substance, the Big Bang occurred.

The followers of the idea of Big Bang pass over the absurdity of this hypothesis in silence, viz. – how could the **infinite** Universe be compressed and go into a **limited** volume of the size of the solar system!?

k) Vortex Cosmogony

It is obvious from the model of vortex gravitation that the main source of the origin and motion of celestial objects in the Universe is the vortex rotation of the cosmic ether which creates the vortex gravitation. The latter, in turn, at the moment of its appearance, gives a unique property to the torsion, namely – the ability to draw in any cosmic dust, which forms a celestial object at certain stages of the existence of this torsion.

Principal scheme of vortex cosmogony.

Since it was shown in Section 3.2 that all the cosmic torsions and (or) celestial objects-satellites move by a spiral toward the parent torsion center, it is straightforward to arrive at the following conclusion:

- all the torsion-satellites were created in periphery sides of the parent torsions.

The parent torsion formed in the periphery of the grand-parent torsion of a higher order, etc.

Formation of torsion-satellites in the periphery of a parent torsion is accounted for by the fact that the ether vortex rotation weakens significantly in these layers of a parent torsion, and, in addition, the intersection of ether flows from two or more neighbor parent torsions are feasible there. These circumstances, on the basis of the hydro- aerodynamics laws, provide favorable conditions for the turbulence arising and, hence, for the appearance of local vortexes.

Thus, the following scheme of the celestial objects and torsions creation can be proposed:
- satellite torsions formed in the periphery of planet torsions; planet torsions formed in the periphery of star torsions; star torsions - in the periphery of galaxy torsions; the latter – in the periphery of metagalaxy torsions. This sequence may represent a very long, probably infinite, row.

*Therefore, **the Universe is a system of interrelated plane cosmic vortexes**.*

Initial orbital motion of any celestial object or their systems was caused by the ether orbital motion in a certain cosmic torsion, taking into account a possible tearing off of a local torsion from a periphery orbital massive of the ether and sharp braking of this torsion at the first moments of its existence due to the mass increase of this torsion. If the new-acquired orbital motion of the torsion produced the centrifugal force, which balanced the vortex gravitation force acting onto the local torsion, then this torsion should turn into a satellite of the parent torsion. Farther, the orbital motion of this cosmic object changed its characteristics in accordance with the laws presented in Section 3.2.

If the orbital speed of the satellite gets lower values, then the forces of the vortex gravitation should exceed the centrifugal forces, and this local torsion rushes toward the parent torsion center and finishes there its existence. If the orbital motion of the local torsion get a momentum with a high speed, then the centrifugal forces acting onto this torsion exceeds the gravitation forces, and this torsion must tear off from the parent torsion gravitation field and disappear in the cosmic space as a meteorite, asteroid, comet, etc.

A newly-formed celestial object must permanently decrease the rotation velocity proportionally to the mass increase on the basis of the rotation angular momentum conservation law.

The proposed principle of formation of torsion-satellites in the joint of two parent torsions allows explanation of the appearance of small planets – asteroids, comets; revolving of Venus in the direction opposite to that for other planets; revolving of some satellites in the direction opposite to that for the planets; considerable difference in the rotation speeds of Venus and its atmosphere; and other astronomy facts.

l) Beginnings of Substance

In modern astrophysics, the origin of elementary particles is explained by thermonuclear reactions occurring in the star cores. That is, in the concluding stage of evolution, the star becomes unstable. Weakening nuclear reactions can not support inside the star such values of temperature and pressure which would ensure the stability of the enormous star mass. As the result, the gravitation, losing the control, causes the immediate compression (collapse) of the star. A giant ejection of energy as neutrino and impact waves, originating from the star interior, really blows away the outer star layers to the environment space, scattering heavy elements all over the galaxy. Such an ejection is usually called as nova outburst. Each nova outburst enriches the galaxy by negligibly small (trace) quantities of elements necessary for formation of the planets such as Earth, and further, for the origin and evolution of life in all the forms populating the Earth.

It is obvious that the principle of beginnings of substance described above has an unconvincing character, because it treats the appearance of substance (in cosmic space) from substance (star cores).

From the viewpoint of vortex gravitation and cosmogony, the possibility appears to explain the origin of any material particle using other properties of matter presented in this article.

That is, in the peripheries of cosmic torsions, there exists a possibility of the origin of torsions of any volume, not only those of large celestial objects. Particularly, these could be the torsions of a size of nucleons, electrons, atoms, and other elementary particles. The number of these micro-torsions in the Universe can be infinite. Created in unlimited quantities, elementary particles in these micro-torsions serve as "bricks" of the tangible matter. In turn, the ether particles – amers – can be a "material" for creation of the elementary particles.

m) Relation Between Rotation Speed And Mass

On the basis of the principle of vortex cosmogony (Section 3.8), it is obvious that the rotation of a celestial object around its axis was resulted from the rotation of a corresponding ether torsion. Therefore, the higher is the cosmic torsion rotation speed, the higher is the speed of the celestial object created in the center of this torsion.

On the other hand, it is evident from formula 10 that the torsion rotation speed determines the gravitation

Global Journal of Science Frontier Research (A) Volume XII Issue I Version I January 2012

force in this torsion. The higher is the gravitation force, the higher is the degree of "sucking in" of the cosmic dust by this torsion and the greater should be the mass of the object created in the torsion center.

Consequently, comparing these qualities, one can see that ***the mass of a celestial object should be directly proportional to the speed of rotation of this object around its axis.***

Besides, the number of local torsions, in which satellites are created, also depends on the value of the parent torsion gravitation force.

The above-indicated analytical interrelations between the planet masses and the number of satellites are confirmed by all the astronomy catalogues. It is known that the biggest and the "fastest" planet in the solar system is Jupiter. Saturn yields only to Jupiter in its rotation speed and mass. The order of magnitude of the masses of other planets also corresponds to the order of magnitude of the speeds of rotation around theirs axes.

It should be noted that Venus has a low rotation speed and a mass commensurate with that of Earth. This discrepancy with the above-said is explained by the fact that the planet masses are proportional not only to the ether pressure gradient and torsion rotation speed, but also they are proportional to the time of existence of this planet (torsion). That is, it is quite probable that Venus has weak gravitation force (which is confirmed by the absence of satellites), but it has a rather long term of existence, during which its rotation speed reduced in accordance with the angular momentum conservation law; this term was sufficient to accumulate the present volume. This suggestion proves additionally the fact that the Venus orbit plane coincides with the sun torsion central plane (Section 3.3). Consequently, the Venus torsion was formed on the outer, the very distant, periphery of the sun torsion, and not on a lateral one; further it moved by a spiral through all the sun torsion. Hence, Venus is the very old planet.

The insignificant speed of rotation of the Sun is also explained by the term of existence of this star which essentially exceeds the term of existence of the planets (see Section 3.7).

Therefore, the galaxies rotate around their axes with a speed which is less than that of the star rotation by several orders of magnitude.

n) Masses of Celestial Objects

Modern methods of calculation of masses of the planets and Sun are based on the Newton law, implying that the substance mass of a celestial body is directly proportional to the gravitation force directed to this body. Knowing the gravitation force and the body volume, researchers deduce the mass of the object from these data.

According to the actual reference catalogues, some celestial objects have the following densities, which are rather doubtful:

Sun – 1.4 ton/cub. m.

Earth – 5.5 - / -

Saturn – 0.7 - / -

As was shown above, the model of vortex gravitation excludes a direct dependence of the gravitation force on the object mass. Therefore, the densities and masses used today by astrophysicists have incorrect values, underestimated by an order of magnitude.

On the basis of the model of vortex gravitation, the possibility appears to determine the planet masses using other physical laws, particularly, the angular momentum conservation law. That is, comparing the rotation speed of ether with that of the celestial object (in one torsion), one can determine the mass increase as an inversely proportional dependence of the rotation speed reduction for the celestial object in the torsion center in comparison with the ether rotation speed. Such a calculation scheme is valid provided that the ether rotation braking is small and one may neglect this value.

On the basis of this principle, the following densities are obtained:

Sun – 30 ton/cub. m.

Earth - 23 ton/cub. m.

Mass of Earth – **2.5 x 10 ^{25} kg.**

o) Age of Celestial Objects

Modern theories of interior structure of celestial bodies, as well as planetary cosmogony, as an initial experimental basis for the estimation of the age of celestial objects, use the results of investigation of the age of mining rocks, sun neutrino, and other data obtained at studying the outer layer of the celestial object.

Since, on the basis of the model of vortex cosmogony, the celestial objects were created by means of accumulation of cosmic matter, one can arrive at a conclusion that any inner layer should have its own age exceeding the age of the outer layer of this planet or star. Therefore, it is impossible to estimate the age of the interior substance or that of the celestial object on the whole from the data of study of outer rocks or any radiations from these rocks.

On the basis of vortex gravitation and creation of celestial objects, it is permissible to determine the age of planets by a mere division of the planet mass by a corresponding annual increase of the mass of this planet.

Taking into account the above-said, the following ages were obtained:

- Earth – 15.6 milliard years.

p) Dark Matter

It is known that in the middle last century, during the study of the galaxy structure, a discrepancy between the star distribution and the gravitation potential distribution has been found.

Scientific opinion has divided into two groups.

Some scientists state that the Newtonian theory of gravitation, developed on the basis of observation of planets in solar system, is not valid in larger astronomical scales.

Most researchers agree that part of matter (30%) does not emit photons, and therefore it is invisible. However, just this matter balances the gravitation potential in the galaxy. This invisible matter was called dark matter.

Obviously, in the theory of vortex gravitation, there are no difficulties in the explanation of this astronomy "paradox", because the world gravitation force does not depend on the masses of stars, but it only depends on the vortex rotation speed and the galaxy ether pressure gradient. The value of vortex gravitation in any point can be determined as described in Section 2. The obtained value of vortex gravitation completely balances the centrifugal forces of stars, and therefore there is no need to use that hypothetical dark matter.

The above-discussed discrepancy of the masses of celestial objects with the gravitation, not only in the galaxies, but in the solar system too (see Section 4), additionally demonstrates the invalidity of the Newton's theory.

q) Earth Evolution

On the basis of vortex cosmogony, it is possible to reconstruct the physical state of our planet in the past. Using the formulas from Section 3.2, one determines that 1 milliard year ago, the planet of Earth had the following properties as compared to the present:

- the mass was 6% less,
- the radius of Earth was 2% less
- the day duration – 22.5 hours
- the vortex gravitation force was 4% higher, centrifugal forces were 13% higher, and therefore all the bodies were 9% lighter.

It should be noted that these properties directly affected on minerals, atmosphere, flora and fauna of that time. This is of high importance for researchers in various fields of natural history. Particularly, a weaker gravity mainly accounts for the existence of giant plants and animals that time.

The rotation speed of Earth round its axis must decrease, and hence a day must lengthen by $\mathbf{0.55 \times 10^{-5}}$ **sec a year**.

Galileo was the first who had observed in 1695 the Earth rotation slowing down. From his observations, this slowing down was $\mathbf{2 \times 10^{-5}}$ **sec a year**. Sixty years later, Kant has explained this effect by a flow friction.

On the basis of the above-presented calculations, the Earth rotation slowing differs insignificantly from the results of astronomy observations of Galileo. The divergence in the results is accounted for by an error in the Earth mass determination [1] and its annual increase, as well as by the accuracy of astronomy observations.

It is to be noted that, on the basis of vortex cosmogony, the Earth rotation slowing down has an explanation which differs absolutely from the hypothesis of Kant.

IV. Conclusion

It is obvious that the above-presented principles of vortex gravitation and cosmogony are based on commonly-accepted basic physical laws.

On the other hand, the classical law of universal gravitation is based on merely the evident equality of centrifugal forces Fc and gravitation forces Fg. Further calculations to support this are connected with simple mathematical transformations:

- the proportionality $\mathbf{V \sim R^{-2}}$ is substituted into the equation $\mathbf{Fg = Fc = mv^2 / R}$ from the 3rd Kepler's law whence it is obtained that $\mathbf{Fg \sim m / R^2}$

In order to turn this ratio into a formula, I. Newton had advanced a hypothesis stating that all the bodies possessed the gravity with a force proportional to their masses. These masses were "prescribed" by a method of selection, and the gravitation constant was "introduced" in order that these masses were correct; it turned out to be necessary to give an absurd unity to this constant – $\mathbf{N\ m^2 / kg^2}$

It is known that Newton himself was not sure in gravitation properties of physical bodies, and later he has suggested that the cosmic substance (ether) density change might be the cause of gravitation. However, no argumentation of the decrease of this density was presented so far. Huygens was known to call the Newton's hypothesis of gravitation properties of the bodies to be ridiculous.

In the theory of relativity, A. Einstein has grounded his more precise calculations on determination of the gravitation forces on the basic principles of I. Newton, i.e. on the central-symmetrical action of the gravity forces and on the gravitation properties of celestial objects.

According to the Newton equation, the gravitation forces from any celestial object stretch over infinite distances, and, since the number of these objects is also infinite, classical theories of gravitation encounter a paradox called the Seliger paradox. That is, under these conditions, all the world space would be filled by infinite gravitation forces.

The model of vortex gravitation removes this paradox, because the action of gravitation is limited by the size of the torsion.

Also, on the basis of the above-discussed classical theories, it is impossible to understand the cause of creation and motion of celestial objects.

It is known that there exists the discordance in modern science concerning the speed of gravitation. From the classical physics, the speed of gravitation is infinite. According to the relativistic ideas, the speed of gravitation is equal to the speed of light. On the basis of vortex cosmology, the gravitation is obviously an inalienable property of any torsion. Therefore, the speed of gravitation corresponds to the speed of the appearance of a cosmic torsion.

It should be noted that many researchers advanced, and still continue to advance, the hypothesis on gravitation properties of the ether. However, up to date, nobody yet proposed a physical and mathematical ground of the interconnection of the ether motion with the change of its density, and the method for its calculation as well.

. . .

The author thanks Dr. A. A. Velichko for his help with mathematical calculations in Section 2.

References Références Referencias

1. V A Atsurovskiy. *General ether-dynamics*. Energoatomizdat. Moscow, Russia. 1990. Page 278.
2. L V Kiknadze, Yu G Mamaladze. *Classical hydrodynamics for physicists-experimentalists.* Tbilisi University Press. Tbilisi, Georgia. 1979. Page 136.
3. A P Babichev, N. A. Babushkina et al. *Physical constants Handbook*. Energoatomizdat. Moscow, Russia.1991. Page 1232.
4. C K Kadyrov. *Physical Theory of Unified Field*. Kyrgyz zer. Bishkek, Kyrgyzstan. 2001. Page 33.
5. A P Gulyaev. *Astronomy calendar*. Cosmosinform. Moscow, Russia. 1993. Page 285.

Global Journal of Science Frontier Research
Physics & Space Science
Volume 12 Issue 1 Version 1.0 January 2012
Type : Double Blind Peer Reviewed International Research Journal
Publisher: Global Journals Inc. (USA)
Online ISSN: 2249-4626 & Print ISSN: 0975-5896

Deformation due to various sources in micropolar elastic solid with voids under inviscid liquid half space

By Rajneesh Kumar, K.D.Sharma, S.K.Garg
Kurukshetra University Kurukshetra, Kurukshetra

Abstract - The present investigation deals with the deformation of a micropolar elastic solid with void overlying a semi-infinite inviscid fluid subjected at the plane interface due to various sources. Laplace and Fourier transform techniques have been used to solve the problem. The expressions of the displacement components, stress, couple stress and change in volume fraction field are obtained in the transformed domain. As an application of the approach (i) concentrated force (ii) uniformly distributed force (iii) linearly distributed force (iv) moving couple have been taken to illustrate the utility of the approach. A particular case of interest have been deduced from the investigation.

GJSFR-A Classification : FOR Code: 010599

DEFORMATION DUE TO VARIOUS SOURCES IN MICROPOLAR ELASTIC SOLID WITH VOIDS UNDER INVISCID LIQUID HALF SPACE

Strictly as per the compliance and regulations of :

Deformation due to various sources in micropolar elastic solid with voids under inviscid liquid half space

Rajneesh Kumar[α], K.D.Sharma[Ω], S.K.Garg[β]

Abstract - The present investigation deals with the deformation of a micropolar elastic solid with void overlying a semi-infinite inviscid fluid subjected at the plane interface due to various sources . Laplace and Fourier transform techniques have been used to solve the problem. The expressions of the displacement components, stress, couple stress and change in volume fraction field are obtained in the transformed domain. As an application of the approach (i) concentrated force (ii) uniformly distributed force (iii) linearly distributed force (iv) moving couple have been taken to illustrate the utility of the approach. A particular case of interest have been deduced from the investigation.

I. Introduction

A non-linear theory concerning solid elastic materials consisting of various pores (voids) distributed throughout the body has been formulated by Nunziato and Cowin (1979). Later, Cowin and Nunziato (1983) developed a theory of linear elastic materials with voids, for the mathematical study of the mechanical behavior of porous solids. They introduced the presence of pores in the classical continuum model by assigning an additional degree of freedom to each material particle, namely fraction of elementary volume which results void of matter; consequently, the bulk mass density of such materials is given by the product of two fields, the void volume fraction and the mass density of matrix material.

Classical mechanics deals with the basic assumption that the effect of the microstructure of a material is not essential for describing mechanical behavior. Such an approximation has been shown in many well-known cases. Often, however, discrepancies between the classical theory and experiments are observed, indicating that the microstructures might be important. For example, discrepancies have been found in the stress concentrations in the areas of holes, notches and cracks; elastic vibrations characterized by a high frequency and small wavelengths, particularly in granular composites consisting of stiff inclusions embedded in a weaker matrix, fibers or grains; and the mechanical behavior of complex fluids such as liquid crystals, polymeric suspensions, and animal blood. In general, granular composites, for example, porous materials are widely used in the area of passive noise control as sound absorbers and the aspect of acoustical waves characterized by high frequencies and small wavelengths become significant.

To explain the fundamental departure of microcontinuum theories from classical continuum theories, the formal is continuum model embedded with microstructures to describe the microscopic motion or a non local model to describe the long range material interaction. This extends the application of the continuum model to microscopic space and short time scales. Micromorphic Theory (Eringen and Suhubi, 1964; Eringen, 1999) treats a material body as continuous collection of a large number of deformable particles, with each particle possessing finite size and inner structure. Using assumptions such as infinitesimal deformation and slow motion, micromorphic theory can be reduced to Mindlin's Microstructure Theory (1964) . When the microstructure of the material is considered rigid, it becomes the micropolar theory (Eringen, 1966) . Eringen's micropolar theory is more appropriate for geological materials like rocks, soils, since their theory takes into account the intrinsic rotation and predicts the behavior of the material with inner structure.

Different researchers has discussed different type of problems in micropolar elasticity with voids. Scarpetta (1990), Marin (1996-a, 1996-b) , discussed some problems in micropolar theory of elastic solids with voids. Passarella (1996) derived the constitutive relations and field equations for anisotropic micropolar porous theomoelastic materials and also derived some basic results.

Mondal and Acharya (2006) studied the effect of voids on the propagation of surface waves in a homogeneous micropolar elastic solids medium which contains distribution of vacuous pores, Kumar, Deswal and Tomar (2002) , discussed the surface wave propagation in micropolar liquid saturated porous layer over a micropolar liquid saturated porous half space of different elastic properties. Kumar and Deswal (2000) studied the propagation of surface waves in a micropolar liquid saturated porous solids line under a uniform layer of liquid.

Author α : Department of Mathematics, Kurukshetra University Kurukshetra, Kurukshetra. E-mail : Rajneesh_kuk@rediffmail.com
Author Ω : Department of Mathematics, Swami Devi Dyal Institute of Engineering &Technology, Barwala .
E-mail : kd_sharma33@rediffmail.com
Author β : Department of Mathematics, Deenbandhu Chhotu Ram University, Murthal (Sonipat). E-mail : skg1958@gmail.com

Kumar and Ailawalia (2007) studied the interaction in a micropolar thermoelastic medium with voids due to distributed loads. Kumar and Ailawalia (2009) studied the influence of various sources in micropolar thermoelastic medium with voids. Kumar and Kumar (2009) studied the analysis of waves motion in transversely isotropic medium with voids under a inviscid liquid layer.

Ghiba (2008) studied the asymptotic partition of energy in the micropolar mixture theory of porous media. Huang and Zhao (2009) developed a mixture theory for multicomponent micropolar porous media with a combination of the hybrid mixture theory and the microcontinuum theory. Madeo and Gavrilyuk (2010) studied the propagation of acoustic waves in porous media and their reflection and transmission at a pure-fluid/porous-medium permeable interface. Tomar and Khurana (2011) investigated the reflection and transmission phenomena of plane longitudinal wave from a plane interface between two distinct micropolar porous elastic solid half space in welded contact. Kumar and Kumar (2011) studied the wave propagation in transversely isotropic generalized thermoelastic half space with voids under initial stress and discusses the reflection characteristics of these waves under consideration of stress free, thermally insulated or isothermal boundary conditions. Kumar and Kumar (2011) studied the wave propagation in orthotropic generalized thermoelastic half space with voids under initial stress.

In this paper the deformation due to various sources in micropolar elastic with void overlying a semi-infinite invicsid fluid is studied. The expressions for components of displacement , stress and acoustic pressure are obtained by using Laplace and Fourier Transforms due to concentrated force, uniformly distributed force, linearly distributed force and moving couple .

II. Basic Equations

Following Eringen (1968) and Iesan (1985) the equations of motion and constitutive relations in a homogenous isotropic micropolar material with voids are given by:

$$(\lambda+2\mu+K)\nabla\left(\nabla.\vec{u}\right)-(\mu+K)\nabla\times\nabla\times\vec{u}+K\left(\nabla X\vec{\phi}\right)+\xi\nabla\psi=\rho\frac{\partial^2\vec{u}}{\partial t^2}\ , \tag{1}$$

$$(\alpha+\beta+\gamma)\nabla\left(\nabla.\vec{\phi}\right)-\gamma\nabla\times\left(\nabla\times\vec{\phi}\right)+K\left(\nabla\times\vec{u}\right)-2K\vec{\phi}=\rho j\frac{\partial^2\vec{\phi}}{\partial t^2}\ , \tag{2}$$

$$d\nabla^2\psi-\xi\nabla.\vec{u}-\omega_1^*\frac{\partial\vec{\psi}}{\partial t}-a\psi=\rho\chi\frac{\partial^2\psi}{\partial t^2}\ , \tag{3}$$

$$t_{ij}=\lambda\delta_{ij}u_{r,r}+\mu\left(u_{i,j}+u_{j,i}\right)+K\left(u_{j,i}-\in_{ijk}\phi_k\right)+\xi\psi\delta_{ij}\ , \tag{4}$$

$$m_{ij}=\alpha\phi_{r,r}\delta_{ij}+\beta\phi_{i,j}+\gamma\phi_{j,i}+\varsigma\psi\delta_{ij}\ , \tag{5}$$

where the list of symbols is given at the end of the paper.

III. Problem Formulation

We consider a homogeneous isotropic micropolar elastic half space with void (medium M1) and underlying a uniform homogeneous inviscid liquid(medium M2). We take the rectangular coordinate system $(Ox_1x_2x_3)$ with origin at the interface of M1and M2 and X_3 - axis is pointing normally into the medium M1.

We restrict our analysis to the plane deformation parallel to x_1x_3 plane with displacement vector $\vec{u}$ and microrotation vector $\vec{\phi}$. For two-dimensional problem, we take

$$\vec{u}=(u_1,0,u_3)\ ,\quad \vec{\phi}=(0,\phi_2,0) \tag{6}$$

We introduce the non-dimensional quantities defined by the expressions

$$x_1' = \frac{\omega^*}{c_1}x_1, \quad x_3' = \frac{\omega^*}{c_1}x_3, \quad u_1' = \frac{\omega^*}{c_1}u_1, \quad u_3' = \frac{\omega^*}{c_1}u_3, \quad \phi'_2 = \left(\frac{\rho c_1^2}{k}\right)\phi_2$$

$$\psi' = \left(\frac{\rho c_1^2}{k}\right)\psi, \quad \phi'^f = \frac{\omega^*}{c_1^2}\phi^f, \quad t'_{31} = \frac{t_{31}}{\mu}, \quad t'_{33} = \frac{t_{33}}{\mu}, \quad m'_{32} = \frac{m_{32}}{\mu}\frac{\omega^*}{c_1}$$

$$t' = \omega^* t, \quad \omega^{*2} = \frac{k}{\rho j}, \quad \bar{u}^{f'} = \frac{\omega^* \bar{u}^f}{c_1}, \quad p' = \frac{p}{\lambda^f} \tag{7}$$

Equations (1) - (3) with the aid of (6) and (7) after suppressing the primes, yield

$$a_1\frac{\partial e}{\partial x_1} + a_2\nabla^2 u_1 - a_3\frac{\partial \phi_2}{\partial x_3} + a_4\frac{\partial \psi}{\partial x_1} = \frac{\partial^2 u_1}{\partial t^2}, \tag{8}$$

$$a_1\frac{\partial e}{\partial x_3} + a_2\nabla^2 u_3 + a_3\frac{\partial \phi_2}{\partial x_1} + a_4\frac{\partial \psi}{\partial x_3} = \frac{\partial^2 u_3}{\partial t^2}, \tag{9}$$

$$a_5\nabla^2\phi_2 + a_6\left(\frac{\partial u_1}{\partial x_3} - \frac{\partial u_3}{\partial x_1}\right) - 2a_7\phi_2 = \frac{\partial^2 \phi_2}{\partial t^2}, \tag{10}$$

$$a_8\left(\frac{\partial^2 \psi}{\partial x_1^2} + \frac{\partial^2 \psi}{\partial x_3^2}\right) - a_9 e - a_{10}\frac{\partial \psi}{\partial t} - a_{11}\psi = \frac{\partial^2 \psi}{\partial t^2}, \tag{11}$$

where

$$a_1 = \frac{\lambda+\mu}{\rho c_1^2}, a_2 = \frac{k+\mu}{\rho c_1^2}, a_3 = \frac{k^2}{\rho^2 c_1^4}, a_4 = \frac{\xi k}{\rho^2 c_1^4}, a_5 = \frac{\gamma}{\rho j c_1^2}, a_6 = \frac{c_1^2}{j\omega^{\bullet 2}},$$
$$a_7 = \frac{k}{\rho j\omega^{\bullet 2}}, a_8 = \frac{d}{\chi\rho c_1^2}, a_9 = \frac{\xi c_1^2}{\chi k\omega^{\bullet 2}}, a_{10} = \frac{\omega_1^*}{\chi\rho\omega^{\bullet}}, a_{11} = \frac{a}{\chi\rho\omega^{\bullet 2}}, \tag{12}$$

The displacement components u_1 and u_3 are related to the potential functions as,

$$u_1 = \frac{\partial \Phi}{\partial x_1} - \frac{\partial \Psi}{\partial x_3}, \quad u_3 = \frac{\partial \Phi}{\partial x_3} + \frac{\partial \Psi}{\partial x_1}, \tag{13}$$

Substituting the values of u_1 and u_3 from equation (13) in the equations (8)-(11), we obtain,

$$\nabla^2\Phi + a_4\psi - \frac{\partial^2 \Phi}{\partial t^2} = 0, \tag{14}$$

$$a_2\nabla^2\Psi + a_3\phi_2 - \frac{\partial^2 \Psi}{\partial t^2} = 0, \tag{15}$$

$$a_5\nabla^2\phi_2 - a_6\nabla^2\Psi - 2a_7\phi_2 - \frac{\partial^2\phi_2}{\partial t^2} = 0 \,, \tag{16}$$

$$a_8\nabla^2\psi - a_9\nabla^2\Phi - a_{10}\frac{\partial\psi}{dt} - a_{11}\psi - \frac{\partial^2\psi}{dt^2} = 0 \,. \tag{17}$$

We define Laplace Transforms as

$$\bar{f}(x_1,x_3,s) = \int_0^\infty f(x_1,x_3,t)e^{-st}dt \tag{18}$$

and its inverse as

$$f(x_1,x_3,t) = \frac{1}{2\pi}\int_{x-i\infty}^{x+i\infty} f(x_1,x_{3,}s)e^{st}ds \tag{19}$$

Fourier Transforms as

$$\hat{\bar{f}}(\xi,x_3,s) = \int_{-\infty}^{\infty} \bar{f}(x_1,x_3,s)e^{-i\xi x_1}dx \tag{20}$$

and its inverse as

$$\bar{f}(x_1,x_3,s) = \frac{1}{2\pi i}\int_{-\infty}^{\infty} \hat{\bar{f}}(\xi,x_3,s)e^{i\xi x_1}d\xi \tag{21}$$

Applying Laplace and Fourier Transform defined by (18) and (20) on (14) - (17) and after simplification, we obtain,

$$\left(\frac{d^4}{dz^4} + A\frac{d^2}{dz^2} + B\right)\left(\hat{\bar{\Phi}},\hat{\bar{\psi}}\right) = 0 \,, \tag{22}$$

$$\left(\frac{d^4}{dz^4} + C\frac{d^2}{dz^2} + D\right)\left(\hat{\bar{\phi}}_2,\hat{\bar{\Psi}}\right) = 0 \,, \tag{23}$$

where

$$A = -\left[1 + b_7 s + b_8 + b_6 s^2 + (\xi^2 + s^2) + b_9\right]$$

$$B = (\xi^2 + s^2)\left[b_7 s + b_8 + b_6 s^2 + \xi^2\right] - b_9\xi^2$$

$$C = b_1 b_3 - 2(b_4 + \xi^2) - s^2(b_5 + b_2)$$

$$D = (b_2 s^2 + \xi^2)(b_5 s^2 + 2b_4 + \xi^2) - b_1 b_3 \xi^2$$

$$\hat{\bar{\psi}} = \left(\frac{s^2}{b_{14}\nabla^2 + a_4 - b_{15}s - b_{16} - s^2}\right)\hat{\bar{\Phi}}$$

$$\hat{\bar{\phi}}_2 = \left(\frac{s^2}{b_{10}\nabla^2 + a_3 - 2b_{11} - b_{12}s^2}\right)\hat{\bar{\Psi}} \tag{24}$$

The solution of equations (20) and (21) satisfying radiation conditions that $\hat{\Phi}, \hat{\psi}, \hat{\phi}_2, \hat{\Psi} \to 0$ as $x_3 \to \infty$ are

$$\hat{\Phi} = A_1 e^{-m_1 x_3} + A_2 e^{-m_2 x_3} \tag{25}$$

$$\hat{\psi} = A_1 d_1 e^{-m_1 x_3} + A_2 d_2 e^{-m_2 x_3} \tag{26}$$

$$\hat{\Psi} = B_1 e^{-m_3 x_3} + B_2 e^{-m_4 x_3} \tag{27}$$

$$\hat{\phi}_2 = B_1 d_3 e^{-m_3 x_3} + B_2 d_4 e^{-m_4 x_3} \tag{28}$$

where

$$d_1 = \left(\frac{s^2}{b_{14}(m_1^2 - \xi^2) + a_4 - b_{15}s - b_{16} - s^2} \right)$$

$$d_2 = \left(\frac{s^2}{b_{14}(m_2^2 - \xi^2) + a_4 - b_{15}s - b_{16} - s^2} \right)$$

$$d_3 = \left(\frac{s^2}{b_{10}(m_3^2 - \xi^2) + a_3 - 2b_{11} - b_{12}s^2} \right)$$

$$d_4 = \left(\frac{s^2}{b_{10}(m_4^2 - \xi^2) + a_3 - 2b_{11} - b_{12}s^2} \right)$$

Substituting the values of $\hat{\Phi}, \hat{\Psi}$ from (25) and (27) in (13) and with the aid of (18) and (20) yield the displacement components as

$$\hat{\tilde{u}}_1 = -i\xi\left(A_1 e^{-m_1 x_3} + A_2 e^{-m_2 x_3}\right) + \left(m_3 B_1 e^{-m_3 x_3} + m_4 B_2 e^{-m_4 x_3}\right) \tag{29}$$

$$\hat{\tilde{u}}_3 = -\left(m_1 A_1 e^{-m_1 x_3} + m_2 A_2 e^{-m_2 x_3}\right) - i\xi\left(B_1 e^{-m_3 x_3} + B_2 e^{-m_4 x_3}\right) \tag{30}$$

From equations (4)-(7), (13),(18),(20) and with the help of (25)-(28) , we obtain the components of stresses, couple stress as

$$\hat{\tilde{t}}_{33} = \left(f + g m_1^{\,2} + h d_1\right) A_1 e^{-m_1 x_3} + \left(f + g m_2^{\,2} + h d_2\right) A_2 e^{-m_2 x_3} + \left(f m_3 + i\xi g m_3\right) B_1 e^{-m_3 x_3} + \left(f m_4 + i\xi g m_4\right) B_2 e^{-m_4 x_3} \tag{31}$$

$$\hat{\tilde{t}}_{31} = K m_1 A_1 e^{-m_1 x_3} + K m_2 A_2 e^{-m_2 x_3} - \left(\xi^2 + b_{18} d_3 + b_{17} m_3^{\,2}\right) B_1 e^{-m_3 x_3} + \left(\xi^2 + b_{18} d_4 + b_{17} m_4^{\,2}\right) B_2 e^{-m_4 x_3} \tag{32}$$

$$\hat{\tilde{m}}_{32} = -b_{22}\left(m_3 d_3 B_1 e^{-m_3 x_3} + m_4 d_4 B_2 e^{-m_4 x_3}\right) \tag{33}$$

Following Achenbach (1973), the field equations in terms of velocity potential for inviscid fluid are given by

$$p = -\rho^f \frac{\partial \varphi^f}{\partial t} \tag{34}$$

$$\nabla^2\varphi^f = \frac{1}{\alpha^{f^2}}\frac{\partial^2\varphi^f}{\partial t^2} \tag{35}$$

$$u_3{}^f = \frac{\partial\varphi^f}{\partial x_3} \tag{36}$$

$$\vec{u}^{\,f} = \nabla\varphi^f \tag{37}$$

where ρ^f is the density, p is the acoustic pressure, $u_3{}^f\left(=\frac{\partial\varphi^f}{\partial x_3}\right)$ is the normal component of velocity $\vec{u}^{\,f}$.

Applying Laplace & Fourier Transform defined by (18) and (20) on (34)-(37) , we obtain

$$\hat{\bar{u}}_3{}^f = -m_5 D e^{-m_5 x_3}, \tag{38}$$

$$\hat{\bar{p}} = -b_{13} s e^{-m_5 x_3}. \tag{39}$$

where

$$m_5 = \sqrt{\xi^2 + \delta_1{}^2 s^2} \tag{40}$$

Boundary Conditions : At the surface $x_3 = 0$ are,

$$\begin{aligned}
&1)\quad t_{33} - p = -F_1(x,t)\ , \\
&2)\quad t_{31} = 0\ , \\
&3)\quad m_{32} = 0\ , \\
&4)\quad \frac{d\psi}{dx_3} = 0\ , \\
&5)\quad \dot{u}_3 = u_3^f\ ,
\end{aligned} \tag{41}$$

Where F(x,t) is the known function. Applying the Laplace and Fourier Transform defined by (18)-(21) on (34) and with the help of (29) to (34), we obtain the system of five non-homogeneous equations and after some calculations, we obtain the stress components and acoustic pressure as

$$\hat{\bar{t}}_{33} = \frac{1}{\Delta}\left(\Delta_{A_1} J e^{-m_1 x_3} + \Delta_{A_2} \mathrm{R} e^{-m_2 x_3} + \Delta_{B_1} V e^{-m_3 x_3} + \Delta_{B_2} U e^{-m_4 x_3}\right)\ , \tag{42}$$

$$\hat{\bar{t}}_{31} = \frac{1}{\Delta}\left(\Delta_{A_1} K m_1 e^{-m_1 x_3} + \Delta_{A_2} K m_2 e^{-m_2 x_3} - \Delta_{B_1} G e^{-m_3 x_3} - \Delta_{B_2} H e^{-m_4 x_3}\right)\ , \tag{43}$$

$$\hat{\bar{m}}_{32} = -\frac{b_{22}}{\Delta}\left(m_3 d_3 \Delta_{B_1} e^{-m_3 x_3} + m_4 d_4 \Delta_{B_2} e^{-m_4 x_3}\right)\ , \tag{44}$$

$$\hat{\bar{p}} = -\frac{b_{13} s}{\Delta}\left(\Delta_D e^{-m_5 x_3}\right)\ , \tag{45}$$

where

$$\Delta = \begin{vmatrix} J & R & V & U & L \\ Km_1 & Km_2 & G & H & 0 \\ 0 & 0 & -b_{22}m_3d_3 & -b_{22}m_4d_4 & 0 \\ m_1d_1 & m_2d_2 & 0 & 0 & 0 \\ m_1 & m_2 & i\xi & i\xi & -m_5 \end{vmatrix}$$

$$\Delta = m_4d_4(2GQ + GTR + YKVm_5 + i\xi Y) - m_3d_3(HQ + THR + YUKm_5) - S(G+H) \tag{46}$$

$$\Delta_{A_1} = \hat{\bar{F}}_1(\xi,s)m_5d_2m_2b_{22}(Gm_4d_4 - Hm_3d_3) \tag{47}$$

$$\Delta_{A_2} = \hat{\bar{F}}_1(\xi,s)m_5d_1m_1b_{22}(Gm_4d_4 - Hm_3d_3) \tag{48}$$

$$\Delta_{B_1} = \hat{\bar{F}}_1(\xi,s)m_5d_4m_4b_{22}Km_1m_2(d_2 - d_1) \tag{49}$$

$$\Delta_{B_2} = -\hat{\bar{F}}_1(\xi,s)m_5d_3m_3b_{22}Km_1m_2(d_2 - d_1) \tag{50}$$

$$\Delta_D = \hat{\bar{F}}_1(\xi,s)[b_{22}m_1m_2(d_1 - d_2)\{d_3m_3(H - Ki\xi) - d_4m_4(G - Ki\xi)\}] \tag{51}$$

Applying the Inverse Laplace and Fourier transform defined by (19) and (21) on (42)-(45) , we obtain the components of stress, normal velocity and pressure in the fluid as

$$t_{33} = \frac{1}{4\pi i}\int_{x-i\infty}^{x+i\infty}\int_{-\infty}^{\infty}\frac{1}{\Delta}\left(\Delta_{A_1}Je^{-m_1x_3} + \Delta_{A_2}\mathrm{R}e^{-m_2x_3} + \Delta_{B_1}Ve^{-m_3x_3} + \Delta_{B_2}Ue^{-m_4x_3}\right)e^{i\xi x}e^{st}\,d\xi ds \tag{52}$$

$$t_{31} = \frac{1}{4\pi i}\int_{x-i\infty}^{x+i\infty}\int_{-\infty}^{\infty}\frac{1}{\Delta}\left(\Delta_{A_1}Km_1e^{-m_1x_3} + \Delta_{A_2}Km_2e^{-m_2x_3} - \Delta_{B_1}Ge^{-m_3x_3} - \Delta_{B_2}He^{-m_4x_3}\right)e^{i\xi x}e^{st}\,d\xi ds \tag{53}$$

$$m_{32} = -\frac{1}{4\pi i}\int_{x-i\infty}^{x+i\infty}\int_{-\infty}^{\infty}\frac{b_{22}}{\Delta}\left(m_3d_3\Delta_{B_1}e^{-m_3x_3} + m_4d_4\Delta_{B_2}e^{-m_4x_3}\right)e^{i\xi x}e^{st}\,d\xi ds \tag{54}$$

$$p = -\frac{1}{4\pi i}\int_{x-i\infty}^{x+i\infty}\int_{-\infty}^{\infty}\frac{b_{13}s}{\Delta}\left(\Delta_D e^{-m_5x_3}\right)e^{i\xi x}e^{st}\,d\xi ds \tag{55}$$

IV. Particular Case

In the absence of voids effect $\xi, d, \chi, w_1^* \to 0$, the boundary conditions given by (41) reduce to

1) $t_{33} - p = -F_1(x,t)$
2) $t_{31} = 0$
3) $m_{32} = 0$ (56)
4) $u_3 = u_3^f$

and the components of stress and acoustic pressure reduces to

$$t_{33}=\frac{1}{4\pi i}\int_{x-i\infty}^{x+i\infty}\int_{-\infty}^{\infty}\frac{1}{\Delta}\left(\Delta_{A_1}Je^{-m_1x_3}+\Delta_{A_2}\,\mathrm{Re}^{-m_2x_3}+\Delta_{B_1}Ve^{-m_3x_3}+\Delta_{B_2}Ue^{-m_4x_3}\right)e^{i\xi x}e^{st}d\xi ds \tag{57}$$

$$t_{31}=\frac{1}{4\pi i}\int_{x-i\infty}^{x+i\infty}\int_{-\infty}^{\infty}\frac{1}{\Delta}\left(\Delta_{A_1}Km_1e^{-m_1x_3}+\Delta_{A_2}Km_2e^{-m_2x_3}-\Delta_{B_1}Ge^{-m_3x_3}-\Delta_{B_2}He^{-m_4x_3}\right)e^{i\xi x}e^{st}d\xi ds \tag{58}$$

$$m_{32}=\frac{1}{4\pi i}\int_{x-i\infty}^{x+i\infty}\int_{-\infty}^{\infty}\left(-\frac{b_{22}}{\Delta}\left(m_3d_3\Delta_{B_1}e^{-m_3x_3}+m_4d_4\Delta_{B_2}e^{-m_4x_3}\right)\right)e^{i\xi x}e^{st}d\xi ds \tag{59}$$

$$p=\frac{1}{4\pi i}\int_{x-i\infty}^{x+i\infty}\int_{-\infty}^{\infty}\left(-\frac{b_{13}s}{\Delta}\left(\Delta_De^{-m_5x_3}\right)\right)e^{i\xi x}e^{st}d\xi ds \tag{60}$$

where

$$\Delta=\begin{vmatrix} N & V & U & L \\ Km_1 & -G & -H & 0 \\ 0 & -b_{22}m_3d_3 & -b_{22}m_4d_4 & 0 \\ 0 & 0 & 0 & 0 \\ m_1 & i\xi & i\xi & -m_5 \end{vmatrix}$$

$$\begin{aligned}\Delta=&-m_3d_3b_{22}[m_5(m_1KU+NH)+b_{13}sm_1(H+Ki\xi)]+\\ &b_{22}m_4d_4[m_5(NG+KVm_1)+b_{13}sm_1(Ki\xi+G)]\end{aligned} \tag{61}$$

$$\Delta_{A_1}=\hat{\bar{F}}_1(\xi,s)m_5b_{22}(Gm_4d_4-Hm_3d_3) \tag{62}$$

$$\Delta_{B_1}=\hat{\bar{F}}_1(\xi,s)m_5m_1m_4d_4b_{22}K \tag{63}$$

$$\Delta_{B_2}=-\hat{\bar{F}}_1(\xi,s)m_5m_3m_1d_3b_{22}K \tag{64}$$

$$\Delta_D=\hat{\bar{F}}_1(\xi,s)[d_4m_4b_{22}m_1(Ki\xi+G)-d_3m_3b_{22}m_1(Ki\xi+H)] \tag{65}$$

V. Application

As an application of the approach, we consider the following cases.

Case I : Concentrated force

Here $F(x,t)=F(x)\delta(t)$

To determine stress components and pressure due to concentrated force described by Dirac delta function $F(x)=\delta(x)$ must be used with

$$\hat{\bar{F}}(\xi,s)=F \tag{66}$$

Case II : The solution due to uniformly distributed force over a strip of dimensionless width 2a applied on the liquid half is obtained by setting

$$F(x,t)=[H(x+a)-H(x-a)]\ \delta(t) \tag{67}$$

in equations (50) – (54).

Using (66) and then apply Laplace and Fourier transform defined by (18) and (20) on (67), we obtain

$$\hat{\bar{F}}(\xi,s)=\frac{2\sin(\xi a)}{\xi} \tag{68}$$

Case III : The solution due to linearly distributed force is obtained by using

$$\begin{aligned} F(x,t) &= \left[1-\frac{|x|}{a}\right]\delta(t) \quad ,if\,|x|\le a \\ &=0 \qquad ,if\,|x|>a \end{aligned} \tag{69}$$

Its Laplace and Fourier transform yield

$$\hat{\bar{F}}(\xi,s)=\frac{2(1-\cos\xi a)}{\xi^2 a} \tag{70}$$

Case IV : Moving couple:

The boundary condition for a couple with its axis parallel to x_2-axis and moving along x_1-axis with constant speed V are given by

$$F_1(x,t)=H(t)\frac{\partial}{\partial x_1}\delta(x_1-Vt) \tag{71}$$

and its Laplace and Fourier transforms yields,

$$\hat{\bar{F}}_1(\xi,s)=\frac{F_0(i\xi)}{(s-i\xi V)} \tag{72}$$

Substituting the values of $\hat{\bar{F}}_1(\xi,s)$ from (66),(68),(70) and (72) in (57) - (60) we obtain the components of stress and acoustic pressure for (i) concentrated force (ii) uniformly distributed force (iii) linearly distributed force (iv) moving couple.

In the absence of void effect the corresponding results reduces to micropolar elastic with void under an inviscid fluid.

VI. Nomenclature

λ,μ – lame's constant

K, α, β, γ – micropolar constant

$a,\xi,\varsigma,d,w_1^*,\chi$ – material constant due to presence of void

ρ – density constant

j – microinertia

$\vec{u}$ – displacement vector

$\vec{\phi}$ – microrotation vector

ψ – change in volume fraction field

t_{ij} – component of stress tensor

m_{ij} – component of couple stress tensor

δ_{ij} – Kronecker delta.

t – time

$\in_{ijk}$ – alternative tensor

References Références Referencias

1. Achenbach J.D., "Wave propagation in elastic solid", North-Holland, Newyork (1973).
2. Cowin, S.C. and Nunziato, J.W., (1983); Linear elastic materials with voids; Journal of Elasticity, 13(2), 125-147.
3. Eringen, A.C. (1966); Linear theory of micropolar elasticity; Journal of Mathematical Mechanics, 16, 909-923.
4. Eringen, A.C. (1999); Microcontinuum field theories 1 : Foundations and Solids; Springer-Verlag, NewYork.
5. Eringen, A.C. and Suhubi , E.S. (1964); Nonlinear Theory of Simple MIcropolar Solids 1&II, Int.J.Engng.Sci.2 389-404.

6. Eringen, A.C.(1968); Theory of micropolar elasticity in fracture;Vol.2,chapter 7,Academic Press, New York,NY.
7. Ghiba, I.D., Asymptotic partition of energy in the micropolar mixture theory of porous media; Meccanica, 43 (2008), 639-649.
8. Huang, L. and Zhao, C., A micropolar mixture theory of multicomponent porous media; Appl. Math. Mech.– Engl. Ed., 30 (5) (2009), 617-630.
9. Iesan,D.,(1985); "Shock waves in micropolar elastic materials with voids";Al.J.Cuza,Lasi 31. 177-186.
10. Kumar R., Ailawalia P., Influence of various sources in micropolar thermoelastic medium with voids, Structural Engineering and Mechanics; 31 (2009) no. 6, 717-735.
11. Kumar R., Ailawalia P., Interaction in a micropolar thermoelastic medium with voids due to distributed loads; Int. J. Applied Mechanics and Engng., 12 (2007), no. 4, 987-1007.
12. Kumar R., Kumar Rajeev, analysis of waves motion in transversely isotropic medium with voids under a inviscid liquid layer; Can. J. Phys., 87 (2009), 377-388..
13. Kumar R., Kumar Rajeev, Wave propagation in orthotropic generalized thermoelastic half space with voids under initial stress; "International Journal of Applied Mathematics and Mechanics (IJAMM)" 7(13) (2011), 17-44.
14. Kumar R., Deswal S. (2000); Surface wave propagation in microliquid saturated porous solid line under a uniform layer of liquid; Bulletin of Calcutta Mathematical Society, 92, 99-110.
15. Kumar R., Deswal S. and Tomar S.K. (2002); A note on surface wave dispersion of a 1-layer micropolar liquid saturated half-space; ISET Journal of Earthquake Technology, Technical note, 39, 367-382.
16. Kumar, R. and Kumar, R., Wave propagation in transversely isotropic generalized thermoelastic half space with voids under initial stress; Multidis. Modeling Materials struct., accepted (2011).
17. Madeo, A. and Gavrilyuk, S., propagation of acoustic waves in porous media and their reflection and transmission at a pure-fluid/porous-medium permeable interface; European J. Mech.-A/Solids, 29(5) (2010), 897-910.
18. Marin, M. (1996-a); Some basic theorems in elastostatics of micropolar materials with voids; Journals of Computational and Applied Mathematics, 70, 115-126.
19. Marin, M. (1996-b); Generalized solutions in elasticity of micropolar bodies with voids; Renista de La Academia Canaria de Cieneias, 8, 101-106.
20. Mindlin, R.D. (1964); Microstructures in linear elasticity; Archive Rational Mechanics and Analysis, 16, 51-78.
21. Nunziato, J.W and Cowin, S.C. (1979); A non-linear theory of elastic materials with voids; Archive Rational Mechanics and Analysis, 72(2), 175-201.
22. Passarella,F.;Some results in micropolar thermoelasticity, Mechanics Research Communications, 23(1996), 349-357.
23. Scarpetta, E.; On the fundamental solutions in micropolar elasticity with voids . Acta. Mechanica , 82(1990) 151-158.
24. Tomar, S.K. Khurana, A., Transmission of longitudinal wave through microporous elastic solid interface; Int. J. Engng. Sci. and Tech.; 3(2) (2011), 12-21.

Global Journal of Science Frontier Research
Physics & Space Science
Volume 12 Issue 1 Version 1.0 January 2012
Type : Double Blind Peer Reviewed International Research Journal
Publisher: Global Journals Inc. (USA)
Online ISSN: 2249-4626 & Print ISSN: 0975-5896

Effect of Heat Treatment on the Formation and Distribution of Dispersoid Particles in AlMgSi

By Farh Hichem, Guitoume Djamal Eddine, Djemmall Karim, Guemini Rebai , Serradj Fares
Université d'Oum el Bouaghi, Algérie

Abstract - In this paper we studied the effect of heat treatment on the formation and distribution of dispersoid particles which were formed as a function of heat treatment in AlMgSi alloy containing transition elements in AlMgSi alloy which contained the transition elements such as Mn and Cr. The extrapolation technique of Cliff et al (1983) has been used to determine the composition of dispersoid particles.

Keywords : AlMgSi alloys, dispersoids, precipitation, recrystallization.

GJSFR-A Classification : FOR Code: 020304,020201

EFFECT OF HEAT TREATMENT ON THE FORMATION AND DISTRIBUTION OF DISPERSOID PARTICLES IN ALMGSI

Strictly as per the compliance and regulations of :

Effect of Heat Treatment on the Formation and Distribution of Dispersoid Particles in AlMgSi

Farh Hichem[α], Guitoume Djamal Eddine[Ω], Djemmall Karim[β], Guemini Rebai[ψ], Serradj Fares[¥]

Abstract - In this paper we studied the effect of heat treatment on the formation and distribution of dispersoid particles which were formed as a function of heat treatment in AlMgSi alloy containing transition elements in AlMgSi alloy which contained the transition elements such as Mn and Cr. The extrapolation technique of Cliff et al (1983) has been used to determine the composition of dispersoid particles.

Keywords : AlMgSi alloys, dispersoids, precipitation, recrystallization.

I. Introduction

Aluminum alloys are widely used for fabricating high strength and light weight structures in automotive and aerospace applications Miao et al (1999). 6XXX alloys (AlMgSi based) have been studied extensively because of their high strength, good formability, weldability and corrosion resistance, Mondolfo (1979).

The addition of small amounts of the transition elements such as Zr, Mn and Cr to AlMgSi alloys showed that these elements inhibit recrystallization when the alloys are pre-heated prior to deformation. The transition elements produce fine dispersoid particles which retard the crystallisation and increase the microstructure stability at high temperature due to their low solid solubility and diffusivity in aluminium, Jones et al (1977), Belov et al (1996). In AlMgSi aluminum alloys, the nucleation of different kinds of dispersoids, i.e., Zr-, Mn-, and Cr-containing dispersoids, which play the role of recrystallization inhibition, has been investigated. Lodgaard et (2000), Cabibbo et al (2006), Lodgaard et al (2000), Jeniski et al (1996). For example the addition of Mn in the AlMgSi alloy is used to produce fine dispersoid particles during homogenization so as to retard recrystallization and grain growth during subsequent processing, Humphreys et al (1995).

The β-Mg_2Si phase and several associated metastable phases, such as β' phase, are considered to be the nucleation sites for the Mn-containing dispersoids. Matsuda et al (2000), Marioara et al (2001).

Auther [α Ω] : Unité de Recherche en Technologie Industriel URTI/CSC, BP1037. Site Université Badji Mokhtar, Chaiba, 23000. Annaba, Algérie. Telephone: +213790259221, E-mail : farhichem@gmail.com
Auther [β ψ] : Département de Physique, Faculté des Sciences Exactes, Université d'Oum el Bouaghi, Algérie
Auther [¥]: Laboratoire de Propriétés Thermodynamiques et des Traitements des Surfaces des Matériaux (LPTTSM), Université de Constantine 25000, Algérie.

II. Experimental Procedures

a) Materials

The AlMgSi alloy was provided by the Banbury Laboratories of Alcan International Ltd. They were prepared by direct chill casting process (DC) in a 178 mm diameter mould The chemical composition of the investigated alloys is given in table I.

b) Heat treatment

The alloy was solution treated at heating rate of 100°Ch-1 for 30 min at 550°C in order to follow the formation and growth of dispersoid, isothermally aged at different temperatures and then water quenched.

c) Thin foil preparation

Thin foils for TEM were prepared by spark machining to form discs 3 mm in diameter. The discs were subsequently grounded with fine silicon-carbide emery paper to about 200 μm thick. Final thinning was by jet polishing using a Struers Tenupol Unit with a solution of 33% HNO_3 in Analar grade methanol at -10 to -15 volts and a temperature of -20 to -30°C. When the electropolishing was completed the specimens were removed from the solution as quickly as possible and washed with Analar methanol. The specimens were dried between filter papers and then stored in a specimen grid box under vacuum.

d) Electron microscopy

Electron microscopy examination was carried out with an EM400T and EM430 analytical electron microscope. It was carried out by using the extrapolation technique of Cliff et al (1983). A liquid nitrogen-cooled decontaminator, an eccentric goniometer and double tilt holder were used in order to prevent the contamination after extended observation of an area of the thin foil.

Table I : chemical compositions of the investigated alloy (wt.%)

Si	Fe	Cu	Mn	Mg	Cr	Al
1.30	0.23	0.004	0.65	0.79	0.001	bal

III. Results and Discussion

Transmission electron micrographs of the alloy showing the development of the microstructure during ramp heating at 100°C h-1 to (a) 300°C, (b) 350°C, (c) 400 °C and (d) 550 °C are shown in Figure 1. Dispersoid

Global Journal of Science Frontier Research (A) Volume XII Issue I Version I January 2012

particles were observed to precipitate after the dissolution of β'-Mg_2Si. They were observed aligned along <100> matrix directions which coincided with the traces of the habit directions of β'- Mg_2Si, figures 1a and 1d. Dispersoid particles coarsened and became heterogeneously distributed after further increase in ageing temperature, figure 1d. Dispersoid particles were observed losing their distribution along <100> matrix directions observed at their early stage of precipitation, with an increase in ageing temperature.

Figure 2 illustrates a diffraction pattern obtained from one of the dispersoid particles observed. Indexation of the diffraction pattern indicates that the stronger precipitates spots can be indexed as the $[100]_{\text{zone axis}}$ of the FCC aluminum matrix and the weaker ones as the $[100]_{\text{dispersoid}}$ of the dispersoid with a simple cubic structure and a lattice parameter of 1.26 nm, Westengen et al (1980). The relation orientation between the matrix and particle can be written as ($[100]_{\text{matrix}}$ // $[100]_{\text{dispersoid}}$).

Figure 3-a shows the microstructure of the alloy ramp heated and aged at 550°C for 10 hours and 600°C for 110 hours, respectively. A high density of particles inside the grain was observed to decrease with an increase in ageing temperature or holding time. A typical set data for alloy ramp heated and aged at 550°C for 10 hours and 600°C for 110 hours, is shown in figure 4. The main elements in the dispersoid particles are Al, Mn and Si. Some iron was being found to be incorporated within the type of particles α-$Al_{15}Mn_3Si_2$, with an increase in heating temperature or holding time, figure 4-a. We notice some substitution of Mn by Fe, figure 4-b. Their compositions are determined by the extrapolation technique as $Al_{15}Mn_{2.62}Si_{2.40}$ and $Al_{15}Mn_{2.08}Fe_{0.86}Si_{2.41}$ respectively

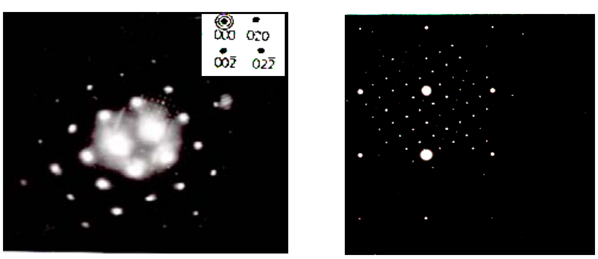

Fig.2 : Selected area diffraction pattern (SADP) from a dispersoid particles of type $Al_{15}(Fe, Mn)_3Si_2$ phase

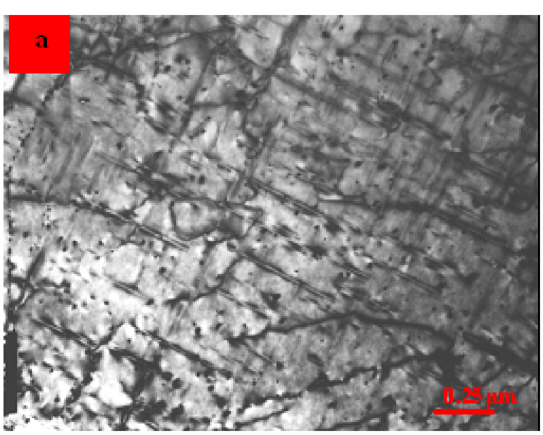

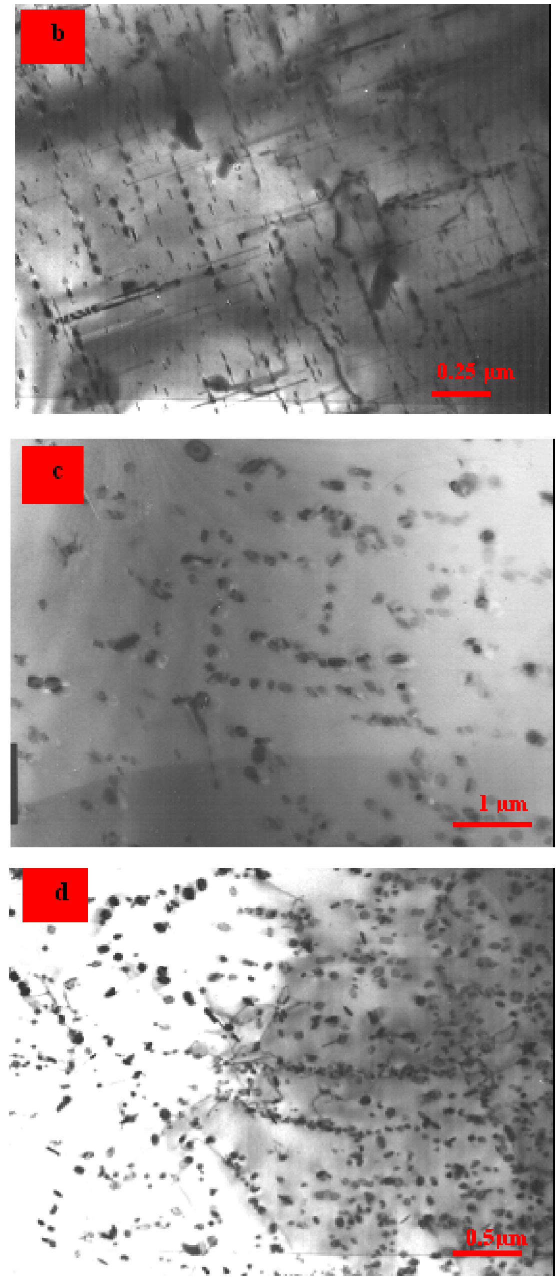

Fig.1 : Transmission electron micrographs showing the development of the microstructure during ramp heating at 100°C h-1 to (a) 300°C, (b) 350°C, (c) 400°C and (d) 550°C

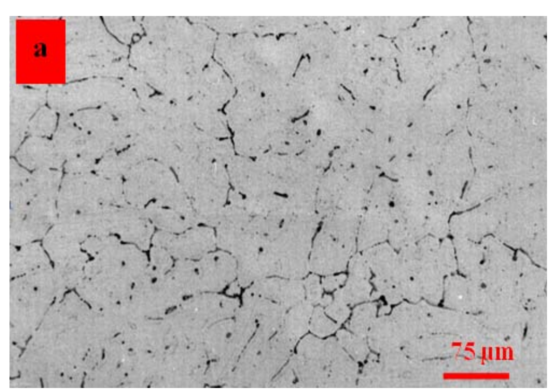

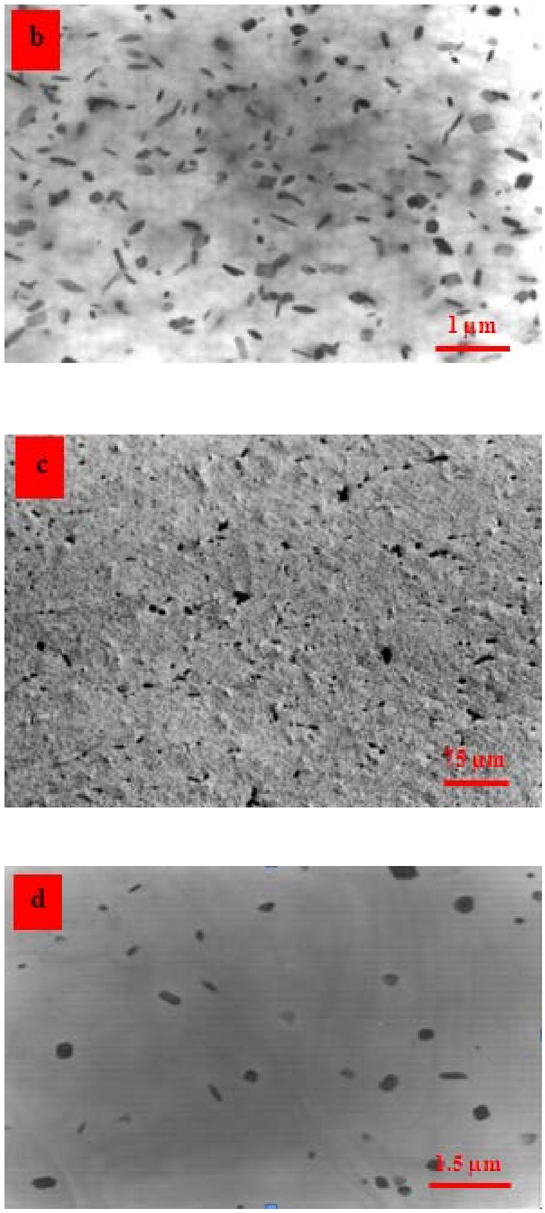

Fig.3 : Optical and transmission micrographs quenched after ramp heating and ageing for
- 10 hours at 550°C (a) and (b)
- 110 hours at 600°C (c) and (d)

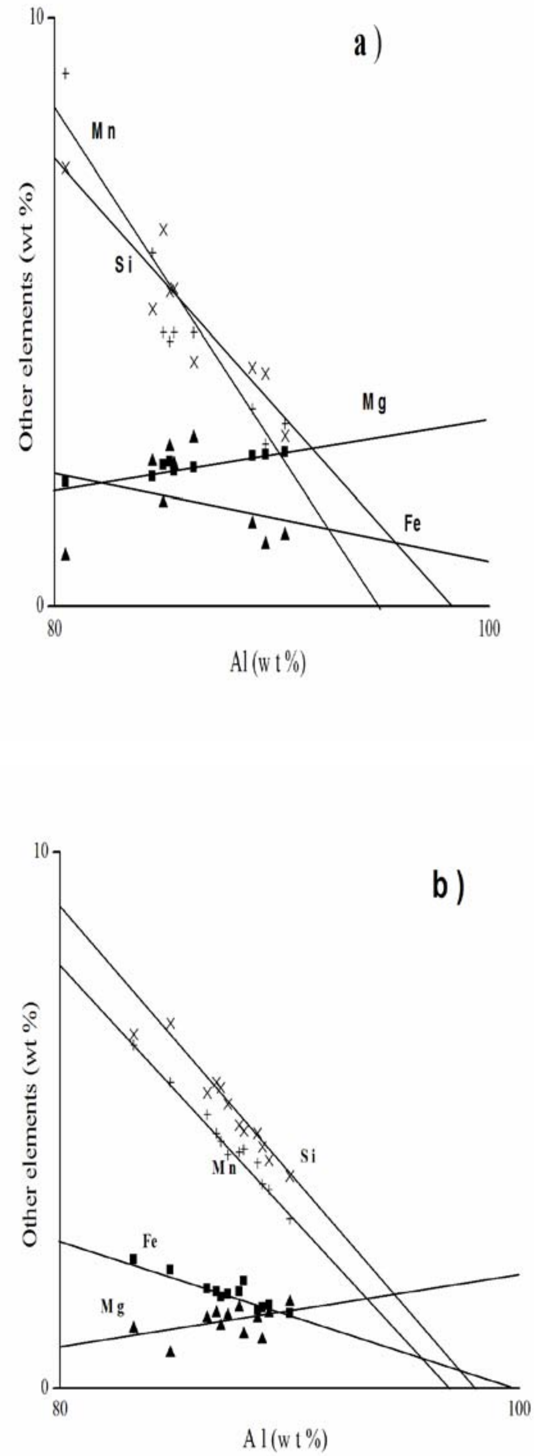

Fig.4 : Chemical composition data of the dispersoid particles in alloy II water quenched after ageing for a) 10 hours at 550°C. The main elements are Al, Mn and Si.
b) 110 hours at 600°C. The main elements are Al, Mn, Fe and Si.

IV. Conclusion

The main experimental results and conclusions can be summarized as follows:

The formation and distribution of the dispersoid particles in the alloy occurred along <100> matrix directions which coincide with the traces of the β' Mg_2Si phase. This orientation is lost and the dispersoid particles become randomly distributed after further increase in ageing temperature.

Precipitation of dispersoid particles of type $Al_{15}Mn_3Si_2$ and $Al_{15}(Mn,Fe)_3Si_2$ were observed after appropriate heat treatments. Some Fe was found to be incorporated with an increase in ageing temperature.

References References Referencias

1. Belov. N. A. (1996). Aluminium Casting Alloys with High Content of Zirconium. Proc.5th Int.Conf.on Al-Alloys and Their Physical and Mechanical Properties (ICAA5), Grenoble, France, Materials Science Forum, Vol. 217-222, P.293-298.
2. Cabibbo. M, Evangelista. E, Scalabroni. C, Bonetti. E. (2006). A Transmission Electron Microscopy Study of the Role of Sc+Zr Addition to a 6082-T8 Alloy Subjected to Equal Channel Angular Pressing. Mat. Sci. Forum, vol. 503-504, 841-46.
3. Cliff. G, Powell. D. J, Pilkington. R, Champness. p. E, Lorimer. G. W. (1983). Electron Microscopy and Analysis. Ed.P.Doig, IOP, London, 63-66.
4. Humphreys. F.J and Hatherly. M. (1995) Recrystallization and Related Annealing Phenomena, Elsevier Science, Inc., Oxford, United Kingdom, 109–14.
5. Jeniski. R.A, Thanaboonsombut. B, Sanders. T.H. (1996). The effect of iron and manganese on the recrystallization behavior of hotrolled and solution-heat-treated aluminum alloy 6013. Metall. Mater. Trans, vol. A27, 19-27.
6. Jones. H, Smallman. R. E, Harris. J. E. (1977). Lattice defects in splat-quenched metals, in "Vacancies", eds., The *Metals Society*, *London*. *175-184*.
7. Lodgaard.L and Ryum. N. (2000). Precipitation of dispersoids containing Mn and/or Cr in Al–Mg–Si alloys. Mater. Sci. Eng, Vol. A283, 144-152.
8. Lodgaard. L and Ryum. N. (2000). Precipitation of chromium containing dispersoids in Al-Mg-Si alloys. Mat. Sci. Technol, vol. 16 (6), 599–604.
9. Matsuda. K, Ikeno. S. (2000). Recent studies on aging phenomena of 6000 series aluminum alloys. J. Japan Inst. Light Metals, vol. 50, 23-36.
10. Marioara. C.D, Andersen. S.J, J. Jansen, Zandbergen. H.W. (2001). Atomic model for GP Zones in a 6082 AlMgSi system. Acta Mater, vol. 49, 321-328.
11. Miao.W and D. Laughlin. (1999). Precipitation hardening in aluminium alloy 6022. Scripta Mater, vol. 40 (7), 873-878.
12. Mondolfo. L. F (1976). Aluminium Alloys, Structures and Properties, Butterworth, 1st edition, London.

Global Journal of Science Frontier Research
Physics & Space Science
Volume 12 Issue 1 Version 1.0 January 2012
Type : Double Blind Peer Reviewed International Research Journal
Publisher: Global Journals Inc. (USA)
Online ISSN: 2249-4626 & Print ISSN: 0975-5896

Study of High Pressure Structural, Mechanical and Thermal Properties of $SrS_{1-x}Se_x$, $SrS_{1-x}Te_x$ and $SrSe_{1-x}Te_x$ Ternary Alloys

By Purvee Bhardwaj
Barkatullah University, Bhopal, India

Abstract - We have developed a new model to study the structural, mechanical and thermal properties of $SrS_{1-x}Se_x$, $SrS_{1-x}Te_x$ and $SrSe_{1-x}Te_x$ ternary alloys. This model includes the Coulomb interaction, TBI interaction, vander Waal interaction overlap repulsive interactions extended up to the second neighbour ions and covalent interaction. The variation of Gibb's free energy, phase transition pressure and the bulk modulus from the concentration using Vegard's law were observed for the three alloys. Our calculated results have revealed reasonably good agreement with the available experimental data on the phase transition pressures and volume collapse. In addition we have calculated other mechanical and thermal properties.

Keywords : *Strontium chalcogenides, Volume collapse, Elastic constants, Phase transition.*

GJSFR-A Classification : *FOR Code: 020304 ,020406*

STUDY OF HIGH PRESSURE STRUCTURAL, MECHANICAL AND THERMAL PROPERTIES OF SRS1-XSEX, SRS1-XTEX AND SRSE1-XTEX TERNARY ALLOYS

Strictly as per the compliance and regulations of :

Study of High Pressure Structural, Mechanical and Thermal Properties of $SrS_{1-x}Se_x$, $SrS_{1-x}Te_x$ and $SrSe_{1-x}Te_x$ Ternary Alloys

Purvee Bhardwaj

Abstract - We have developed a new model to study the structural, mechanical and thermal properties of $SrS_{1-x}Se_x$, $SrS_{1-x}Te_x$ and $SrSe_{1-x}Te_x$ ternary alloys. This model includes the Coulomb interaction, TBI interaction, vander Waal interaction overlap repulsive interactions extended up to the second neighbour ions and covalent interaction. The variation of Gibb's free energy, phase transition pressure and the bulk modulus from the concentration using Vegard's law were observed for the three alloys. Our calculated results have revealed reasonably good agreement with the available experimental data on the phase transition pressures and volume collapse. In addition we have calculated other mechanical and thermal properties.

PACS No : *62.20.de, 62.20.dq, 62.50.-p, 64.00.00*

Keywords : Strontium chalcogenides, Volume collapse, Elastic constants, Phase transition.

I. Introduction

The strontium chalcogenides SrX (X = S , Se and Te), together with other alkaline earth chalcogenides form a very important closed shell ionic system with the NaCl crystal structure at normal conditions. They are technologically important materials, with applications in the area of luminescent devices, radiation dosimetry, fast high-resolution optically stimulated luminescence imaging, and infrared sensitive devices [1–3]. Under higher pressure prior to metallization, they undergo a first order structural phase transition to the CsCl structure. Semiconductor alloys, which are solid solutions of two or more semiconducting elements, have important technological applications, especially in the manufacture of electronic and electro-optical devices [4-6]. One of the easiest ways to change artificially the electronic and optical properties of semiconductors is by forming their alloys. It is possible to combine two different compounds with different optical band gaps and different rigidities in order to obtain a new material with intermediate properties.

There are a number of theoretical works on these compounds concerning electronic band structure, structural phase stability, elastic properties, metallization process and optical properties [7–11]. For the band gap results, there are some discrepancies between different calculations. Recently, Dadsetani et. al. [1] have calculated the optical properties of SrS, SrSe and SrTe compounds using the full potential linearized augmented plane wave method (FP-LAPW). To the best of our knowledge no experimental or theoretical investigations of their ternary alloys have been appeared in the literature, therefore, the purpose of this paper is to study the structural, elastic, and thermodynamic properties as well as to investigate the disorder effects in these strontium alloys using the charge transfer mechanism.

Zimmer et. al. [4] investigated pressure volume relationships and structural transition in CaTe and SrTe at high pressure using X-ray diffraction. Their results show that SrTe transforms from B1 to B2 structure at 12 GPa. Luo. et. al. [5] studied the high pressure phase transformation and the equation of state of SrSe by X-ray diffraction using a synchrotron source. They reported a B1-B2 structural transition at 14.2 GPa with a volume reduction of 10.7%. Khenata et. al. [6] calculated the electronic band structures and the total energies of SrS, SrSe and SrTe in the B1 and B2 structures. They determined the transition and metallization pressure in these compounds.

Metallization is often described in terms of the single particle band and the unoccupied conduction band. The band gaps in these close shell insulating materials are expected to decrease with pressure until finally the empty d-type conduction band drops in energy below the top of the filled p-type valence bands. Saum et. al. [9] measured the fundamental optical absorption of SrS, Sr Se and SrTe in the energy range from 2.5 to 5.8 eV. Cheng Yan et al [10] investigated the transition phase and elastic properties of SrS from NaCl structure (B1) to CsCl structure using the ab-initio plane wave pseudopotential density functional theory and by the quasi-harmonic Debye model. Yang Xiao-Cui et al [11] investigated the structural stabilities and electronic properties of SrX (X=S, Se , T e) under high pressure using the first principles calculation based on density functional theory (DFT) with the plane wave basis.

Jha et al [12] reported the investigation of the pressure induced phase transition of BaSe, BaTe, SrSe, and SrTe, using a three-body potential approach. But, they ignored the van-der Waal and covalency effect. The ab initio full potential linearized augmented plane

Author : High Pressure Research Lab, Department of Physics, Barkatullah University, Bhopal-462026, India.
E-mail : purveebhardwaj@gmail.com Ph: +91-755-2487552, Fax +91-755-2677723

wave (FP-LAPW) method within density functional theory (DFT) was applied to study the effect of composition on the structural, electronic, optical and thermodynamic properties of $SrS_{1-x}Se_x$, $Sr\ S_{1-x}Te_x$ and $SrSe_{1-x}Te_x$ ternary alloys by S Labidi et al [13].

It is seen from the current literature that three body potential model (TBP) used and developed by Singh and coworkers [14-16] has been found to be remarkably successful in giving the unified description of the lattice dynamic, static elastic, optic, dielectric and photo elastic properties of ionic and semi conducting crystals. In this TBP model, the three body interactions owe their origin to the quantum mechanical foundation and also to the phenomenological approach in terms of the transfer (or exchange) of charge between the overlapping electron shells of the adjacent ions in solids. This TBP approach has been extended to include the Hafemeister-Flygare (HF) type [17] overlap repulsion operative upto the second neighbour ions for describing the lattice static and mechanical properties of binary ionic solids and alloys. Also, Tosi and coworkers [18] have demonstrated the significance of van der Waals (vdW) attraction due to the dipole-dipole (d-d) and dipole-quadruple (d-q) interactions to describe the cohesion in ionic solids. The van der Waal interactions are generally ignored in the first principle calculations. Besides, it is noted that Motida [19] has incorporated the effect of covalency to reveal the cohesive and lattice properties of partially ionic crystals.

II. Essentials of Theory and Computational Method

The natural consequence of application of pressure on the crystals is the compression, which in turn leads to an increased charge transfer (or three-body interaction effects) [14] due to the existence of the deformed (or exchanged) charge between the overlapping electron shells of the adjacent ions.

These effects have been incorporated in the Gibbs free energy ($G = \Phi+PV-TS$) as a function of pressure and three body interactions (TBI), which are the most dominant among the many body interactions. Here, Φ is the internal energy of the system equivalent to the lattice energy at temperature near zero and S is the entropy. At temperature T=0K and pressure (P) the Gibbs free energies for rock salt (B1, real) and CsCl (B2, hypothetical) structures are given by:

$$G_{B1}(r) = \phi_{B1}(r) + P_{B1}(Vr) \tag{1}$$

$$G_{B2}(r') = \phi_{B2}(r') + P_{B2}(Vr') \tag{2}$$

With V_{B1} ($=2.00r^3$) and V_{B2} ($=1.54r'^3$) as unit cell volumes for B_1 and B_2 phases respectively. The first terms in (1) and (2) are lattice energies for B_1 and B_2 structures and they are expressed as:

$$\begin{aligned}\phi_{B_1}(r) = {} & \frac{-\alpha_m z^2 e^2}{r} - \frac{(12\alpha_m z e^2 f_m(r))}{r} - [\frac{C}{r^6} + \frac{D}{r^8}] + 6b\beta_{ij}\exp[(r_i + r_j - r)/\rho] \\ & + 6b\beta_{ii}\exp[(2r_i - 1.414r)/\rho] + 6b\beta_{jj}\exp[(2r_j - 1.414r)/\rho]\end{aligned} \tag{3}$$

$$\begin{aligned}\phi_{B_2}(r') = {} & \frac{-\alpha'_m z^2 e^2}{r'} - \frac{(16\alpha'_m z e^2 f_m(r'))}{r'} - [\frac{C'}{r'^6} + \frac{D'}{r'^8}] + 8b\beta_{ij}\exp[(r_i + r_j - r')/\rho] \\ & + 3b\beta_{ii}\exp[(2r_i - 1.154r')/\rho] + 3b\beta_{jj}\exp[(2r_j - 1.154r')/\rho]\end{aligned} \tag{4}$$

With α_m and α'_m as the Madelung constants for NaCl and CsCl structure respectively. C (C') and D (D') are the overall vander Waal coefficients of B1 (B2) phases, β_{ij} (i,j=1,2) are the Pauling coefficients defined as $\beta_{ij}=1+(Z_i/n_i)+(Z_j/n_j)$ with Z_i (Z_j) and n_i (n_j) are the valence and the number of electrons of the i(j)th ion. Ze is the ionic charge and b (ρ) are the hardness (range) parameters, r (r') are the nearest neighbour separations for NaCl (CsCl) structure $f_m(r)$ is the modified three body force parameter which includes the covalency effect with three body interaction r_i (r_j) are the ionic radii of ions i (j).

These lattice energies consist of long range Coulomb energy (first term), three body interactions corresponding to the nearest neighbour separation r (r') (second term), vdW (vander Waal) interaction (third term), energy due to the overlap repulsion represented by Hafemeister and Flygare (HF) type potential and extended up to the second neighbour ions (fourth, fifth and sixth terms).

Covalency effects have been included in the second terms parameters of cohesive energies given by equation (3) and (4) in three-body interaction on the lines of Motida [19]. Now modified three body parameter $f_m(r)$ becomes

$$f_m(r) = f_{TBI}(r) + f_{cov}(r) \tag{5}$$

$$f_{\mathrm{cov}}(r) = \frac{4V^2_{sp\sigma}e^2}{rE_g^{\ 3}}$$

$$\frac{V^2_{sp\sigma}}{E_g^2} = \frac{1-e_s^*}{12}$$

$$E_g = E - I\frac{(2\alpha-1)e^2}{r} \tag{6}$$

With $V_{sp\sigma}$ is the transfer matrix between the outer most P orbital of anion and lowest excited state of cation E_g is the transfer energy of electron from anion to cation. Denoting the static and optical dielectric constant ε_0 and ε respectively and the transverse optical phonon frequency at zone centre by ω_t, e_s represented as

$$(e_s^*)^2 = \frac{9\mu\,\omega_t^2(\varepsilon_0-\varepsilon_\infty)}{4\pi N(\varepsilon_\infty+2)^2}$$

$$and \tag{7}$$

$$\frac{(e_s^*)^2}{(e)^2} = \frac{9v\mu\,\omega_0^2(\varepsilon_0-\varepsilon_\infty)}{4\pi e^2(\varepsilon_\infty+2)^2}$$

Where ν denotes the unit cell volume: $2r^3$, r equilibrium value of the separation of the nearest neighbouring ions, ε_0 the static dielectric constants, μ reduced mass of the ions, and ω_0 the infrared dispersion frequency, these values have been taken from [19].
The values of derivatives of $f_m(r)$ obtained as

$$f_m(r) = f_0 e^{-r/\rho} + f_{\mathrm{cov}}(r)$$ and its first derivative is

$$f_m'(r) = f'(r) + f'_{\mathrm{cov}}(r)$$

Where, various symbols have their usual meanings describe in our earlier paper [20-22]. The mixed crystals, according to the virtual crystal approximation (VCA) [23], are regarded as any array of average ions whose masses, force constants, and effective charges are considered to scale linearly with concentration (x). The measured data on lattice constants in $SrS_{1-x}Se_x$, $Sr\ S_{1-x}Te_x$ and $SrSe_{1-x}Te_x$ have shown that they vary linearly with the composition (x), and hence they follow Vegards law:

$$a\ (A\ B_{1-x}\ C_x) = (1-x)\ a\ (AB) + xa\ (AC) \tag{8}$$

The values of these model parameters are the same for end point members. The values of these parameters for their mixed crystal components have been determined from the application of Vegards law to the corresponding measured data for AB and AC. It is instructive to point that the mixed crystals, according to the virtual crystal approximation, are regarded as an array of average ions whose masses, force constants and effective charges are considered to scale linearly with concentration. It is convenient to find the three parameters for both binary compounds. Furthermore, we assume that these parameters vary linearly with x and hence follow Vegards law:

$$b\ (A\ B_{1-x}\ C_x) = (1-x)\ b\ (AB) + xb\ (AC) \tag{9}$$

$$\rho\ (A\ B_{1-x}\ C_x) = (1-x)\ \rho\ (AB) + x\rho\ (AC) \tag{10}$$

$$f(r)\ (AB_{1-x}\ C_x) = (1-x)\ f(r)\ (AB) + xf(r)\ (AC) \tag{11}$$

a) Thermo Physical Properties

In order to access the relative merit of the present potential we have calculated the molecular force constant (f), infrared absorption frequency (υ_0), Debye temperature (θ_D), Grunneisen parameter (γ) and ratio of volume expansion coefficient (α_v) to specific heat (C_v) at constant volume which are directly derived from the cohesive energy [20-22], $\Phi(r)$.

The compressibility is well known to be given by

$$\beta = \frac{3Kr_0}{f} \tag{12}$$

in terms of molecular force constants

$$f = \frac{1}{3}\left[\phi_{kk'}^{SR}(r) + \frac{2}{r}\phi_{kk'}^{SR}(r)\right]_{r=r_0} \tag{13}$$

With $\Phi_{kk'}^{SR}(r)$ as the short range nearest neighbour ($k\neq k'$) part of Φ (r) given by the last three terms in eq. (3) and (4). This force constant f leads to the infrared absorption frequency with the knowledge of the reduced mass (μ) of the oxide crystals.

$$\nu_0 = \frac{1}{2\pi}\left(\frac{f}{\mu}\right)^{1/2} \tag{14}$$

This frequency gives us the Debye temperature

$$\theta_D = \frac{h\nu_0}{k} \tag{15}$$

With h and k as the Planck and Boltzman constants, respectively. The values of the Grunneisen parameter (γ), have been calculated from the relation

$$\gamma = -\frac{r_0}{6}\left[\frac{\phi'''(r)}{\phi''(r)}\right]_{r=r_0} \tag{16}$$

We have calculated the ratio of the volume expansion coefficient (α_v) to the volume to specific heat (C_v) from its well known expression

$$\frac{\alpha_v}{C_v} = -\left[\frac{\phi'''(r)}{2r\phi''(r)}\right]_{r=r_0} \tag{17}$$

The thermal expansion coefficient (α_v) can be calculated with the knowledge of specific heat (C_v).

III. Results and Discussion

The Three Body potential described in the preceding section for NaCl (B_1) CsCl (B_2) structures contain three model parameters [b ρ, f(r)], namely range, hardness and three body interaction parameter. To calculate these parameters we employed the first and second order space derivatives of lattice energy and equilibrium condition. We have followed the technique of minimization of U_{B1} (r) a nd U_{B2} (r') at different pressures in order to obtain inter ionic separation r and r, for B_1 and B_2 phases respectively. We have evaluated the corresponding $G_{B1}(r)$ and $G_{B2}(r')$ and their respective differences $\Delta G = (G_{B1}(r) - G_{B2}(r'))$. The pressure at which ΔG approaches zero is the phase transition pressure (P_t).

Firstly, the structural properties of the binary compounds SrS, Sr Se and SrTe in the rocksalt structure were analyzed. We model the alloys at some selected compositions with ordered structures described in terms of periodically repeated super cells with eight atoms per unit cell, for the compositions $x = 0.25, 0.5, 0.75$. The values of phase transition pressures of SrX mixed crytals for model-I and model-II at diffrent concentrations are given in Table-1. The values of phase tarnsition of model-I and model-II are compared with experimental and others data for end point members and psedoexperimental data for diffrent concentrations. The variations of Gibb's free energy change ΔG (KJ/mole) with concentration (x) are plotted in Fig 1. The Gibb's free energy change ΔG of SrX are dependent lineraly with concentration (x). The phase transition pressures of $SrS_{1-x}Se_x$, $SrSe_{1-x}Te_x$ and $SrS_{1-x}Te_x$ have been plotted with different concentration (x) in Fig. 2. We have compared our results with theoretical [3,5] and experimental results [6].

The first order phase transition involving a discontinuity in volume takes place at the transition pressure. Experimentally one usually studies the relative volume changes ($-\Delta V/V_0$) associated with the compressions. The discontinuity in volume ($-\Delta V/V_0$) at the transition pressure is obtained from the phase diagram. The negative sign shows compression in crystal. This is the characteristic of first order phase transition. The volume collapse of SrX mixed crystals are given in Table-1. The values of model-I and model-II of end point memers are compared with experiment and other theoretical data. Our values of model-I are better than other theoretical values. The volume collapse of SrX mixed crystals at diffrent concentrations are compared with psedoexperimental data.

Usually, in the treatment of alloy problems, it is assumed that the atoms are located at ideal lattice sites and the lattice constants of alloys should vary linearly with composition x according to Vegard's law [23], however, violations of Vegard's rule have been reported in semiconductor alloys both experimentally [3,5] and theoretically [6,12,13]. To test the mechanical stability of our model, we have computed the elastic properties of proposed materials.

To study the elastic behavior of strontium compounds we have studied second order elastic constants (SOECs) and their combinations. We have made further investigations from the variations of the bulk modulus $B [= (C_{11}+2C_{12})/3]$, the combination of SOEC elastic stiffness $C_L[=(C_{11}+C_{12}+2C_{44})/2]$ and the shear moduli $Cs [= (C_{11}-C_{12})/2]$. The values of these combinations for model-I and model-II are given in Table-2 at P=0 GPa. The values of the bulk modulus B are calculated for the compositions $x = 0.25, 0.5, 0.75$ by S Labidi et al [13] using the ab initio full potential linearized augmented plane wave (FP-LAPW) method within density functional theory (DFT). We have calculated the bulk modulus B at the same concentration for both the models and compared them with FP-LAPW results. Significant deviations of the bulk modulus from the linear concentration dependence have been plotted in Fig 3. Our results show that the bulk modulus decreases with an increase of the Se and Te concentration x which is same as S Labidi et al [13]. This suggests that as x increases from x = 0 t o 1 the alloys become generally more compressible.

In order to investigate elasticity of SrX compounds in detail, we have used normalized elastic constants c_{ij} [24]. The value of c_{ij} is obtained by dividing a specific elastic constant by the bulk modulus

$$c_{ij} = c_{ij}/B = 3c_{ij}/(c_{11} + 2c_{12}).$$

Divided by the bulk modulus, the interatomic forces are normalized with an average restoring force of the system. At zero pressure, if a cubic crystal is elastically ideal, namely an isotropic Cauchy solid. The normalized elastic constants of $SrS_{1-x}Se_x$, $SrSe_{1-x}Te_x$ and $SrS_{1-x}Te_x$ have been summarized in Table-3.

Besides we have calculated thermo physical properties of SrX. The thermo physical properties provide us the interesting information about the substance. The Debye characteristic temperature θ_D reflects its structure stability, the strength of bonds between its separate elements, structure defects availability (dislocations in crystalline structure of mineral grains, pores, microcracks) and its density.

Compressibility is used in the earth science to quantify the ability of a soil or rock to reduce in volume with applied pressure.The calculated thermo physical properties have been listed in Table 4. Due to the lack of experimental data, we could not compare them with our results.

In view of the overall achievements, it may be concluded that there is reasonably good agreement of modified MTBP (Model-I) with the experimental values than computed from TBP (Model-II). The success achieved in the present investigation can be ascribed to the realistic approach of our model. The charge transfer effect seems to be of great importance at high pressure when the inter-ionic separation reduces considerably and the coordination number increases. For the study of the phase transitions in partially covalent chalcogenides, we have incorporated, probably for the first time, the effect of covalency in the TBP model along with the van der Waals interactions. The consistency of the results obtained from the TBI potential arose because the electron-shell deformation, when the nearest neighbour ions overlap, is enhanced under pressure. This supports our view of a partially ionic character and a charge transfer. It is thus obvious from the overall results that the present TBI mechanism is adequately suited for a description of the phase transition phenomena and mechanical properties, and we stress that the TBI gives a realistic representation of interionic interaction capable of explaining the elastic behaviour.

Finally, it may be concluded that the present modified interaction potential model (MIPM) has successfully predicted the phase transition pressures, associated volume collapses, elastic and thermophysical properties correctly for the present group of compounds. The inclusion of three body interactions with covalency effect has improved the prediction of phase transition pressures over that obtained from the two-body potential and TBI without covalency.

References Références Referencias

1. M. Dadsetani and A. Pourghazi, Phys. Rev. B, 73 (2006), 195102-195109.
2. R. Khenata, H. Baltache M, Rerat M Driz. M, Sahnoun, B. Bouhafs, B. Abbar, Physica B, 371 (2006), 12-19.
3. H. G. Zimmer., H. Winze and K. Syassen, Phys. Rev.B, 32 (1985) 4066-4070; K. Syassen, Phys. Stat. Sol. (a)91 (1985) 11.
4. A. Chakrabarti, Phys. Rev.B, 62 (2000), 1806-1814.
5. Huan Luo, Raymond G. Green and Arthur L. Ruff, Phys. Rev. B, 49, (1994), 15341-15343.
6. Khenata R, Baltache H, Rerat M, Driz M. Sahnoun, M, Bouhafs, B, Abbar, B. Physica B 339 (2003) 208-215.
7. T.A. Grzybowski, L. Ruoff, Phys. Rev. B 27 (1983) 6502.
8. T.A. Grzybowski, L. Ruoff, Phys. Rev. Lett. 53 (1984) 489.
9. G.A. Saum, E.B. Hensley, Phys. Rev. 113 (1959) 1019.
10. Yan Cheng, Lai-Yu Lu, Ou-He Jia, Qing-Quan Gou, Commun. Theor. Phys. 49 (2008) 1611.j
11. Xiao-Cui Yang, Ai-Min Hao, Jie Yang, Yong-Hao Han, Gang Peng, Chun-Xiao Gao, Guang-Tian Zou, Chin. Phys. Lett. 25 (5) (2008) 807.
12. P.K. Jha, U.K. Sakalle, S.P. Sanyal, J. Phys. Chem. Solids 59 (1998) 1633.
13. S. Labidi, H. Meradji, M. Labidi, S. Ghemid, S. Drablia and F. El Haj Hassan, Physics Procedia 2 (2009) 1205–1212.
14. R.K. Singh, Phys. Reports 85 (1982) 259.
15. R.K. Singh Sadhna Singh, Phys. Rev. B 45 (1992) 1019.
16. R.K. Singh Sadhna Singh, Phase Transit. 15 (1989) 127.
17. Hafemiester D W and Flygare H F 1965 J. Chem. Phys. 43 795.
18. Tosi M P and Fumi F G 1962 J. Phys. Chem. Solids 23 359; Tosi M P 1964 Solid State Physics 16 1.
19. K. Motida, J. Phys. Soc. Jpn. 55 (1986) 1636.
20. Purvee Bhardwaj, Sadhna Singh and N. K. Gaur, Mat. Res. Bull. 44 (2009) 1366-1374.
21. Purvee Bhardwaj, Sadhna Singh and N. K. Gaur, J. Cetr. Euro. J. Phys. 6, 2 (2008) 223-229.
22. Purvee Bhardwaj, Sadhna Singh and N. K. Gaur, J. of Molecular Structure: THEOCHEM 897 (2009) 95-99.
23. R J Elliot and R A Leath, IIE 386 (1996).
24. Sadhna Singh and Purvee Bhardwaj J of Opto. and Advanced Material 12 (2010) 2261 – 2271.

Captions of Figures

1. Gibb's free energy ΔG (kj/mole) with concentration (x) of $SrS_{1-x}Se_x$, $SrSe_{1-x}Te_x$ and $SrS_{1-x}Te_x$ respectively.
2. Phase transition pressure with concentration (x) of SrX solid squares (■), solid circles (●) solid triangles (▲), and represent for $SrS_{1-x}Se_x$, $SrSe_{1-x}Te_x$ and $SrS_{1-x}Te_x$ respectively.
3. Bulk modulus of SrX with concentration (x) solid squares (■), solid circles (●) solid triangles (▲), and represent for $SrS_{1-x}Se_x$, $SrSe_{1-x}Te_x$ and $SrS_{1-x}Te_x$ respectively.

Global Journal of Science Frontier Research (A) Volume XII Issue I Version I January 2012

Table-1 : Phase transition and volume collapse of SrX at different concentration

Alloys/ Concentration	Phase Transition Pressure (GPa)				Volume Collapse (%)			
	Present		Expt.	Others	Present		Expt.	Others
	Model-I	Model-II			Model-I	Model-II		
$SrS_{1-x}Se_x$ 0	18.2	18.6	18[a]	18.17[b]	10.46	10.12	11.4[a]	10.8[b]
0.25	17.08	17.28	17.13[a]	17.6[b]	10.32	9.95	11.22[a]	10.59[b]
0.5	15.96	15.96	16.26[a]	17.03[b]	10.19	9.78	11.05[a]	10.38[b]
0.75	14.84	14.64	15.39[a]	16.46[b]	10.05	9.61	10.87[a]	10.17[b]
1	13.7	13.3	14.5	15.87[b]	9.92	9.45	10.7[a]	9.96[b]
$SrSe_{1-x}Te_x$ 0	13.7	13.3	14.5[a]	15.87[b]	9.92	9.45	10.7[a]	9.96[b]
0.25	13.23	12.78	13.88[a]	15.22[b]	10.05	9.60	10.8[a]	9.70[b]
0.5	12.76	12.26	13.26[a]	14.57[b]	10.18	9.76	10.9[a]	9.44[b]
0.75	12.29	11.74	12.64[a]	13.92[b]	10.31	9.92	11.0[a]	9.18[b]
1	11.8	11.2	12[a]	13.24[b]	10.44	10.08	11.1[a]	8.92[b]
$SrS_{1-x}Te_x$ 0	18.2	18.6	18[a]	18.17[b]	10.46	10.12	11.4[a]	10.8[b]
0.25	16.6	16.7	16.5[a]	16.94[b]	10.455	10.11	11.32[a]	10.33[b]
0.5	15.0	14.9	15.0[a]	15.71[b]	10.450	10.10	11.25[a]	9.86[b]
0.75	13.4	13.05	13.5[a]	14.48[b]	10.445	10.09	11.17[a]	9.39[b]
1	11.8	11.2	12[a]	13.24[b]	10.44	10.08	11.1[a]	8.92[b]

a-ref [3,5], b-ref [6].

Table-2 : Bulk modulus and shear modulus of SrX at different concentration

Alloys/ Concentration	Bulk modulus (GPa)				Shear modulus (GPa)			
	Present		Expt.	Others	Present		Expt.	Others
	Model-I	Model-II			Model-I	Model-II		
$SrS_{1-x}Se_x$ 0	51.9	51.53	58[a]	46.3[b]	58.65	58.7	-	61.9[b]
0.25	50.84	50.48	54.75[a]	45.6[b]	56.8	56.89	-	56.63[b]
0.5	49.78	49.43	51.5[a]	44.8[b]	54.95	55.08	-	51.36[b]
0.75	48.72	48.38	48.25[a]	43.5[b]	53.1	53.27	-	46.09[b]
1	47.66	47.31	45[a]	41.1[b]	51.25	51.46	53.3[a]	40.8[b]
$SrSe_{1-x}Te_x$ 0	47.66	47.31	45[a]	41.1[b]	51.25	51.46	53.3[a]	40.8[b]
0.25	44.69	44.4	43.75[a]	38.1[b]	49.5	49.71	-	42.31[b]
0.5	41.72	41.49	42.5[a]	34.0[b]	47.85	47.96	-	43.82[b]
0.75	38.75	38.58	41.25[a]	32.0[b]	46.15	46.21	-	45.32[b]
1	35.76	35.64	40[a]	31.8[b]	44.44	44.46	-	46.85[b]
$SrS_{1-x}Te_x$ 0	51.9	51.53	58[a]	46.3[b]	58.65	58.7	-	61.9[b]
0.25	47.87	47.56	53.5[a]	41.6[b]	55.1	55.14	-	58.13[b]
0.5	43.84	43.59	49[a]	37.5[b]	51.55	51.58	-	54.37[b]
0.75	39.81	39.62	44.5[a]	33.5[b]	48.0	48.02	-	50.61[b]
1	35.76	35.64	40[a]	31.8[b]	44.44	44.46	-	46.85[b]

a-ref [3,5], b-ref [13]

Table-3 : Normalized Elastic constants

Normalized elastic constants	SrS		SrSe		SrTe	
	Model-I	Model-II	Model-I	Model-II	Model-I	Model-II
C'_{11}	2.50	2.51	2.43	2.45	2.65	2.66
C'_{12}	0.246	0.238	0.283	0.274	0.171	0.168
C'_{44}	0.960	0.933	0.709	0.705	1.12	1.12

Table 4 : Thermo physical properties of SrX.

Crystal	f (10^4dyn/cm)	υ_0 (10^{12} Hz)	θ_D (K)	γ	α_v/c_v (10^3 J)
SrS	12.2	14.51	694.32	1.85	6.42
SrSe	8.29	8.9	430.38	3.16	9.80
SrTe	1.20	3.05	146.16	2.30	6.23

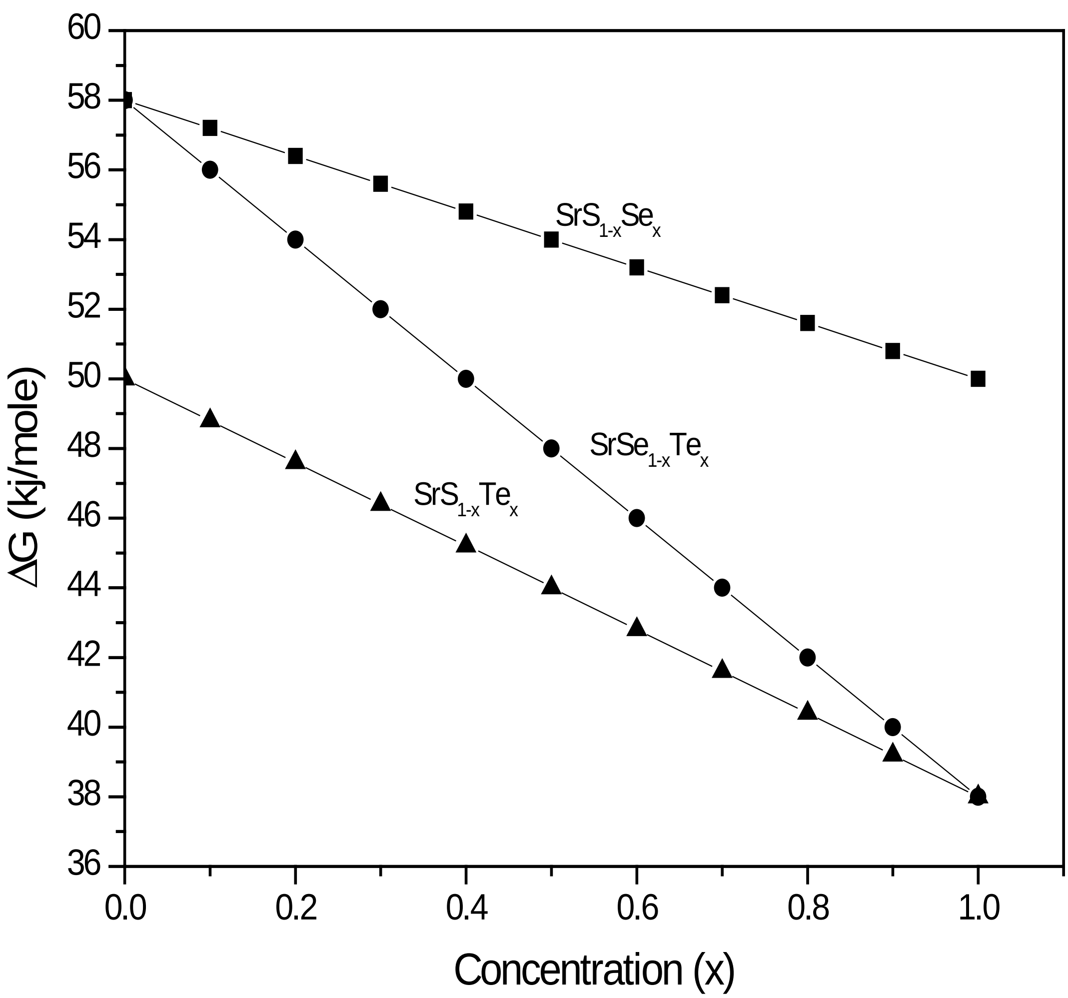

Fig 1.

Global Journal of Science Frontier Research (A) Volume XII Issue I Version I January 2012

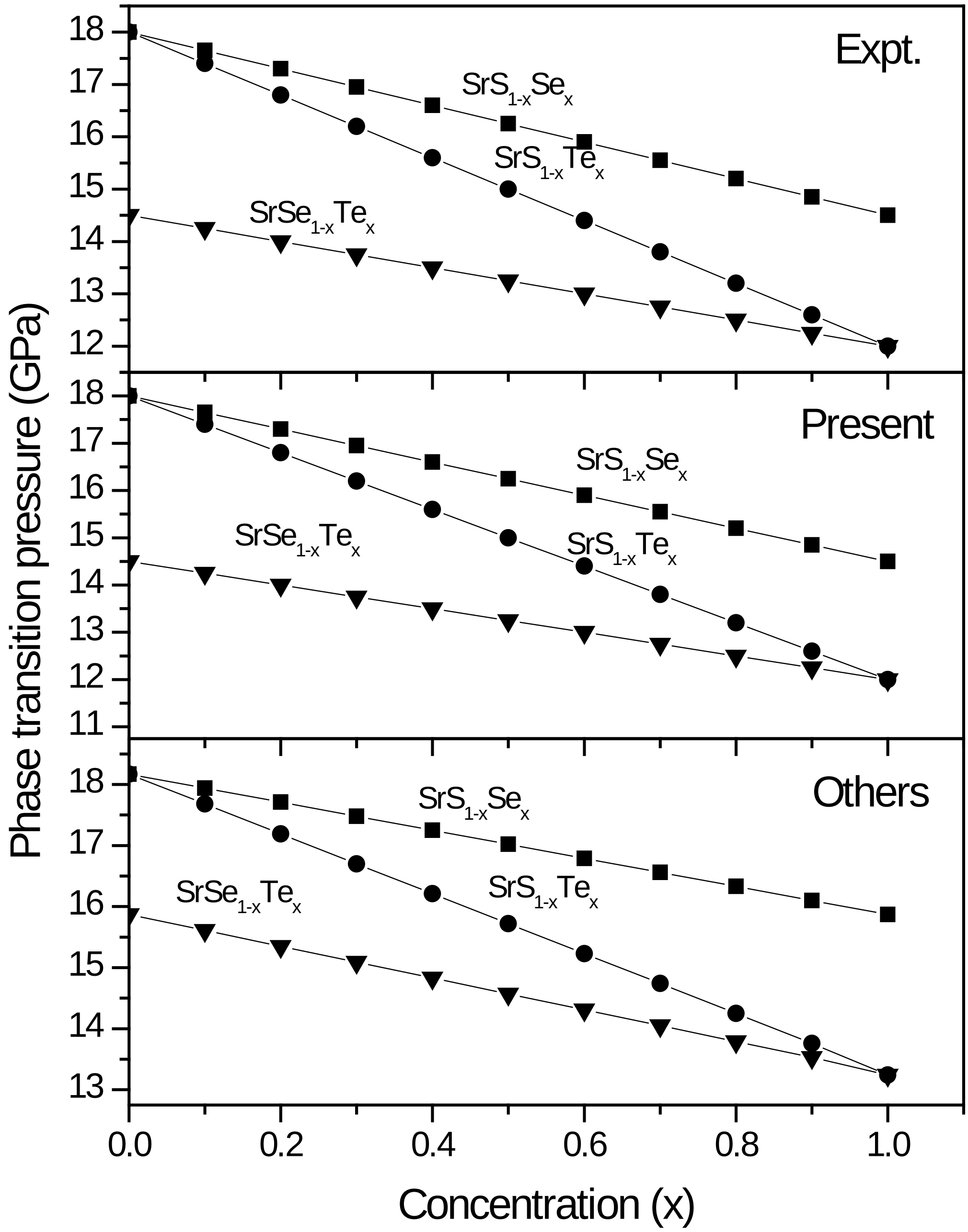
Expt.
Present
Others
SrS1-xSex
SrS1-xTex
SrSe1-xTex
Phase transition pressure (GPa)
Concentration (x)
0.0
0.2
0.4
0.6
0.8
1.0

Fig 2.

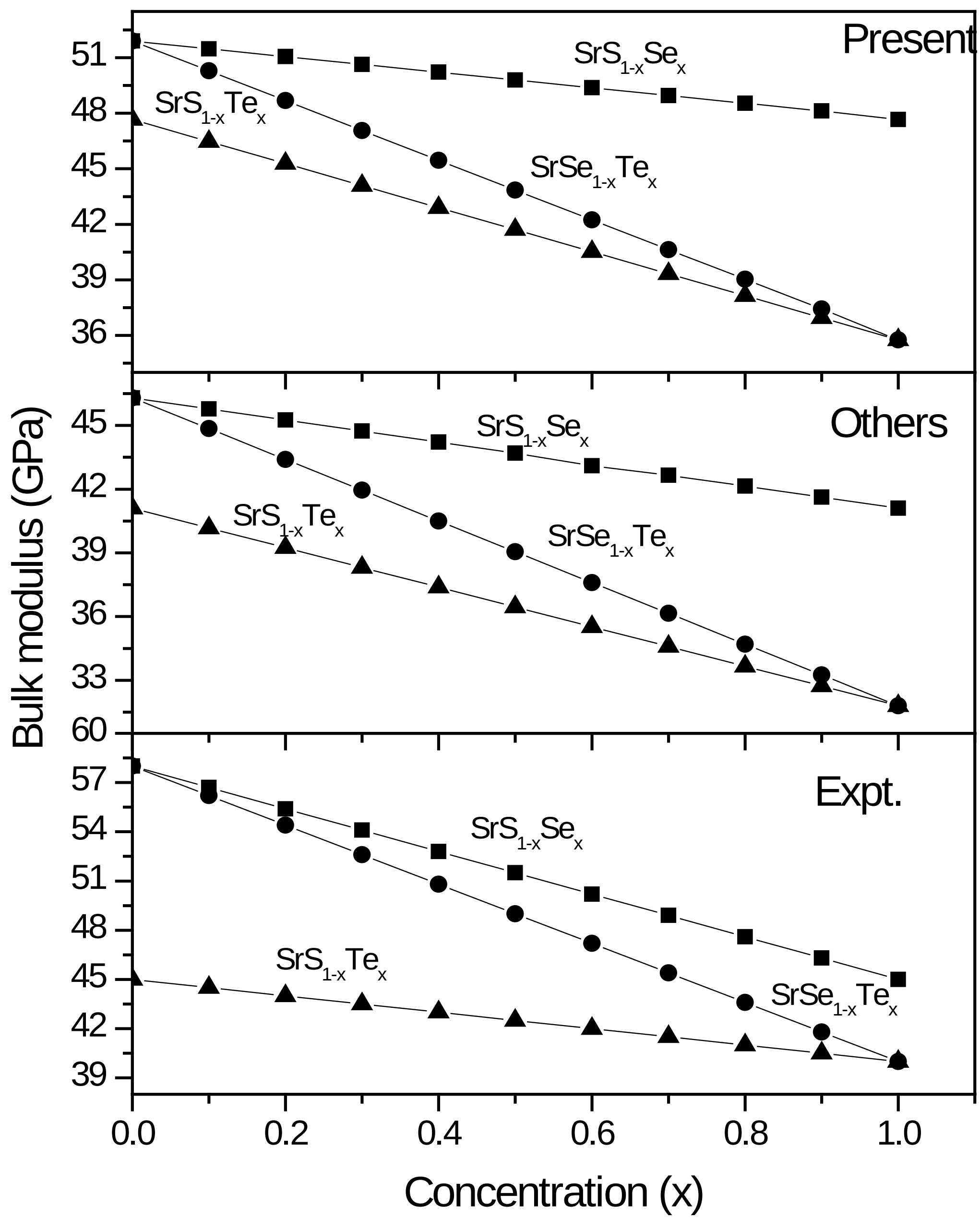
Present
$SrS_{1-x}Se_x$
$SrS_{1-x}Te_x$
$SrSe_{1-x}Te_x$
Others
$SrS_{1-x}Se_x$
$SrS_{1-x}Te_x$
$SrSe_{1-x}Te_x$
Expt.
$SrS_{1-x}Se_x$
$SrS_{1-x}Te_x$
$SrSe_{1-x}Te_x$
Bulk modulus (GPa)
Concentration (x)
0.0
0.2
0.4
0.6
0.8
1.0
51
48
45
42
39
36
45
42
39
36
33
60
57
54
51
48
45
42
39

Fig 3.

This page is intentionally left blank

Global Journal of Science Frontier Research
Physics & Space Science
Volume 12 Issue 1 Version 1.0 January 2012
Type : Double Blind Peer Reviewed International Research Journal
Publisher: Global Journals Inc. (USA)
Online ISSN: 2249-4626 & Print ISSN: 0975-5896

Empirical Model for the Estimation of Global Solar Radiation in Makurdi, Nigeria

By Isikwue, B.C., Amah, A.N., Agada, P. O.
Federal University of Agriculture Makurdi, Benue State, Nigeria

Abstract - This work proposes the coefficients for Angstrom - Prescott type of model for the estimation of global solar radiation in Makurdi, Nigeria using relative sunshine duration alongside the measured global solar radiation data (2001-2010). The model constants a and b obtained in this investigation for Makurdi are .138 and 0.488 respectively. The correlation coefficient of 89% (P=0.00) between the clear sky index and relative sunshine duration, as well as the coefficient of determination, R2 of 79.5 obtained shows that this model fits the data very well. Hence, the very low mean standard error of 0.025 showed a good agreement between the measured and estimated global solar radiation. Consequently, the developed model in this work can be used with confidence for Makurdi, and other locations with similar climate conditions.

Keywords : global solar radiation, extraterrestrial radiation, solar constant, clear sky index, sunshine hours, empirical model and Makurdi, Nigeria.

GJSFR-A Classification : FOR Code: 020109

EMPIRICAL MODEL FOR THE ESTIMATION OF GLOBAL SOLAR RADIATION IN MAKURDI, NIGERIA

Strictly as per the compliance and regulations of :

Empirical Model for the Estimation of Global Solar Radiation in Makurdi, Nigeria

Isikwue, B.C.[α], Amah, A.N.[Ω], Agada, P. O.[β]

Abstract - This work proposes the coefficients for Angstrom - Prescott type of model for the estimation of global solar radiation in Makurdi, Nigeria using relative sunshine duration alongside the measured global solar radiation data (2001-2010). The model constants a and b obtained in this investigation for Makurdi are .138 and 0.488 respectively. The correlation coefficient of 89% (P=0.00) between the clear sky index and relative sunshine duration, as well as the coefficient of determination, R^2 of 79.5 obtained shows that this model fits the data very well. Hence, the very low mean standard error of 0.025 showed a good agreement between the measured and estimated global solar radiation. Consequently, the developed model in this work can be used with confidence for Makurdi, and other locations with similar climate conditions.

Keywords : global solar radiation, extraterrestrial radiation, solar constant, clear sky index, sunshine hours, empirical model and Makurdi, Nigeria.

I. Introduction

The high dependence on the depleting fossil fuel energy in Nigeria may not meet up with the increasing demand for energy, hence the need for the alternating source of energy. The widely used renewable resources are solar and wind energies

However, the facilities for global solar radiation measurement are available only in few locations in the country. Consequently, there in need to use some empirical relations to estimate global solar radiations from some measured meteorological parameters, such as relative sunshine hours.

There are various models for estimating solar radiation using relative sunshine durations and other meteorological data. The commonly used model which relates the global solar radiation to sunshine duration was first developed by Angstrom [1]. Subsequently, other models [2, 3] were developed.

In Nigeria several researches have been carried out for estimating solar radiation at different locations [4 - 9]. However, none has been found in the literature of the models developed for estimating global solar radiation for Makurdi and its environs of similar meteorological parameters. Hence this work is aimed at developing an Angstrom-type of empirical model for the estimation of global solar radiation for Makurdi and other surrounding towns of similar meteorological conditions.

Author α Ω : Department of Physics, Federal University of Agriculture Makurdi, Benue State, Nigeria.
Author β : Department of Maths /Statistics /Computer science, Federal University of Agriculture Makurdi, Benue State, Nigeria.

Makurdi, having an area of about 33.16 km^2 is located at latitude 7°.41' N and longitude 8°.37'E. It is the capital of Benue State, Nigeria, having a population of as about 297, 398 people. Makurdi is noted for its hotness during the dry season with an average air temperature of about 33 °C. This high temperature is attributed to the presence of River Benue (the second largest river in Nigeria) which cuts across the middle of the city, and serves a heat reservoir. This work will help in utilizing the solar energy potential to solve the energy problems in the state. The global solar radiation and sunshine hour data used in this research was obtained from the Gunn - Bellani radiation integrator, Air force Base Makurdi, Nigeria located at an altitude of about 106.4 m.

II. Methodology

The Angstrom- Prescott regression equation which has been used to estimate the monthly average daily solar radiation on a horizontal surface in Nigeria or other places is given as

$$\frac{\bar{H}_m}{\bar{H}_o} = a + b\left(\frac{\bar{n}}{\bar{N}}\right) \qquad (1)$$

$\bar{H}_m$ is the monthly average daily global solar radiation measured on a horizontal surface (M J m^{-2} day^{-1}); $\bar{H}_o$ is the monthly average daily extraterrestrial solar radiation measured on a horizontal surface (M J m^{-2} day^{-1}); $\bar{n}$ is the monthly average daily number of hours of bright sunshine; $\bar{N}$ is the monthly average daily maximum number of hours of possible sunshine (or day length); and **a** and **b** are regression constants to be determined.

Values of $\bar{N}$ are computed from Cooper's formula [10]:

$$\bar{N} = \left(\frac{2}{15}\right)\cos^{-1}(-\tan\Phi\tan\delta) \qquad (2)$$

$\bar{H}_o$ was obtained from [7] as

$$\bar{H}_o = \frac{24}{\pi} I_{sc}\left(1 + 0.33\cos\frac{360\bar{n}}{365}\right)\left(\cos\Phi\cos\delta\sin w_s + \frac{2\pi w_s}{360}\sin\Phi\sin\delta\right) \qquad (3)$$

$w_{s\ and\ \delta}$ are sunset hour angle and solar declination respectively and are defined as

$$w_s = \cos^{-1}[\cos(-\tan\Phi\tan\delta)) \qquad (4)$$

$$\delta = 23.45\sin\left(360\,\frac{284+d}{365}\right) \qquad (5)$$

d is the day of year (known as the Julian day).Usually, the solar declination is calculated on the 15th of each month.

In this work, $\bar{H}_o$ and $\bar{N}$ were computed for each month using equations (2) and (3). The values of the monthly average daily global solar radiation, $\bar{H}_m$ and $\bar{n}$ were obtained from daily measurements covering a period of nine (9) years. The SPSS computer software was applied to obtain the regression constants **a** and **b**. Mean Bias Error (MBE) was also obtained to assess the validity of estimation made through equations (1)

III. Result and Discussion

The input parameters used in this analysis are presented in Table 1.

Month	$\bar{H}_m$	$\bar{H}_o$	$\frac{\bar{H}_m}{\bar{H}_o}$	$\frac{\bar{n}}{\bar{N}}$
Jan	14.055	33.255	0.423	0.620
Feb	15.618	35.572	0.439	0.563
Mar	15.555	37.446	0.415	0.578
Apr	14.792	38.085	0.389	0.603
May	14.355	37.271	0.385	0.558
June	13.655	36.462	0.375	0.495
July	12.009	37.348	0.322	0.402
Aug	11.355	37.490	0.303	0.348
Sept	13.064	37.566	0.348	0.399
Oct	14.864	36.015	0.413	0.517
Nov	15.691	33.666	0.467	0.592
Dec	15.264	32.379	0.471	0.648

Table 1 : input parameters for estimation of monthly daily global solar radiation for Makurdi, Nigeria

The model constants, **a** and **b** obtained in this investigation were **0.138** and **0.488** respectively. Hence the first order polynomial developed for Makurdi is

$$\frac{\bar{H}_m}{\bar{H}_o} = 0.138 + 0.488\left(\frac{\bar{n}}{\bar{N}}\right) \qquad (6)$$

The coefficient of determination, R^2 of **79.5** obtained for this analysis shows that this model fits the data very well. The relationship between the relative sunshine duration, $\frac{\bar{n}}{\bar{N}}$ and clear sky index (K_T) or $\frac{\bar{H}_m}{\bar{H}_o}$ for Makurdi are presented in Figure 1

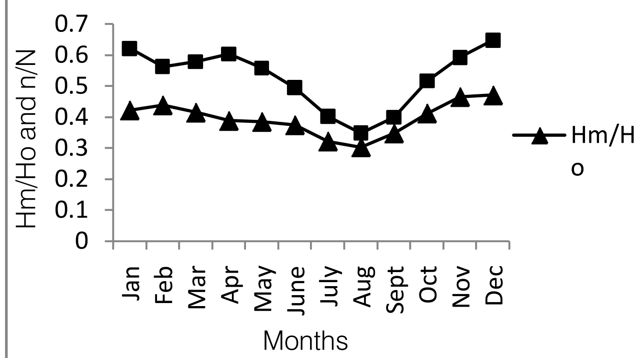

Fig. 1 : Relationship between the clearness index and the relative sunshine duration in Makurdi, Nigeria

The value of K_T (=0.303) corresponding to the lowest value of $\frac{\bar{n}}{\bar{N}}$ (=0 .348) and $\bar{H}_m$ (=11.355 (M J m $^{-2}$ day $^{-1}$) in the month of August indicate poor sky conditions. These conditions correspond to the wet or rainy season (June -September) observed in Nigeria during which there is much cloud cover. Hence, the correlation coefficient between K_T and $\frac{\bar{n}}{\bar{N}}$ is as high as 89% (p=0.00). Figure 2 demonstrates the relationship between the measured and the estimated global solar radiation

Observation from Fig. 2 shows that both the estimated and the measured vary correspondingly except in February, May and April, where they respectively exhibit under estimation and over estimation of the predicted values. This could be due to variability in atmospheric parameters during the measurement. However, the estimated value of the global solar radiation correlates well with the measured, hence, the Means Standard Error (MSE) between the measured and the estimated global solar radiation is as 0.025. This shows a good agreement between the measured and estimated values.

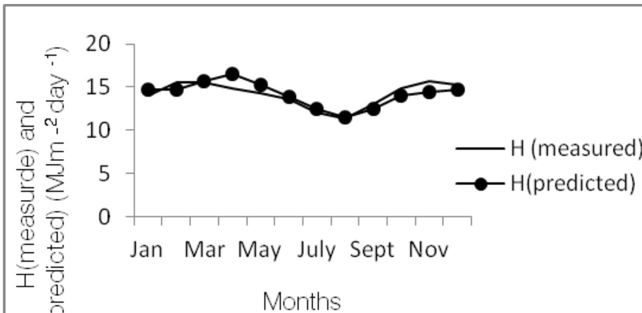

Fig. 2 : Relationship between the and measured the estimated monthly average daily global solar radiations in Makurdi, Naigeria

Figure 2 also shows that the maximum solar radiation in Makurdi, were obtained for the period 2001-2010 in (February – March) and (October- November). In the rainy season, the lowest solar radiation was obtained in August (probably due to rain bearing clouds which pervaded the sky), where as in the dry season, the highest was measured in November and the lowest in December and January (probably due to hamartan dust which scattered the solar radiation at that time.

Under clear perfect sky condition, the transmission of the atmosphere for global; solar radiation is given as the sum of the regression coefficients a + b, where as the transmissivity of an over cast atmosphere is interpreted as the intercept a. From this investigation, the atmosphere transmissivity, under clear sky for Makurdi is obtained as 0.63 which compares well with the values of 0. 67, 0.70 reported for humid to tropics [7].

The best month, November with $\overline{H}_m$ of 15.69 M J m $^{-2}$ day $^{-1}$ contributed about 9 % of the annual total, while the worst month, August, with $\overline{H}_m$ of 11.36 M J m $^{-2}$ day $^{-1}$ contributed 7 % of the annual total.

Finally our model fits adequately with the radiation data presented in Table 1. Consequently, equation (6) can be used with confidence for Makurdi, and other locations with similar climate conditions.

References Références Referencias

1. A. S. Angstrom, "Solar and Terrestrial Radiation" Q.J.Roy. Met. Soc. 50, Pp. 126, 1924
2. J. A. Prescott , "Evaporation from a Water Surface in Relation to Solar Radiation", Trans. R Soc. Austr. pp 114 – 118, 1940.
3. J. N. Black, C.W. Bonython and J. A. Prescott, "Solar Radiation and Duration of Sunshine," Q. J. R. Meteoro. Soc. 80, pp 231 - 235, 1954.
4. A.S.Sambo, "Empirical Model for the Correlation of Global Solar Radiation with Meteorological Data for Northern Nigeria," Solar and Wind Technology vol. 3 no. 2 pp 89 - 93, 1986.
5. F .W. Burari and A. S. Sambo, "Model for the Prediction of Global Solar Radiation for Bauchi, Using Meteorological Data", Nigeria Journal of Renewable Energy, vol. 91 pp 30 - 33, 2001.
6. E.C.Okogbue and J.A Adedokun, "On the Estimation of Solar Radiation at Ondo, Nigeria", Journal of Physics, vol.14, pp 97 - 99, 2002.
7. L .E. Akpabio and S. E. Etuk, "Relationship between Global Solar Radiation and Sunshine Duration for Onne, Nigeria", Turkish Journal of Physics, vol. 27, pp 161 - 167, 2003.
8. L .E. Akpabio; S .O Udo, and S. E Etuk, "Empirical Correlations of Global Solar Radiation with Meterological Data for Onne, Nigeria", Turkish Journal of Physics, vol. 28, no.3, pp 301 - 3o7, 2004
9. E.O. Falayi; J.O. Adepitan and A.B. Rabiu, "Empirical Models for the Correlation of Global Solar Radiation with Meteorological Data for Iseyin, Nigeria,' International Journal of Physical Sciences, vol. 3, no. 9, pp 210 - 216, 2008.
10. P. I Cooper, "The Absorption of Radiation on Solar Stills", Solar Energy, vol. 12, no. 3, pp 333 - 346, 1969.

This page is intentionally left blank

Global Journal of Science Frontier Research
Physics & Space Science
Volume 12 Issue 1 Version 1.0 January 2012
Type : Double Blind Peer Reviewed International Research Journal
Publisher: Global Journals Inc. (USA)
Online ISSN: 2249-4626 & Print ISSN: 0975-5896

Study of additional heating Systems by Electron cyclotron and Alfven waves in Tokamak Machine

By Naima Ghoutia Sabri, Tayeb Benouaz

University of Bechar, Bechar, Algeria

Abstract - Electron cyclotron (EC) absorption in tokamak plasma is based on interaction between wave and electron cyclotron movement when the electron passes through a layer of resonance at a fixed frequency and dependent magnetic field. This technique is the principle of additional heating (ECRH) and the generation of non-inductive current drive (ECCD) in modern fusion devices. In this paper we are interested by the problem of EC absorption which used a microscopic description of kinetic theory treatment versus the propagation which used the cold plasma description. The power absorbed depends on the optical depth which in turn depends on coefficient of absorption and the order of the excited harmonic for O-mode or X-mode. There is another possibility of heating by dissipation of Alfven waves, based on resonance of cold plasma waves, the shear Alfven wave (SW) and the compressional Alfven wave (FW). Once the (FW) power is coupled to (SW), it stays on the magnetic surface and dissipates there, which is cause the heating of bulk plasmas. This present calculation allows us to compare the two heating systems.

Keywords : electron cyclotron, additional heating, plasma, Alfven waves, resonance.

GJSFR-A Classification : 020201

STUDY OF ADDITIONAL HEATING SYSTEMS BY ELECTRON CYCLOTRON AND ALFVEN WAVES IN TOKAMAK MACHINE

Strictly as per the compliance and regulations of :

Study of additional heating Systems by Electron cyclotron and Alfven waves in Tokamak Machine

Naima Ghoutia Sabri[α], Tayeb Benouaz[Ω]

Abstract - Electron cyclotron (EC) absorption in tokamak plasma is based on interaction between wave and electron cyclotron movement when the electron passes through a layer of resonance at a fixed frequency and dependent magnetic field. This technique is the principle of additional heating (ECRH) and the generation of non-inductive current drive (ECCD) in modern fusion devices. In this paper we are interested by the problem of EC absorption which used a microscopic description of kinetic theory treatment versus the propagation which used the cold plasma description. The power absorbed depends on the optical depth which in turn depends on coefficient of absorption and the order of the excited harmonic for O-mode or X-mode. There is another possibility of heating by dissipation of Alfven waves, based on resonance of cold plasma waves, the shear Alfven wave (SW) and the compressional Alfven wave (FW). Once the (FW) power is coupled to (SW), it stays on the magnetic surface and dissipates there, which is cause the heating of bulk plasmas. This present calculation allows us to compare the two heating systems.

Keywords : electron cyclotron, additional heating, plasma, Alfven waves, resonance.

I. Introduction

Energy is essential to whole life; is a major scientific and strategic challenge to discover a new method of energy production that has an impact as low as possible on health, and the environment and the overall functioning of the planet, with sufficient energy to several million years. Energy produced from thermonuclear fusion reactions had been known for some decades in the sun and stars, is likely safe and doesn't produce greenhouse gas emissions and its radioactive wastes is less expensive to manage. These reactions require special conditions of temperature (100 million degrees) and pressure. In this case, the more promoter configuration to realize them is tokamak which is a machine governed by Lawson criterion (Sabri. N.G, 2010), (n density, T temperature and t_E confinement time) and to achieve these high temperatures, it is necessary to heat the plasma.

The ohmic regime is the first natural heating mechanism. Unfortunately, this effect is proportional to the resistance of the plasma which tends to collapse when the temperature increases. We therefore use additional heating systems. Radio-frequency heating (Wang[†] .S and Tang. J, 2004) is one of important of these systems. It is based on the phenomenon of wave-particle resonance where the waves can be transferred their energy to the charged particles in the plasma, which in turn collide with other plasma particles, thus increasing the temperature of the bulk plasma.

The injection of electron-cyclotron (EC) waves is nowadays a well-established method for coupling energy to plasma electrons in modern fusion devices (Harvey. R.W. and al., 1996, Mandrin. P., 1999), with primary applications the plasma heating ECRH (Electron Cyclotron Resonance Heating),(Arnoux. G., 2005) and the generation of non-inductive current drive ECCD (Electron Cyclotron Current Drive), (Dumont. R., 2001, Nikkola .P, 2004).

In this sense, the ECRH studies are formally split in the experiments involving the injection of EC waves on the one hand, and on the other in the theoretical investigations related to the propagation (Fontanesi. M and Bernabei. P, 1971) and absorption (Orefice. A, 1988), of the radiation. With respect to the theory, it is very important to have a quantitative model for the way the wave propagates and is absorbed inside the plasma (Bornaciti. M, 1982), as well as for the effects the resonant electrons have on the wave. The cold plasma model is used to describe the propagation (Stix. T.H, 1962), and the absorption is described with kinetic model (Rönnmark. K. G., 1985).

The Alfvén wave is a fundamental electromagnetic oscillation in magnetically confined plasmas. Alfvén waves can be either excited spontaneously by instabilities or driven by external sources. It is also believed that Alfvén waves play a crucial role in the heating of bulk plasmas in both magnetic fusion devices and the solar corona. The Alfvén waves band are divided into slow shear Alfven wave (SW) (Appert, 1986) and the fast compressional Alfven wave (FW), (Cross. R. C and Lehane. J. A., 1967).

Heating plasma by resonant absorption of Alfvén waves is a technique that combines low-frequency conventional technology and low cost of installed capacity. The TCA Tokamak, acronym of heating in tokamak Alfven wave. The TCA/Sw refers to

Author [α] : University of Bechar, POB 417, Street of Kenadsa, 080000, Bechar, Algeria. Telephone: +213.7.73.14.69.65,
E-mail : sabri_nm@yahoo.fr
Author [Ω] : University of Abou bekr Belkai, Tlemcen, POB119, 13000, Tlemcen, Algeria. Telephone:+213.43.21.59.99 ,
E-mail : b_tayeb@yahoo.com

Global Journal of Science Frontier Research (A) Volume XII Issue I Version I January 2012

the circular section tokamak of CRPP (Center for Research in Plasma Physics, Switzerland) with the main objective is to investigate the possibility of plasma heating by dissipation of Alfven waves (Cheethan 1980, TCA Team 1985, Chambrier. A. D., 1987) and TCA/Br refers to the Brazilian tokamak with Alfvén wave heating (Elfimov. A. G. and al. 1995, Ruchlto. L and al, 1994) is the largest machine and the most powerful and best equipped in diagnostics which provided the most detailed results on the spectrum and heating by Alfven waves. Its purpose is to study the excitation and absorption Alfvén waves in plasma (Hasegawa, 1975, 1982), showing the usefulness of these waves in the additional heating.

In this paper, we examine in some depth, two types of plasma additional heating systems in a tokamak machine. The emphasis is on electron cyclotron heating. First, we briefly come back to the main non-collisional heating mechanisms and to the particular features of the quasilinear theory absorption in the electron cyclotron range of frequencies (ECRF). Then, the Alfvén wave heating is covered more briefly. Where applicable, the prospects for ITER are commented.

II. Wave Propagation

a) *Cold Plasma*

In this approximation the plasma pressure is assumed very small compared to the magnetic pressure $\beta \ll 1$. Where The parameter β represents the ratio of thermal pressure (kinetic) $p = nk_BT$ and the magnetic pressure $B^2/2\mu_0$. With k_B is the Boltzmann constant; T and n are respectively the temperature and the density of electrons. B is the magnetic field and μ_0 the magnetic permeability in vacuum. In this case the thermal motion of electrons may be negligible in terms of oscillations of the wave $v_\varphi \gg v_{th}$ where v_φ is the phase velocity of the wave and v_{th} is the thermal velocity of electrons and the Larmor radius is small compared to the wavelength (Bertrand. P, 2004). The relation between $\vec{j}$ and $\vec{E}$ can be written as

$$\vec{j}(\vec{k},\omega) = \bar{\bar{\sigma}}(\vec{k},\omega).\vec{E}(\vec{k},\omega) \quad (1)$$

Where $\vec{k}$ is the wave vector, $\bar{\bar{\sigma}}$ is the conductivity of the plasma that is a tensor in case of anisotropic plasma. Considering plane wave solutions of Maxwell's equations, such as fluctuating quantities vary as $exp\,(i\,(\vec{k}\,.\vec{r} - \omega t))$. In Fourier space, we can find from the Maxwell's equations a wave equation of the form (Moncuque. M, 2001):

$$k^2\vec{E} - \vec{k}(\vec{k}\vec{E}) - \left(\frac{\omega^2}{c^2}\right)\vec{D} = 0 \quad (2)$$

Where $\vec{D} = \bar{\bar{K}}\vec{E}$ is the electrical induction vector, $\bar{\bar{K}}$ is the dielectric tensor (permittivity), $\vec{E}$ is the vector of wave electric field. In the cold plasma approximation, the dielectric tensor $\bar{\bar{K}}$ can be written in the following matrix form (Sabri. N.G, 2010, Moncuque. M, 2001) :

$$\bar{\bar{K}} = \begin{pmatrix} S & -iD & 0 \\ iD & S & 0 \\ 0 & 0 & P \end{pmatrix} \quad (3)$$

Where in the domain of electron cyclotron wave frequency $(\omega \gg \omega_{ci}, \omega_{pi})$, S, D and P are given by

$$S = 1 - \frac{\omega_{pe}^2}{(\omega^2 - \omega_{ce}^2)} \quad (4)$$

$$D = -i\frac{\omega_{ce}}{\omega}\frac{\omega_{pe}^2}{(\omega^2 - \omega_{ce}^2)} \quad (5)$$

$$P = 1 - \frac{\omega_p^2}{\omega^2} \quad (6)$$

$$R = 1 - \frac{\omega_p^2}{\omega(\omega+\omega_c)}\,;\; L = 1 - \frac{\omega_p^2}{\omega(\omega-\omega_c)} \quad (7)$$

With $\omega_{pe}^2 = \frac{4\pi n_e e^2}{m_e}$, $\omega_{ce} = \frac{eB_0}{m_e c}$. Where n_e is the electron density, $-e$ the electron charge and m_e its mass.

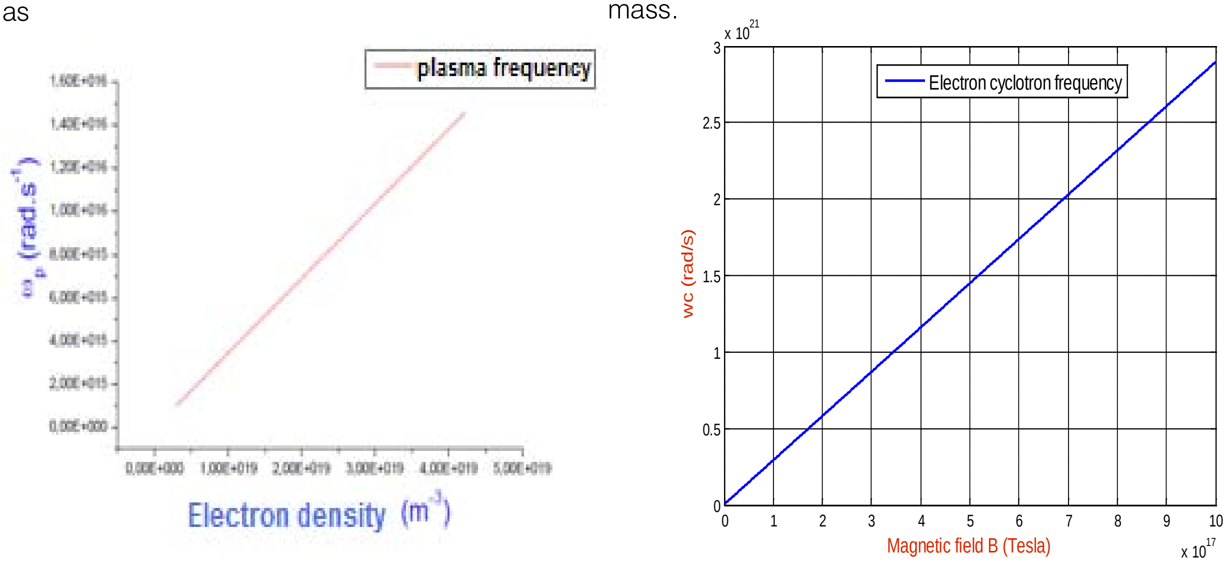

Fig.1 : Description of above image : the figure describes in (a) the plasma frequency as a function of density and in (b) the electron cyclotron frequency as a function of .

As the refractive index $\vec{N}$ is written $\vec{N} = \frac{\omega}{c}\vec{k}$; the equation (2) becomes $\bar{\bar{M}}_{k,\omega}\vec{E} = \vec{N}\wedge\vec{N}\wedge\vec{E} + \bar{\bar{K}}.\vec{E} = 0$ and the nontrivial solutions are obtained for: $\det\left(\bar{\bar{M}}_{k,\omega}\right) = 0$, such as $\bar{\bar{M}}_{k,\omega}$ is a matrix representing the operator $\left(\vec{k}\wedge\vec{k}\wedge\square + \frac{\omega^2}{c^2}\bar{\bar{K}}.\square\right)$. So we can write:

$$\begin{pmatrix} S - N^2cos^2\theta & -iD & N^2cos^2\theta sin^2\theta \\ iD & S - N^2 & 0 \\ N^2cos^2\theta sin^2\theta & 0 & P - N^2sin^2\theta \end{pmatrix}\begin{pmatrix} E_x \\ E_y \\ E_z \end{pmatrix} = 0 \quad (8)$$

The following system may take the form of the dispersion equation as follows:

$$AN^4 + BN^2 + C = 0 \quad (9)$$

With $A = Ssin^2\theta + Pcos^2\theta$, $B = RLsin^2\theta + PS(1 + cos^2\theta)$ and $C = PRL$.

To generate current, the power of the electron cyclotron wave must be effectively absorbed by the plasma. However, the quality of the interaction depends on the state of polarization of this wave. It is useful, in this frequency range, using a proper mode (ordinary or extraordinary), chosen according to the plasma conditions, and assume that it propagates up the resonance without modification. In the case of perpendicular propagation to magnetic field ($N_{II} = 0$).

We obtain two solutions of equation (9) for the perpendicular refractive index, which can be written:

$$N_O^2 = P = 1 - \frac{\omega_p^2}{\omega^2}, \quad (10)$$

$$N_X^2 = \frac{S^2 - D^2}{S} = 1 - \frac{\omega_{pe}^2}{\omega^2}\frac{(\omega^2 - \omega_{pe}^2)}{(\omega^2 - \omega_{pe}^2 - \omega_{ce}^2)} \quad (11)$$

These electromagnetic solutions are well known by the names of ordinary mode (O) and extraordinary (X),(Sabri, N.G & Benouaz T, 2011).

- The ordinary mode (O): The electric field is parallel to the confining magnetic field and transverse$(\vec{E}\perp\vec{k})$. This mode does not have any resonance and propagate for $\omega > \omega_{pe}$ because of the cut-off.
- The extraordinary mode (X): The electric field is elliptically polarized in the perpendicular plane to $\overrightarrow{B_0}$. This mode has two cut-offs and two resonances.

According to the phase velocity ω/k, there are two modes X, fast (F) and slow (S) as it is shown in Figure 2 and in Figure 3. This figure shows the dispersion relations of ordinary (O) and extraordinary (X) fast (F) and slow (S) waves propagating across the magnetic field.

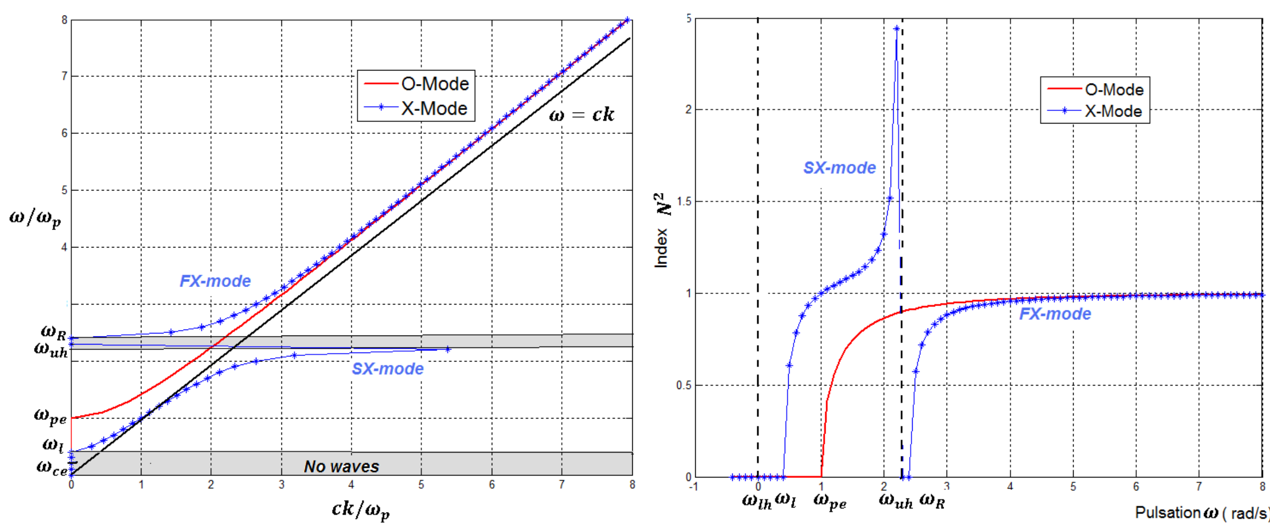

Fig.2 : (a) The dispersion diagram (b) $N^2 = f(\omega)$ for perpendicular propagation

The electron temperature, coupled with their average speed, such as

$$k_\perp\rho_L = N_\perp n\sqrt{k_B T_e/(m_e c^2)} \quad (12)$$

Where $N_\perp = k_\perp c/\omega$ is the refractive index of the wave in plasma. The two branches of propagation (ordinary and extraordinary) appear and we can see that the ordinary mode propagates for frequencies such that $\omega > \omega_{pe}$. The extraordinary mode is propagative for $\omega_L < \omega < \omega_{uh}$, evanescent for $\omega_{uh} < \omega < \omega_R$. It becomes propagative when $\omega > \omega_R$. With ω_R, ω_L are the cutoff frequencies of the X mode, called right and left modes, defined by:

$$\omega_{R,L} = \frac{1}{2}\left[\mp\omega_c + \left(\omega_c^2 + 4\omega_p^2\right)^{1/2}\right] \quad (13)$$

The X mode has a cold resonance ($N_\perp \to \infty$), given by:

$$\omega_{uh} = \sqrt{\omega_c^2 + \omega_p^2} \quad (14)$$

Global Journal of Science Frontier Research (A) Volume XII Issue I Version I January 2012

This resonance is called upper hybrid (UH) is not available if $\omega > \omega_c$. There is also a lower hybrid resonance (Swanson. D.G, 1989), it is well below the electron cyclotron frequency domain and therefore not interferes here.

b) Electron Cyclotron Wave Absorption

The cyclotron resonance is, in principle, an interaction between the wave and particle motion (see Figure 3).

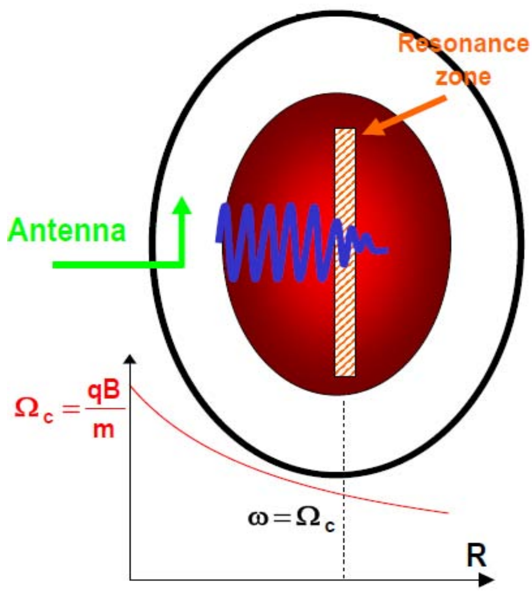

Fig.3 : The principle of EC heating.

In other words, it involves the microscopic structure of the plasma. We shall use the kinetic theory (as opposed to the fluid theory), to accurately reflect the phenomena occurring at the particle scale.

The hot plasma model under certain approximations, leads to a new expression of dielectric tensor that can be expressed by a correction of the type:

$$\overline{\overline{K}}_{hot} = \overline{\overline{K}}_{cold}\left(\omega, B_0, n_{e,0}\right) + \widetilde{K}\left(\omega, B_0, n_{e,0}, T_{e,0}\right) \tag{15}$$

The hot correction $\widetilde{K}$ depends explicitly on the wave vector $\vec{k}$ and the electron temperature at equilibrium, $T_{e,0}$. To calculate the elements of $\overline{\overline{K}}_{hot}$, we start from the relativistic Vlasov equation (Arnoux. G, 2005, Dumont. R, 2001). In the relativistic formalism, the distribution function of electrons is written as $f_e(\vec{r},\vec{p},t)$ with the relation $\vec{p} = m_{e,0}.\gamma.\vec{v}$ where $m_{e,0}$ is rest mass. The distribution function is solution of the relativistic Vlasov equation given by:

$$\frac{\partial f_e}{\partial t} + \frac{\vec{p}}{m_e\gamma}\frac{\partial f_e}{\partial \vec{r}} - e\left(\vec{E} + \frac{1}{m_e\gamma}\vec{p}\wedge\vec{B}\right)\frac{\partial f_e}{\partial \vec{p}} = 0 \tag{16}$$

Where $m_e^2 = m_{e,0}^2 + (p/c)^2 = m_{e,0}^2\gamma^2$ is the relativistic mass of the electron and $\gamma = 1/\sqrt{1 - (\mathrm{v}/c)^2}$ (Pochelon. A, 1994) , the relativistic Lorentz factor, $\gamma = 1$ for a non-relativistic plasma. The distribution function f_e is written as $f_e(\vec{r},\vec{p},t) = f_{e,0}(\vec{p}) + f_{e,1}(\vec{r},\vec{p},t)$ the sum of two distribution functions f_{e0} for equilibrium state and f_{e1} for the perturbed state. Similarly to distribution function f_e , the magnetic and electric fields (Baea, Y.S, Namkung, W, 2004), can be written as $\vec{B} = \overrightarrow{B_0} + \overrightarrow{B_1}$ and $\vec{E} = 0 + \overrightarrow{E_1}$. A perturbed state of linearized Vlasov equation takes the form

$$\frac{\partial \mathrm{f}_{e,1}}{\partial t} + \frac{\vec{\mathrm{p}}}{\mathrm{m_e}}\frac{\partial \mathrm{f}_{e,1}}{\partial \vec{\mathrm{r}}} + \frac{\mathrm{e}}{\mathrm{m_e}}\left(\vec{\mathrm{p}} \wedge \overrightarrow{\mathrm{B}_0}\right)\frac{\partial \mathrm{f}_{e,1}}{\partial \vec{\mathrm{p}}} = -\mathrm{e}\left(\vec{\mathrm{E}} + \frac{\vec{\mathrm{p}}\wedge\vec{\mathrm{B}}_1}{\mathrm{m_e}}\right).\frac{\partial \mathrm{f}_{e,0}}{\partial \vec{\mathrm{p}}} \tag{17}$$

The integration of equation (17) gives the relativistic dielectric tensor:

$$K_{ij} = \delta_{ij} - \frac{\omega_p^2}{\omega^2}\frac{\mu^2}{2k_2(\mu)}\int_{-\infty}^{+\infty} d\overline{p}_{II}\int_0^{+\infty}\overline{p}_{\perp}d\overline{p}_{\perp}\frac{e^{-\mu\gamma}}{\gamma}U \tag{18}$$

$$U = \sum_{n=-\infty}^{n=\infty}\frac{P_{i,j}^n(p_\perp, p_{II})}{\gamma - n\frac{\omega_{ce}}{\omega} - n_{II}\overline{p}_{II}} \tag{19}$$

Where $\overline{p} = p/(m_{e,0}c) = \overline{p}_\perp + \overline{p}_{II}$, $n_{II} = ck_{II}/\omega$ is the index refraction for parallel direction to $\overrightarrow{B_0}$ and $k_n(z)$ is the modified Bessel function of second kind (or McDonald function) of index n (here $n = 2$) and argument z.

If we decompose respectively the dielectric tensor in hermitian and anti-hermitian parts as $\overline{\overline{K}} = \overline{\overline{K}}_h + i\overline{\overline{K}}_a$. And if one decompose the hot correction $\boldsymbol{\widetilde{K}}$ in real and imaginary part as $\widetilde{K} = \widetilde{K}' + i\widetilde{K}''$. The expression (15) can be written:

$$\overline{\overline{K}}_{hot} = \underbrace{\begin{pmatrix} S + \widetilde{K}_q{}' & -i\left(D - \widetilde{K}_q{}'\right) \\ i\left(D - \widetilde{K}_q{}'\right) & S + \widetilde{K}_q{}' \end{pmatrix}}_{hermitian} + i\underbrace{\begin{pmatrix} \widetilde{K}_q{}'' & i\widetilde{K}_q{}'' \\ -i\widetilde{K}_q{}'' & \widetilde{K}_q{}'' \end{pmatrix}}_{anti-hermitian} \tag{20}$$

It can be shown that the first hermitian part $\overline{\overline{K}}_h$ characterizes the propagation while the second anti-hermitian part $\overline{\overline{K}}_a$ characterizes the absorption (Swanson. D.G, 1989). If $T_e \to 0$, we obtain $\overline{\overline{K}}_a = 0$ and $\overline{\overline{K}}_h = \overline{\overline{K}}_{cold}$; which justifies the use of the cold approximation to describe wave propagation (Brambilla. M , 1998).

c) The Relation of Relativistic Resonance

The relation of resonance is given by the relativistic resonance condition as follows:

$$\gamma - k_{II}v_{II} - n\frac{\omega_{c,0}}{\omega} = 0 \tag{21}$$

The term $k_{II}v_{II}$ describes longitudinal Doppler shift [9], $(k_{II} \neq 0)$. The term $n\omega_{ce}/\omega$ describes the gyration of the electron; n is the order of the harmonic excited. This relation expresses the equality between the frequency of the wave and the relativistic cyclotron frequency of rotation corrected by the Doppler shift which caused by the electron parallel velocity. The energy of resonant electrons at ω_{ce} and given n_{II} can be written as:

$$E = m_e c^2 (k_{II} v_{II} + n\frac{\omega_{ce}}{\omega} - 1) \qquad (22)$$

An increase of the electron parallel velocity of the quantity Δv_{II} translates into a gain in elementary current $\Delta j = -e\Delta v_{II}$. Energy expense is increased by the electron $\Delta E = m_e . v_{II} . \Delta v_{II}$. So we deduce

$$\Delta j = e\frac{\Delta E}{me.v_{II}} \qquad (23)$$

This relation translates the generation of electron cyclotron current drive (ECCD) which is an important tool for current profile shaping in magnetically confined plasmas, thanks to the highly localized power deposition of the EC wave and the ease of external control of its deposition location.

d) Absorption Coefficient

We take the viewpoint of geometrical optics by considering a plane monochromatic wave type $\vec{E}(\vec{r},t) = \vec{E}(\vec{k},\omega)\, exp\{i[\vec{k}.\vec{r} - \omega t]\}$ for which one trying to describe the dissipation by introducing the concept of absorption coefficient. For there to be absorption, it is necessary that $k = k' + ik_a''$ avec the imaginary part of wave vector $k_a'' = (\omega/c)N'' \neq 0$. Then the absorption coefficient (Bornatici M. and al.,1983, Tsironis.C, Vlahos.L, 2006) is given by

$$\alpha = -2k_a''.\frac{\vec{v_g}}{v_g} \qquad (24)$$

With $\vec{v_g} = \frac{d\vec{r}}{dt}$ is the group velocity

For the explicit calculation of the absorption coefficient, we introduce a Another approach based on energy conservation, using the anti-Hermitian part of the dielectric tensor. Poynting's theorem (Sabri, N.G, Benouaz T.and Cheknane *A.*, 2009) writes:

$$\frac{\partial W_{0,t}}{\partial t} + \vec{\nabla}.\vec{S}_{0,t} = \frac{\partial}{\partial t}\frac{1}{2}\left(\frac{|\vec{B_t}|^2}{\mu_0} + \varepsilon_0|\vec{E}_t|^2\right) + \frac{1}{\mu_0}\vec{\nabla}.Re(\vec{E}_t \wedge \vec{B}_t) = -\vec{J}_t.\vec{E}_t \qquad (25)$$

$\partial W_{0,t}/\partial t$, contains respectively the magnetic $|B_t|^2/(2\mu_0)$ and electrostatic $\frac{1}{2}\varepsilon_0|E_t|^2$ energies. $\vec{S}_{0,t}$ is the instantaneous Poynting vector in vacuum describing the flow of electromagnetic energy. The source term, $-\vec{J}_t.\vec{E}_t$, describes the interactions of the wave with the plasma. By performing the time average over a few periods of oscillations: $\langle E_t \rangle t = E_1(\vec{r})\, exp(i\vec{k}.\vec{r})$, and separating explicitly the parties hermitian and antihermitienne of dielectric tensor introduced into the source term, we can be extracted from equation (25) the absorption coefficient:

$$\alpha = \frac{\varepsilon_0 \omega \vec{E_1^*} \bar{\bar{K}}_a \vec{E_1}}{|\vec{S}|} \qquad (26)$$

Where $\vec{E_1^*}$ is the complex conjugate of $\vec{E_1}$ and $\vec{S} = \vec{S}_0 + \vec{Q}_s$ with

$$\vec{S}_0 = \frac{1}{4\mu_0} Re(\vec{E}_1^* \wedge \vec{B}_1 + \vec{E}_1 \wedge \vec{B}_1^*) \qquad (27)$$

$$\vec{Q}_s = -\frac{1}{4}\varepsilon_0 \omega \vec{E}_1^* \frac{\partial \bar{\bar{K}}_h}{\partial k}.\vec{E}_1 \qquad (28)$$

And for wave polarized in X-mode, the absorbed power density is given by the numerator of (26) as:

$$D = \varepsilon_0 \omega \vec{E_1^*} \bar{\bar{K}}_a \vec{E_1} = \alpha|\vec{S}| \qquad (29)$$

A useful quantity is the optical depth τ (Arnoux. G, 2005, Westerhof. E, 2006 and Mandrin. P, 1999). [2], [15], [16], which is defined as the integral of the absorption coefficient α along the trajectory s of the wave: $\tau = \int -\alpha \, ds$. The total absorbed power P_{abs} in the plasma can then be written as

$$P_{abs} = P_{inj}\,(1 - exp(-\tau)) \qquad (30)$$

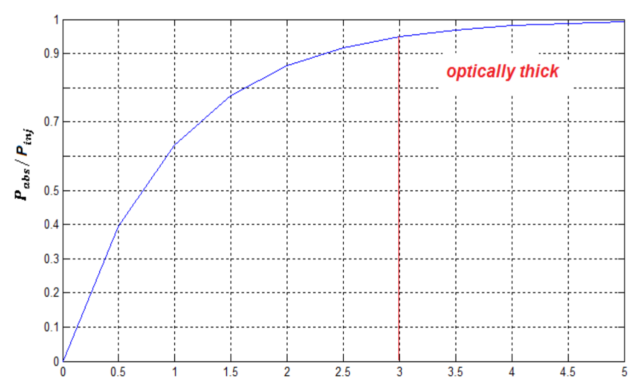

Fig.4 : The fraction of absorbed power as a function of optical depth $\boldsymbol{\tau}$, (cas $\boldsymbol{\tau} > 3$).

We can see an illustration of the function P_{abs}/P_{inj} on the Figure 4 where we define that the plasma is optically thick when $\tau > 3$, i.e. when the fraction of absorbed power $P_{abs}/P_{inj} > 95\%$.

Table 1 present the optical depths of a plasma slab in which the magnetic field varies as $B \sim 1/R$ and we obtained:

1. For the O-mode, the optical depth is given for perpendicular propagation and for all harmonics $n \geq 1$.

2. Similarly for the X-mode and the harmonics $n \geq 2$.
3. The optical depth for the fundamental harmonic $n = 1$ of the X-mode is given for oblique propagation.

Table 1 : The optical depth of EC waves (Westerhof. E, 2006).

mode	expression
O-mode-$\perp$ $n \geq 1$	$\tau = \frac{\pi^2 n^{2(n-1)}}{2^{n-1}(n-1)!} N_O^{2n-1} \left(\frac{\omega_p}{\omega_c}\right)^2 \left(\frac{v_t}{c}\right)^{2n} \frac{R}{\lambda}$
X-mode-$\perp$ $n \geq 2$	$\tau = \frac{\pi^2 n^{2(n-1)}}{2^{n-1}(n-1)!} A_n \left(\frac{\omega_p}{\omega_c}\right)^2 \left(\frac{v_t}{c}\right)^{2(n-1)} \frac{R}{\lambda}$ With $A_n = N_X^{2n-3}\left(1 + \frac{\left(\frac{\omega_p}{\omega_c}\right)^2}{n(n^2-1-\omega_p^2/\omega_c^2)}\right)$
X-mode oblique $n = 1$	$\tau = \pi^2 N_X^5 \left(1 + \frac{\omega_p}{\omega_c}\right)^2 \left(\frac{\omega_c}{\omega_p}\right)^2 \left(\frac{v_t}{c}\right)^2 cos^2\theta \frac{R}{\lambda}$

In the table, $v_{th} = (k_B T_e/m_e)^{1/2}$ is the thermal velocity of the electrons. In most current ECRH tokamak experiments either the fundamental O-mode or second harmonic X-mode are employed. Except near the edges of the plasma, optical depths of the order of one or significantly larger are generally achieved for both the fundamental O- and second harmonic X-mode resulting in complete single pass absorption.

e) Electron Cyclotron Absorption in Tokamak Plasma

In current fusion machines, the accessibility conditions usually require to inject the electronic cyclotron waves from low-field side. This imposes constraints on the polarization and the chosen mode from firstly of the propagation characteristics of ordinary and extraordinary modes and secondly from the absorption characteristics. So it is advantageous to use low-order harmonics of the interaction, to maximize absorption.

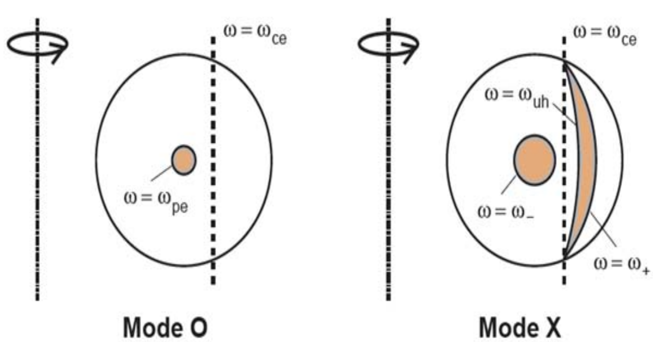

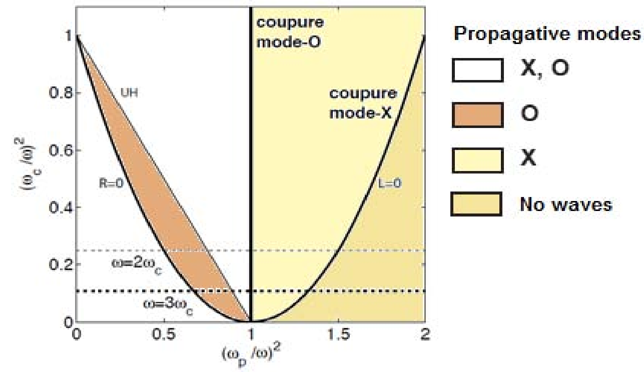

Fig.5 : (a) Typical cuts-off and resonances of a tokamak plasma in the case of perpendicular injection from the low-field side. Ordinary mode (left) and extraordinary mode (right); (b) CAM diagram.

The Figure 5 (a) shows the typical shapes of cut-offs right (ω_R), left (ω_L), and cut-off plasma ω_{pe}, the high hybrid resonance ω_{uh} and cyclotron frequency ω_{ce} in the poloidal plane. A very synthetic way to represent this problem of choosing the mode and propagation is the CMA diagram, as is shown on the Figure 5(b), (Dumont. R, 2001).

III. Alfven Waves Heating

a) Alfven Waves Dispersion

Branches of dispersion oblique propagation have a complicated expression because the continuation between θ = π / 2 and θ = 0. In this case the wave propagates with a low frequency approximation checking the magnetohydrodynamic (MHD) $\omega \ll \omega_{ci}, \omega_{pi}$. The elements of dielectric tensor are given by:

$$S = 1 + \frac{\omega_{pi}^2}{\omega_{ci}^2 - \omega^2} + \frac{\omega_{pe}^2}{\omega_{pe}^2 - \omega^2} \approx 1 + \frac{\omega_{pi}^2}{\omega_{ci}^2} = 1 + \frac{c^2}{v_a^2} \qquad (31)$$

$$D \approx \frac{i\omega}{\omega_{ci}} \frac{c^2}{v_a^2} \approx 0 \qquad (32)$$

$$P \approx 1 - \frac{\omega_{pi}^2 + \omega_{pe}^2}{\omega^2} \approx 1 - \frac{c^2}{v_a^2}\frac{\omega_{ci}\omega_{ce}}{\omega^2} \approx -\frac{\omega_{pe}^2}{\omega^2} \gg 1$$
$$P \to \infty \qquad (33)$$

Here, we used the quasi-neutral plasma, which is written $\omega_{pe}^2/\omega_{ce} = -\omega_{pi}^2/\omega_{ci}$ and the system of eigenvalues (8) reduces to

$$\begin{cases} \left(-n^2 cos^2\theta + 1 + \frac{c^2}{v_a^2}\right) \mathrm{E_x} = 0 \\ \left(-n^2 + 1 + \frac{c^2}{v_a^2}\right) \mathrm{E_y} = 0 \\ (\infty) E_z = 0 \end{cases} \qquad (34)$$

Global Journal of Science Frontier Research (A) Volume XII Issue I Version I January 2012

b) Shear Alfven wave (tortional Alfven Wave)

The first equation of system (34) gives the dispersion relation

$$n^2 cos^2\theta = 1 + \frac{c^2}{v_a^2} \quad (35)$$

It is fairly easy to show, from the definitions of the plasma and cyclotron frequencies that $\frac{\omega_{pi}^2}{\omega_{ci}^2} = \frac{c^2}{v_a^2}$. Here, $\rho \simeq nm_i$ is the plasma mass density, and

$$v_a = \sqrt{\frac{B_0^2}{\mu_0 \rho}} \quad (36)$$

is called the *Alfven velocity.* Thus, the dispersion relations of the two low-frequency waves can be written

$$\omega \approx kv_a cos\theta \equiv k_{//} v_a \quad (37)$$

With a phase velocity

$$v_\varphi \approx v_a^2 cos^2\theta \quad (38)$$

It is interesting to note that the magnetic perturbation induces torsion of field lines and is therefore called *slow* or *shear* Alfvén wave (Dumont.R, France 2005 and Fitzpatrick.R , 2008); see Figure 8.

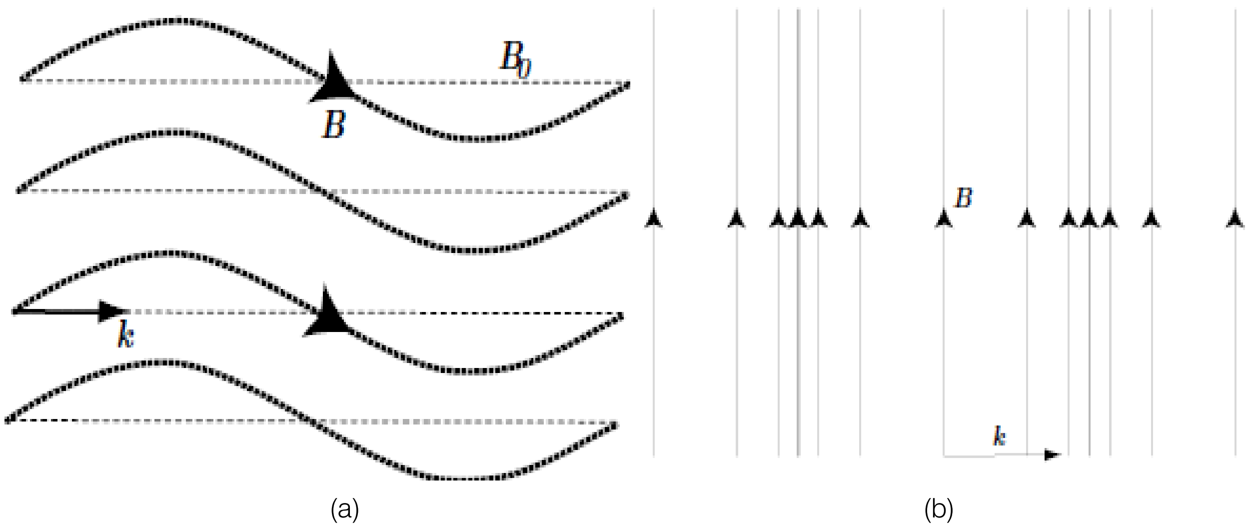

Fig.7 : Magnetic field perturbation associated with a (a) Shear-Alfven wave; (b) Compressional Alfven-wave.

c) Principle of Alfven wave heating

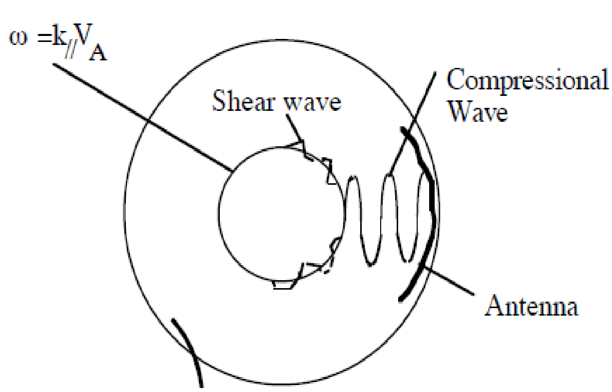

Fig.8 : The principle of Alfven wave heating. Poloïdal cross-section of the tokamak (Elfimov. A. G and al., 1995, Chambrier.A. D,1987).

The dispersion relation (35) implies that the shear Alfvén wave can propagate only along the field lines and in an inhomogeneous plasma there is only one surface, close to a magnetic surface, where for a given $N_{//}$ this wave dispersion relation is satisfied. So, the shear Alfvén wave can propagate only on that surface, as shown on Figure 8, it is trapped on that surface.

Therefore, the idea is to launch from the outside the compressional Alfvén wave, which can propagate in all directions and reach the Alfvén resonance. Once the power is coupled to the shear wave by resonance absorption, it stays on the magnetic surface and dissipates there. The Figure 9 shows a schematic diagram of heating by the shear Alfvén wave resonance whose condition is

$$\omega^2(r) = \frac{k_{//}^2 v_a{}^2}{1+k_{//}^2 v_a^2/\omega_{ci}^2} \quad (42)$$

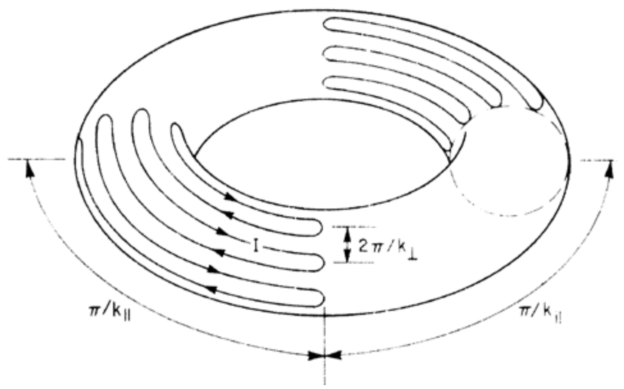

Fig.9 : Schematic diagram of the proposed setting of heating coil using shear Alfvèn wave resonance (Hasagawa. A., Chen. L.,1974).

Note that the wavelength of the compressional wave is of the order of 1m. This means that, for 1m wide or narrower antennas, most of the wave spectrum will be evanescent with an evanescence length of the order of the antenna size (Westerhof. E, 2006). The inclusion of kinetic effects, such as electron and ion temperatures and finite electronic mass, changes the physical picture of processes. This gives rise to an electrostatic wave which propagates in radial direction close to resonant surface of (SW) that called kinetic Alfvèn wave (Veron.D, 1978). In this case, the dissipation of the waves is attributed to Landau damping on electrons (Hasagawa. A., Chen. L.,1974). From the experimental point of view the most extensive experiments and analysis of Alfven wave heating have been performed on the TCA tokamak (Veron.D, 1978).

IV. Summary and Discussion

The application of EC waves to plasmas rests on a wide base of theoretical work which progressed from simple cold plasma models to hot plasma models with fully relativistic physics to quasilinear kinetic Vlasov models. In this case, all the information about the absorption of the EC wave in the inhomogeneous plasma, is finally expressed in terms of the relativistic dielectric tensor which characterizes the propagation with its hermitian part and the absorption with its anti-hermitian one. For a very low electron temperature $T_e \to 0$, the hermitian part of the tensor present the cold dielectric tensor which justifies the use of the cold plasma approximation to describe the wave propagation.

We generally use the cold plasma model to study Alfven waves and especially to describe the damping of the compressional wave by local absorption of power at the position of the shear Alfvén wave resonance.

Although antenna coupling and general Alfvèn wave behavior appeared to be in agreement with the theory, generally speaking little plasma heating was observed while the main effect of the RF was a large density increase, sometimes interpreted as an increase in the particle confinement time. In view of these disappointing results there have been few attempts to apply Alfven wave heating to large tokamaks and this method is usually not mentioned for the heating of ITER or reactors. However, there has been some renewed interest in this field as the conversion to the kinetic Alfven wave may induce poloïdal shear flows, and possibly to generate transport Barriers (Veron.D, 1978).

In constract, electron cyclotron (EC) power has technological and physics advantages for heating and current drive (CD) in a tokamak reactor, and advances in source development make it credible for applications in the International Thermonuclear Experimental Reactor (ITER). Because this heating system (ECH) is a particularly *robust* heating scheme since the physics of wave propagation and absorption is well understood, there is total absorption for all plasma parameters foreseen in ITER.

References References Referencias

1. Sabri, N.G., (2010). Etude de la Propagation d'une Onde Electromagnétique dans un Plasma de Tokamak- Interaction Onde Plasma *; Thèse de Doctorat, U .T*, 200 pages.
2. Arnoux. G., *(2005).* Chauffage de plasma par ondes électromagnétiques à la troisième harmonique de la fréquence cyclotron des électrons dans le tokamak TCV; *Doctorat.*
3. Dumont, R., (2001). Contrôle du profil de courant par ondes cyclotroniques électroniques dans les tokamaks ; *thèse de doctorat*, université de Henri Poincaré, Nancy I.
4. Elfimov, A. G., Assis, A. S., Azevedo, C. A., Grishanov, N. I., Nekrasov, F. M, Potapenkof I. F, Tsypin, V. S. (1995). Analysis in Magnetized Plasma Structures. Brazilian Journal of Physics, vol. 25, no. 3.
5. Bertrand, P. (2004). *Description cinétique de la turbulence dans un plasma de Tokamak*, Ecole d'Aquitaine onde & matière, Maubuisson.
6. Moncuque, M., (2001). *Cours Méthodes numériques de DESS*, Laboratoire d'Etudes Spatiales et d'Instrumentation en Astrophysique (LESIA), Paris.
7. Sabri, N.G. Benouaz, T. (2011). *Study of electron cyclotron absorption in tokamak plasma using kinetic model*', International Seminar on Plasma Physics, SIPP'2011, Algeria,
8. Swanson, D.G. (1989). *Plasma Waves,*Academic Press, San Diego.
9. Pochelon A. (1994). *Electron cyclotron resonance heating*, 36Th Course of the Association Vaudoise des chercheurs en physique, LRP 505/94.
10. Baea, Y.S., Namkung W., (2004). *Plasma Sheath Lab, Theory of Waves in Plasmas*,

11. Brambilla, M. (1998). Kinetic Theory of Plasma Waves*, Clarendon Press, Oxford*,
12. Bornatici, M. Cano, R. De Barbieri, O. Engelmann, F. (1983). Electron cyclotron emission and absorption in fusion plasmas, Nuclear Fusion, vol.23 pp.1153-1257 (Review Paper:390 citations to date)
13. Tsironis. C., Vlahos. L., (2006). Effect of nonlinear wave–particle interaction on electron-cyclotron absorption, *Plasma Phys. Control. Fusion* 48 1297–1310.
14. Sabri, N.G., Benouaz. T., Cheknane *A.,*(2009). *Transfers of Electromagnetic Energy in Homogeneous Plasma,* International Review of Physics, Vol.3,N.1, pp.11-15.
15. Westerhof, E., (2006). *Electron Cyclotron Waves*, Transactions of Fusion Science And Technology Vol. 49.
16. Mandrin,P. (1999). *Production de plasma et démarrage du courant du tokamak TCV avec l'assistance d'onde cyclotron électronique*, LRP 541/99, ISSN 0458-5895.
17. Dumont, R. (2005). Waves in the cold plasma, Interaction wave – plasma, pp 15-20.
18. Fitzpatrick, R. (2008). Course of The Physics of Plasmas, *The University of Texas at Austin*,19-12.
19. Chambrier A. D. (1987). *Mesures de la température ionique dans le plasma du tokamak TCA en présence de chauffage par ondes d'Alfven,* thèse de Doctorat, EPFL, No 71 2.
20. Veron, D. (1978). TFR Report EUR-CEA-FC-980, Fontenay aux Roses.
21. Hasagawa, A. Chen, L. (1974). *Plasma heating by Alfvèn Wave phase mixing*, Physical Review Letters,volume 32, Number 9.

This page is intentionally left blank

Global Journal of Science Frontier Research
Physics & Space Science
Volume 12 Issue 1 Version 1.0 January 2012
Type : Double Blind Peer Reviewed International Research Journal
Publisher: Global Journals Inc. (USA)
Online ISSN: 2249-4626 & Print ISSN: 0975-5896

Static Characterization of InAs/AlGaAs Broadband Self-Assembled Quantum Dot Lasers

By D. Ghodsi Nahri, H. Arabshahi
Islamic Azad University, Mashhad, Iran

Abstract - In this paper we have studied the static-characteristics of InAs/AlGaAs broadband self-assembled quantum-dot laser diodes (SAQD-LDs) solving the rate equations numerically using fourth-order Runge-Kutta method. Energy level, size, and composition distributions of the InAs/AlGaAs broadband quantum-dots (QDs) are considered and their effects on Static-characteristics are investigated. Simulated results of static-characteristics show that nonlinearity appears in light-current characteristics whereas homogeneous broadening (HB) becomes equal to inhomogeneous broadening (IHB). Slope-efficiency increases as the HB heightens up to the IHB. Exceeding the HB from IHB results in degradation of light-current characteristics. In fact, InAs/AlGaAs broadband SAQD-LD has the best performance when HB is equal to IHB. Light-current characteristics degrade and threshold current increases as the IHB enhances. We also investigate the effects of QD coverage on the laser performance and show that there is an optimum QD coverage in which the SAQD-LD operates with lowest possible threshold current and maximum output power as whatever the QD coverage enhances from that optimum amount, the threshold current increases and slope efficiency decreases.

Keywords : InAs/AlGaAs broadband Self-Assembled Quantum dot laser; Static Characterization, inhomogeneous and homogeneous broadening;.

GJSFR-A Classification : FOR Code: 020603

STATIC CHARACTERIZATION OF INASALGAAS BROADBAND SELF-ASSEMBLED QUANTUM DOT LASERS

Strictly as per the compliance and regulations of :

Open Association of Research, Soceity (United States)

Static Characterization of InAs/AlGaAs Broadband Self-Assembled Quantum Dot Lasers

D. Ghodsi Nahri [α], H. Arabshahi [Ω]

Abstract - In this paper we have studied the static-characteristics of InAs/AlGaAs broadband self-assembled quantum-dot laser diodes (SAQD-LDs) solving the rate equations numerically using fourth-order Runge-Kutta method. Energy level, size, and composition distributions of the InAs/AlGaAs broadband quantum-dots (QDs) are considered and their effects on Static-characteristics are investigated. Simulated results of static-characteristics show that nonlinearity appears in light-current characteristics whereas homogeneous broadening (HB) becomes equal to inhomogeneous broadening (IHB). Slope-efficiency increases as the HB heightens up to the IHB. Exceeding the HB from IHB results in degradation of light-current characteristics. In fact, InAs/AlGaAs broadband SAQD-LD has the best performance when HB is equal to IHB. Light-current characteristics degrade and threshold current increases as the IHB enhances. We also investigate the effects of QD coverage on the laser performance and show that there is an optimum QD coverage in which the SAQD-LD operates with lowest possible threshold current and maximum output power as whatever the QD coverage enhances from that optimum amount, the threshold current increases and slope efficiency decreases.

Keywords : InAs/AlGaAs broadband Self-Assembled Quantum dot laser; Static Characterization, inhomogeneous and homogeneous broadening;

I. Introduction

Three-dimensionally quantum confining medium of electrons,, holes, and excitons in semiconductor microstructures known as quantum dots (QDs) is predicted to produce new physical phenomena and improve optoelectronic devices significantly (Liu et al., 2005; Lv et al., 2008; Zhang et al., 2004; Zhang et al., 2008). The atom-like state density in QDs associated with three-dimensional confinement of electrons and holes would cause an increase of optical gain and limit thermal carrier distribution. Therefore, the use of QDs for semiconductor lasers as an active region is expected to provide a remarkable reduction of threshold current and temperature sensitivity. During primary research based on predictions in the early 1980s, QDs have been created by combining lithography and re-growth on a processed substrate. The artificial techniques, however, suffer from non-uniform dot size and composition, poor interface quality, that cause IHB of optical gain and low numerical density. High uniformity is required to achieve the atom-like state density of a dot ensemble. A high optical quality and high numerical density are required to obtain a large gain (Sugawara et al., 1997; Sugawara, 1999; Sun et al., 1999). Here, we characterize the static features of broadband emitting InAs/AlGaAs self-assembled QD lasers examining the effects of energy level distributions that cause homogeneous broadening (HB) of optical gain and the effects of IHB on the static performance of the mentioned QD lasers. These InAs/AlGaAs QDs exhibit a broad photoluminescence (PL) full width at half maximum (FWHM) of 80 meV, which is much wider than that grown on GaAs substrate and it was proposed that this broadband emission is beneficial for broadening the lasing spectrum (Sun et al., 1999; Lv et al., 2008). Broadband QD lasers have been observed experimentally (Djie et al., 2007). This observation is fundamentally different from conventional quantum-well or bulk lasers characteristics and thus the study of broadband characteristics of QD lasers are necessary to obtain a further insight of the carrier processes in the QD semiconductor materials (Tan et al., 2007; Tan et al., 2008).

Author [α] : Department of Physics, Mashhad Branch, Islamic Azad University, Mashhad, Iran.
Author [Ω] : Department of Physics, Payame Noor University, PO Box 19395-3697, Tehran, Iran. E-mail : arabshahi@um.ac.ir

II. Simulation Model

Based on the density-matrix theory, the linear optical gain of QD active region is given as

$$g^{(1)}(E)=\frac{2\pi e^2\hbar N_D}{cn_r e_0 m_0^2}\cdot\frac{\left|p_{cv}^{\sigma}\right|^2(f_c-f_v)}{E_{cv}}\times B_{cv}(E-E_{cv}) \quad (1)$$

where n_r is the refractive index, N_D is the volume density of QDs, $\left|P_{cv}^{s}\right|^2$ is the transition matrix element, f_c is the electron occupation function of the conduction-band discrete state, f_v is that of the valence-band discrete state, and E_{cv} is the interband transition energy. The linear optical gain shows the homogeneous broadening of a Lorentz shape as

$$B_{cv}(E-E_{cv})=\frac{\hbar\gamma_{cv}/\pi}{(E-E_{cv})^2+(\hbar\gamma_{cv})^2} \quad (2)$$

where FWHM is given as $2\hbar\gamma_{cv}$ with polarization dephasing or scattering rate γ_{cv}. Neglecting the optical-field polarization dependence, the transition matrix element is given as

$$\left|P_{cv}^{\sigma}\right|^2 = \left|I_{cv}\right|^2 M^2 \qquad (3)$$

where I_{cv} represents the overlap integral between the envelope functions of an electron and a hole, and

$$M^2 = \frac{m_0^2}{12m_e^*} \cdot \frac{E_g(E_g + D)}{E_g + 2D/3} \qquad (4)$$

as derived by the first-order k.p is the interaction between the conduction band and valence band. Here, E_g is the band gap, m_e^* is the electron effective mass, D is the spin-orbit interaction energy of the QD material. Equation 3 holds as long as we consider QDs with a nearly symmetrical shape (Sugawara et al., 2000). In actual SAQD-LDs, we should rewrite the linear optical gain formula of equation 1 by taking into account inhomogeneous broadening due to the QD size and composition fluctuation in terms of a convolution integral as

$$g^{(1)}(E) = \frac{2\pi e^2 \hbar N_D}{c n_r e_0 m_0^2} \int_{-\infty}^{\infty} \frac{\left|p_{cv}^{\sigma}\right|^2}{E_{cv}} (f_c(E') - f_v(E')) \times$$
$$B_{cv}(E - E') G(E' - E_{cv}) dE' \qquad (5)$$

where E_{cv} is the center of the energy distribution function of each interband transition, $f_c(E')$ is the electron occupation function of the conduction-band discrete state of the QDs with the interband transition energy of E', and $f_v(E')$ is that of the valence band discrete state. The energy fluctuation of QDs are represented by $G(E' - E_{cv})$ that takes a Gaussian distribution function as

$$G(E' - E_{cv}) = \frac{1}{\sqrt{2\pi}\xi_0} \exp(-(E' - E_{cv})^2 / 2\xi_0^2)$$

Whose FWHM is given by $G_0 = 2.35x_0$. The width G_0 usually depends on the band index c and v (Sugawara et al., 1999).

The most popular and useful way to deal with carrier and photon dynamics in lasers is to solve rate equations for carrier and photons (Grundmann, 2002; Markus et al., 2003; Sugawara et al., 2000; Tan et al., 2007; Tan et al., 2008). In our model, we consider an electron and a hole as an exciton, thus, the relaxation means the process that both an electron and a hole relax into the ground state simultaneously to form an exciton. We assume that the charge neutrality always holds in each QD.

In order to describe the interaction between the QDs with different resonant energies through photons, we divide the QD ensemble into j=1, 2,... 2M+1 groups, depending on their resonant energies for the interband transition over the longitudinal cavity photon modes. $j = M$ corresponds to the group and the mode with the central transition energy E_{CV}. We take the energy width of each group equal to the mode separation of the longitudinal cavity photon modes which equals to

$$D_E = ch / 2n_r L_{ca} \qquad (7)$$

where L_{ca} is the cavity length. The energy of the j[th] QD group is represented by

$$E_j = E_{cv} - (M - j)D_E \qquad (8)$$

where $j = 1, 2, ..., 2M + 1$. The QD density j[th] QD group is given as

$$N_D G_j = N_D G(E_j - E_{cv}) D_E \qquad (9)$$

Let N_j be the carrier number in j[th] QD group, According to Pauli's exclusion principle, the occupation probability in the ground state of the j[th] QD group is defined as

$$P_j = N_j / 2N_D V_a G_j \qquad (10)$$

where V_a is the active region volume. The rate equations are as follows (Markus et al., 2003; Sugawara et al., 2000; Sugawara et al., 2005; Tan et al., 2007; Tan et al., 2008)

$$\frac{dN_s}{dt} = \frac{I}{e} - \frac{N_s}{\tau_s} - \frac{N_s}{\tau_{sr}} + \frac{N_w}{\tau_{we}} \qquad (11)$$

$$\frac{d\ _w}{dt} = \frac{NN_s}{\tau_s} + \sum_j \frac{N_j}{\tau_e D_g} - \frac{N_w}{\tau_{wr}} - \frac{N_w}{\tau_{we}} - \frac{N_w}{\overline{\tau}_d}$$

$$\frac{dNj}{dt}=\frac{N_w G_j}{\tau_{dj}}-\frac{N_j}{\tau_r}-\frac{N_j}{\tau_e D_g}-\frac{c\Gamma}{n_r}.g^{(1)}(E)S_m$$

$$\frac{dS_m}{dt}=\frac{\beta N_j}{\tau_r}+\frac{c\Gamma}{n_r}.g^{(1)}(E)S_m-S_m/\tau_p$$

where N_S, N_W, and N_j are the carrier numbers in separate confinement heterostructure (SCH) layer, wetting layer (WL) and j[th] QD group, respectively, S_m is the photon number of m[th] mode, where m=1,2…2M+1, I is the injected current, G_j is the fraction of the j[th] QD group type within an ensemble of different dot size population, e is the electron charge, D_g is the degeneracy of the QD ground state without spin, b is the spontaneous-emission coupling efficiency to the lasing mode. $g_{mj}^{(1)}$ is the linear optical gain which the j[th] QD group gives to the m[th] mode photons where is represented by

$$g_{mj}^{(1)}(E)=\frac{2\pi e^2\hbar N_D}{cn_r\varepsilon_0 m_0^2}.\frac{|p_{cv}^{\sigma}|^2}{E_{cv}}(2p_j-1). \qquad (12)$$
$$G_j B_{cv}(E_m-E_j)$$

the related time constants are as τ_s, diffusion in the SCH region, τ_{sr}, carrier recombination in the SCH region, τ_{we}, carrier reexcitation from the WL to the SCH region, τ_{wr}, carrier recombination in the WL, τ_{dj}, carrier relaxation into the j[th] QD group, τ_r, carrier recombination in the QDs, τ_p, photon lifetime in the cavity, The average carrier relaxation lifetime, $\bar{\tau}_d$, is given as

$$\tau_d^{-1}=\sum_j \tau_{dj}^{-1}.G_j=\tau_{d0}^{-1}(1-P_j)G_j \qquad (13)$$

where τ_{do} is the initial carrier relaxation lifetime. The photon lifetime in the cavity is

$$\tau_p^{-1}=(c/n_r)[\alpha_i+\ln(1/R_1R_2)/2L_{ca}] \qquad (14)$$

where R_1 and R_2 are the cavity mirror reflectivities, and a_i is the internal loss. The laser output power of the m[th] mode from one cavity mirror is given a

$$I_m=\hbar\omega_m cS_m\ln(1/R)/(2L_{ca}n_r) \qquad (15)$$

where w_m is the emitted photon frequency, and R is R_1 or R_2. We solved the rate equations numerically using fourth order Runge-Kutta method to characterize static characteristics of InAs/AlGaAs broadband self-assembled QD lasers by supplying the step-like current at the time of $t=0$. The system reaches the steady-state after finishing the relaxation oscillation.

III. Simulation Results

Fig. 1 shows light-current (L-I) characteristics of the mentioned self-assembled QD laser diode (SAQD-LD) for FWHM of IHB (a) $G_0 = 60meV$ at $\hbar\gamma_{cv}=15, 20, 30,$ and $60meV$, and (b) $G_0 = 80meV$ at $\hbar\gamma_{cv}=20, 30, 40,$ and $50meV$,

As we can see from Fig. 1, non-linear L-I characteristics exist when HB is smaller than IHB. While when the HB becomes equal to IHB, L-I curve has a linear shape. For large HBs, near to IHB up to a bit larger than IHB, output power increases infinitely as the injected current elevates. Besides, Slope efficiency (external quantum differential efficiency) heightens as the HB increases up to the IHB. In addition, when the HB exceeds the IHB, static-characteristics degrade. We can conclude that the broadband SAQD-LD has its best performance when HB is equal to IHB.

Furthermore, Fig. 1 shows that slope efficiency decreases and threshold current also elevates with enhancement of IHB as a result of decreasing the central group density of states (DOS). In some cases such as Fig. 1(a) for FWHM of HB 30 meV and at I= 2.5 mA or Fig. 1(b) for FWHM of HB 40 meV and at I=3.5 mA, all of the central group DOS occupies and the output power reaches its maximum amount, then, it decreases as the injected current increases, as a result of emitting of central group carriers within other modes.

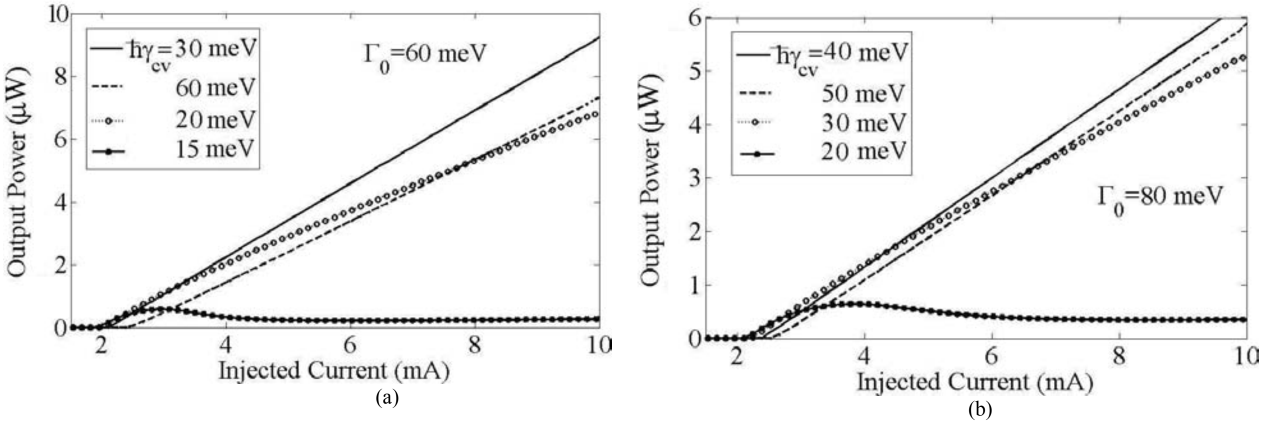

Fig. 1 : light-current characteristics of InAs/AlGaAs broadband SAQD-LD for FWHM of IHB and H $G_0 = 60\,meV$ and $2\hbar\gamma_{cv} = 30, 40, 60, and\ 120\,meV$ and (b) $G_0 = 80\,meV$ at $2\hbar\gamma_{cv} = 40, 60, 80, and\ 100\,meV$.

In addition, the threshold current increases as the HB increases owing to elevating DOS of the central group. This fact is revealed clearly in Fig. 2 where L-I characteristics is shown for HB 0.8 and 80 meV.

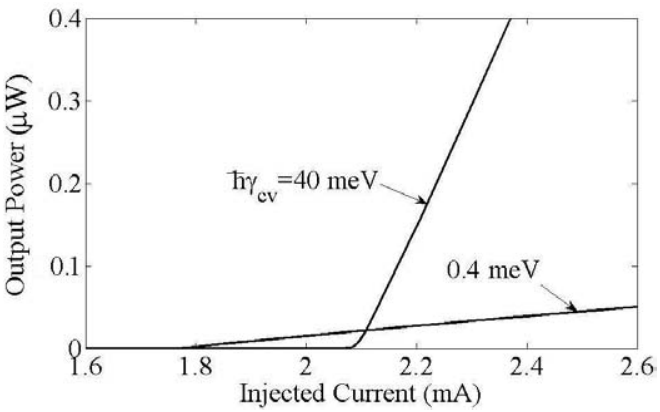

Fig. 2 : Output power as a function of injected current for HB 0.8 and 80 meV.

It is clearly shown that slope efficiency and the threshold current enhance with increase of HB. Fig. 3 shows L-I characteristics for QD coverage as a variable parameter $\xi = 0.04, 0.07, 0.1, 0.2, 0.4,\ and\ 0.8$ and carrier radiative recombination times 2.8 ns in QDs and 3ns in WL.

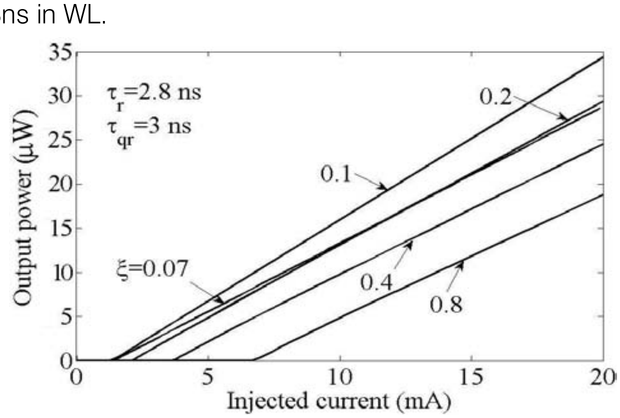

Fig. 3 : shows L-I characteristics for QD coverage as a variable parameter $\xi = 0.04, 0.07, 0.1, 0.2, 0.4,\ and\ 0.8$.

As shown in fig. 3, with increase of QD coverage from 0.1, threshold current increases owing to enhancing the number of QDs or the QD volume (the number of energy levels) and as a result, it is required to provide more QD carriers in order to establish population inversion. Besides, output power and slope efficiency decline due to decreasing occupation probability and accordingly, increasing the relaxation time. It is clearly revealed that the QD coverage 0.1 has the best L-I characteristics and the lowest threshold current. It is concluded that there is an optimum QD coverage.

IV. Conclusion

Considering energy level and size distributions of InAs/AlGaAs broadband self-assembled quantum-dots, we solved the rate equations numerically using fourth-order Runge-Kutta method and simulated light-current characteristics of the mentioned SAQD-LD. Simulated results of the static-characteristics showed that slope efficiency elevates as the HB increases whereas it becomes equal to IHB. Exceeding the HB from IHB and elevating IHB result in degradation of light-current characteristics. Threshold current increases as the HB and IHB enhance. Nonlinearity appears in light-current characteristics whereas HB becomes equal to IHB. The SAQD-LD has the best performance when HB is equal to IHB. We also saw that increasing of HB from IHB leads to declining of static-characteristics of InAs/AlGaAs broadband SAQD-LD. We revealed that there is an optimum QD coverage in which the SAQD-LD operates with lowest possible threshold current and maximum output power as whatever the QD coverage enhances from that optimum amount, the threshold current increases and slope efficiency decreases.

References Références Referencias

1. Djie H S, Ooi B, Fang, Wu X Y, Fastenau J, Liu, X And Hopkinson M (2007). Room-Temperature Broadband Emission Of An InGaAs/GaAs Quantum Dots Laser. Opt. Lett., 32: 44-46.

2. Grundmann M (2002). Nano Optoelectronics. Springer, New York.
3. Liu N, Jin P And Wang Z (2005). Inas/Gaas Quantum-Dot Super Luminescent Diodes With 110 Nm Bandwidth. Electron. Lett., 41: 1400-1402.
4. Lv X, Liu Q, Jin P And Wang Z (2008). Broadband Emitting Super Luminescent Diodes With Inas Quantum Dots In Algaas Matrix. IEEE Photon. Technol. Lett., 20: 1742-1744.
5. Markus A, Chen J, Gauthier-Lafaye O, Provost J, Paranthoen C And Fiore A (2003). Impact Of Intraband Relaxation On The Performance Of A Quantum-Dot Laser. IEEE J. Sel. Top., Quantum Electron., 9: 1308-1314.
6. Sugawara M, Mukai K And Shoji H (1997). Effect Of Phonon Bottleneck On Quantum-Dot Laser Performance. Applied Phys. Lett., 71: 2791-2793.
7. Sugawara M (1999). Self –Assembled Ingaas/Gaas Quantum Dots. Academic Press 60.
8. Sugawara M, Mukai K, Nakata Y And Ishikawa H (2000). Effect Of Homogeneous Broadening Of Optical Gain On Lasing Spectra In Self-Assembled InxGa1àxAsõGaAs Quantum Dot Lasers. Phys. Rev. B, 61: 7595-7603.
9. Sugawara M, Hatori N, Ebe H And Ishida H (2005). Modeling Room-Temperature Lasing Spectra Of 1.3μm Self-Assembled Inas/Gaas Quantum-Dot Lasers: Homogeneous Broadening Of Optical Gain Under Current Injection. Applied Phys., 97: 043523-043530.
10. Sun Z, Ding D, Gong Q, W Zhou, B Xu And Wang Z (1999). Quantum-Dot Superluminescent Diode: A Proposal For An Ultra-Wide Output Spectrum. Opt. Quantum Electron., 31: 1235-1246.
11. Tan C, Wang Y, Djie H And Ooi B (2007). Role Of Optical Gain Broadening In The Broadband Semiconductor Quantum-Dot Laser. Applied Phys. Lett., 91: 061117-061119.
12. Tan C, Wang Y, Djie H And Ooi B (2008). The Role Of Optical Gain Broadening In The Ultrabroadband Ingaas/Gaas Interband Quantum-Dot Laser. Comput. Matter. Sci., 44: 167- 173.
13. Zhang Z, Wang Y, Xu B And Liu F (2004). High Performance Quantum-Dot Superluminescent Diodes. IEEE Photon. Technol. Lett., 16: 27-29.
14. Zhang Y, Hogg P. Jin And Wang Z (2008). High-Power Quantum-Dot Superluminescent LED With Broadband Drive Current Insensitive Emission Spectra Using Tapered Active Region. IEEE Photon. Technol. Lett., 20: 782-784.

This page is intentionally left blank

Global Journal of Science Frontier Research
Physics & Space Science
Volume 12 Issue 1 Version 1.0 January 2012
Type : Double Blind Peer Reviewed International Research Journal
Publisher: Global Journals Inc. (USA)
Online ISSN: 2249-4626 & Print ISSN: 0975-5896

Estimating the Speed of rotation of a rotating X-Ray window

By Dikedi P.N.
King's College, London

Introduction - A rotating membrane is assumed to be a rotating discand appropriate speed of rotation is a key consideration if the material in question must survive the heat flux imparted on it by impinging beam of electrons. 1μm hot spots are assumed to be distributed on the target material such that a circular pattern is formed according to figure 1 .

GJSFR-A Classification : FOR Code: 020202, 020504, 020204

ESTIMATING THE SPEED OF ROTATION OF A ROTATING X-RAY WINDOW

Estimating the Speed of rotation of a rotating X-Ray window

Dikedi P.N.

I. Introduction

A rotating membrane is assumed to be a rotating disc and appropriate speed of rotation is a key consideration if the material in question must survive the heat flux imparted on it by impinging beam of electrons. 1μm hot spots are assumed to be distributed on the target material such that a circular pattern is formed according to figure 1

II. Number of Hot Spots

Radii chosen varied from 1000μm to 50000μm. If we set speed of rotation as 825 *rev/s* (which is a realistically attainable speed)

$$825rev/s = \frac{44xR}{7T} \quad (1)$$

Where *R*=radius of rotating disc, and *T* is the time for 1 rev (period) Consider a circle of diameter 10mm; circumference, of the circle will be, $2\pi R = 2\pi (5\times10^{-3})m = 3.142857\times10^{-2}m$

To arrive at the number of hot spots

We have $\frac{2\pi R}{d} = \frac{3.142857\times10^{-2}}{1\times10^{-6}} = 31428.57$

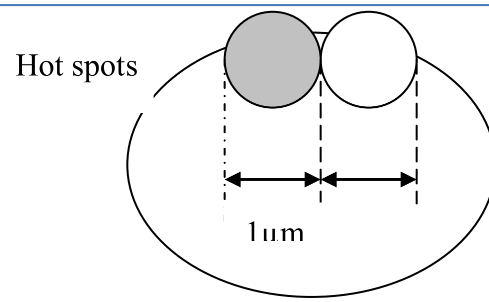

Figure 1 : Rotating disk with 1μm hotspots forming a circular pattern

hot spots where *d* is the diameter of 1 hot spot.

If heat source will theoretically heat up $1\mu m$ hot spot to maximum allowable temperature in say 30ns and we rotate the disc by $1\mu m$ after this assumed time so that a new position is assumed on the circular path of the beam, the circle will make 1 revolution in a time expressed as

T=Number of spots x time per spot

$$=31428.57\times30\times10^{-9}s = 942857.143\times10^{-9}s$$

$$\approx 1\times10^{-3}s$$

$$w = \frac{2\pi R}{T} \div 2\pi R\ (rev/s)$$

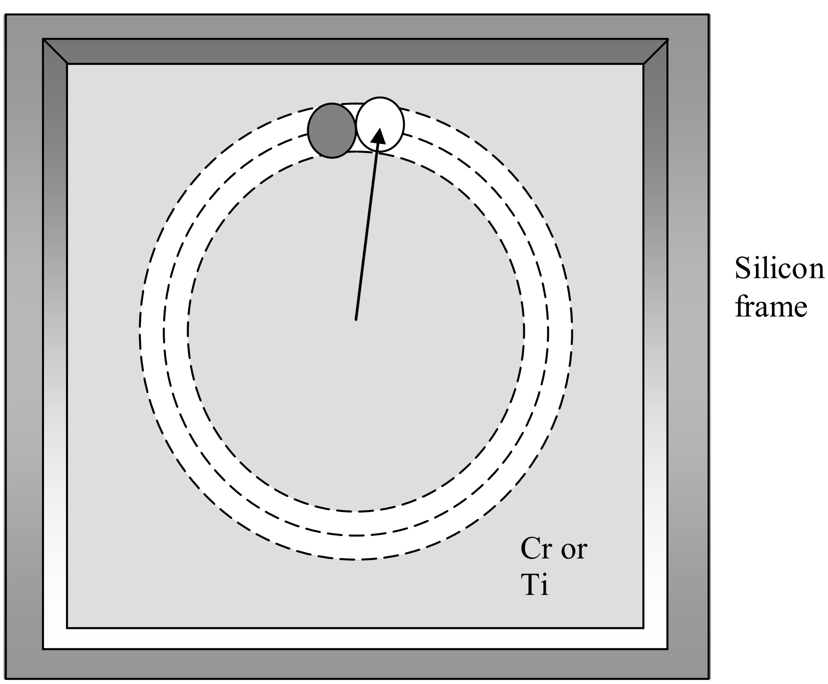

Figure 2 : Circular pattern showing the paths covered by heat flux on a square shaped X-ray window

Author : *Physics Department, King's College, London*

III. Speed and Seat Up Time

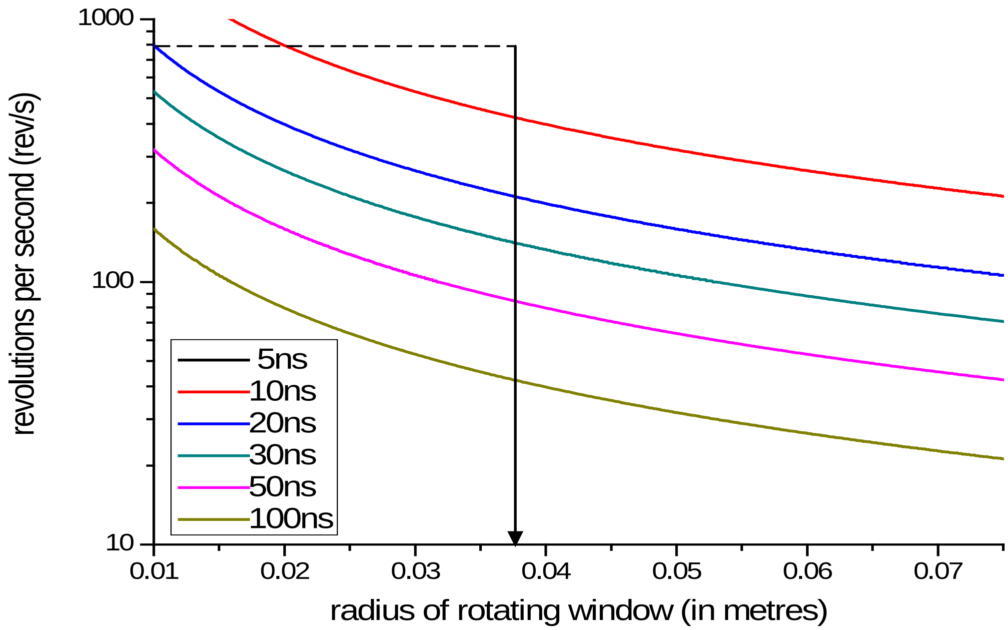

Figure 3 : Graph showing required rotation rate versus radius, for varying heat up times

Figure 2 Describes the rotation of the disk by the circular pattern showing the paths covered by heat flux on a square shaped X-ray window.

Figure 3 simply infers that at lower seating up times, the speed of rotation is greater and has an inverse relationship with radii of rotating window. Window of radius of about 32*mm* been impinged on, by a beam of electrons having heating up time of 5ns will be assumed to rotate at $1000 rev/s$. Rotating discs of radius of $\leq 32mm$ will rotate at $\leq 1000 rev/s$ for heating up times of 5, 10, 20, 30, 50 and 100ns according to figure 1. The graph shows that, assuming a maximum practical radius of 800*rev/s*, a range of heating up time s from 10ns to 100ns can be tolerated and rotating diameters of $\approx 20mm$ to $\approx 100mm$ can be used.

However the speed of an arbitrary hot spot travelling on a circular path in metres per seconds is unaffected by changing radii according to figure **

The maximum practically attainable rotation has 1650 *rev/s* or 100 000 *rev/min* and a more realistic and less problematic value of speed is approximately 825 *rev/s* or 50 000 rev/min. Maximum practical radius of rotation is taken as approximately 50mm. Radii larger than this critical value will cause centrifugal force to tear the rotating disk. Rotating disk of radii $R \leq 28mm$ will rotate at speeds of $w \leq 1100 rev/s$ at heating up times of 5ns, 10ns, 20ns, 30ns, 50ns and 100ns according to figure 3.

IV. Conclusion

A description on how to calculate the number of hot spots have been given; speed of rotation in revolutions per second and seat up time for each hot spot have been derived. In the course of microfabrication, radii of disks must not exceed 50mm, to avoid been torn apart by centrifugal force.

Appendix

Basic Thermal Properties of materials considered in the simulation (From CRC handbook)

Titanium

Thermal conductivity k = 0.219 W/ (cm. K) = 21.9 W/ (m. K) at 300K
Density r = 4500 kg/m3
Heat capacity Cp = 0.125cal/ (g. K) = 523 J/ (kg. K)

Silicon Nitride

Thermal conductivity k = 0.072 cal.cm-1.s-1.k-1 = 30.1 W/ (m. K) @300K
Density r = 3180 kg/m3
Heat capacity Cp = 0.17 cal/ (g. K) = 712 J/(kg. K)

Aluminium

Thermal conductivity k = 2.37 W/ (cm. K) = 237 W/ (m. K) at 300K
Density r = 2700 kg/m3
Heat capacity Cp = 0.215 cal/ (g. K) = 900 J/ (kg. K)

Chromium

Thermal conductivity k = 0.903 W/ (cm. K) = 90.3 W/ (m. K) at 300K
Density r = 7190 kg/m3
Heat capacity Cp = 0.107 cal/ (g. K) = 448 J/ (kg. K)

Global Journals Inc. (US) Guidelines Handbook 2011

www.GlobalJournals.org

FELLOW OF ASSOCIATION OF RESEARCH SOCIETY IN SCIENCE (FARSS)

- 'FARSS' title will be awarded to the person after approval of Editor-in-Chief and Editorial Board. The title 'FARSS" can be added to name in the following manner. eg. Dr. John E. Hall, Ph.D., FARSS or William Walldroff Ph. D., M.S., FARSS
- Being FARSS is a respectful honor. It authenticates your research activities. After becoming FARSS, you can use 'FARSS' title as you use your degree in suffix of your name. This will definitely will enhance and add up your name. You can use it on your Career Counseling Materials/CV/Resume/Visiting Card/Name Plate etc.
- 60% Discount will be provided to FARSS members for publishing research papers in Global Journals Inc., if our Editorial Board and Peer Reviewers accept the paper. For the life time, if you are author/co-author of any paper bill sent to you will automatically be discounted one by 60%
- FARSS will be given a renowned, secure, free professional email address with 100 GB of space eg.johnhall@globaljournals.org. You will be facilitated with Webmail, SpamAssassin, Email Forwarders, Auto-Responders, Email Delivery Route tracing, etc.
- FARSS member is eligible to become paid peer reviewer at Global Journals Inc. to earn up to 15% of realized author charges taken from author of respective paper. After reviewing 5 or more papers you can request to transfer the amount to your bank account or to your PayPal account.
- Eg. If we had taken 420 USD from author, we can send 63 USD to your account.
- FARSS member can apply for free approval, grading and certification of some of their Educational and Institutional Degrees from Global Journals Inc. (US) and Open Association of Research,Society U.S.A.
- After you are FARSS. You can send us scanned copy of all of your documents. We will verify, grade and certify them within a month. It will be based on your academic records, quality of research papers published by you, and 50 more criteria. This is beneficial for your job interviews as recruiting organization need not just rely on you for authenticity and your unknown qualities, you would have authentic ranks of all of your documents. Our scale is unique worldwide.
- FARSS member can proceed to get benefits of free research podcasting in Global Research Radio with their research documents, slides and online movies.
- After your publication anywhere in the world, you can upload you research paper with your recorded voice or you can use our professional RJs to record your paper their voice. We can also stream your conference videos and display your slides online.
- FARSS will be eligible for free application of Standardization of their Researches by Open Scientific Standards. Standardization is next step and level after publishing in a journal. A team of research and professional will work with you to take your research to its next level, which is worldwide open standardization.

- FARSS is eligible to earn from their researches: While publishing his paper with Global Journals Inc. (US), FARSS can decide whether he/she would like to publish his/her research in closed manner. When readers will buy that individual research paper for reading, 80% of its earning by Global Journals Inc. (US) will be transferred to FARSS member's bank account after certain threshold balance. There is no time limit for collection. FARSS member can decide its price and we can help in decision.

MEMBER OF ASSOCIATION OF RESEARCH SOCIETY IN SCIENCE (MARSS)

- 'MARSS' title will be awarded to the person after approval of Editor-in-Chief and Editorial Board. The title 'MARSS" can be added to name in the following manner. eg. Dr. John E. Hall, Ph.D., MARSS or William Walldroff Ph. D., M.S., MARSS
- Being MARSS is a respectful honor. It authenticates your research activities. After becoming MARSS, you can use 'MARSS' title as you use your degree in suffix of your name. This will definitely will enhance and add up your name. You can use it on your Career Counseling Materials/CV/Resume/Visiting Card/Name Plate etc.
- 40% Discount will be provided to MARSS members for publishing research papers in Global Journals Inc., if our Editorial Board and Peer Reviewers accept the paper. For the life time, if you are author/co-author of any paper bill sent to you will automatically be discounted one by 60%
- MARSS will be given a renowned, secure, free professional email address with 30 GB of space eg.johnhall@globaljournals.org. You will be facilitated with Webmail, SpamAssassin, Email Forwarders, Auto-Responders, Email Delivery Route tracing, etc.
- MARSS member is eligible to become paid peer reviewer at Global Journals Inc. to earn up to 10% of realized author charges taken from author of respective paper. After reviewing 5 or more papers you can request to transfer the amount to your bank account or to your PayPal account.
- MARSS member can apply for free approval, grading and certification of some of their Educational and Institutional Degrees from Global Journals Inc. (US) and Open Association of Research,Society U.S.A.
- MARSS is eligible to earn from their researches: While publishing his paper with Global Journals Inc. (US), MARSS can decide whether he/she would like to publish his/her research in closed manner. When readers will buy that individual research paper for reading, 40% of its earning by Global Journals Inc. (US) will be transferred to MARSS member's bank account after certain threshold balance. There is no time limit for collection. MARSS member can decide its price and we can help in decision.

ANNUAL MEMBER

- Annual Member will be authorized to receive e-Journal GJSFR for one year (subscription for one year).
- The member will be allotted free 1 GB Web-space along with subDomain to contribute and participate in our activities.
- A professional email address will be allotted free 500 MB email space.

PAPER PUBLICATION

- The members can publish paper once. The paper will be sent to two-peer reviewer. The paper will be published after the acceptance of peer reviewers and Editorial Board.

Process of submission of Research Paper

The Area or field of specialization may or may not be of any category as mentioned in 'Scope of Journal' menu of the GlobalJournals.org website. There are 37 Research Journal categorized with Six parental Journals GJCST, GJMR, GJRE, GJMBR, GJSFR, GJHSS. For Authors should prefer the mentioned categories. There are three widely used systems UDC, DDC and LCC. The details are available as 'Knowledge Abstract' at Home page. The major advantage of this coding is that, the research work will be exposed to and shared with all over the world as we are being abstracted and indexed worldwide.

The paper should be in proper format. The format can be downloaded from first page of 'Author Guideline' Menu. The Author is expected to follow the general rules as mentioned in this menu. The paper should be written in MS-Word Format (*.DOC,*.DOCX).

The Author can submit the paper either online or offline. The authors should prefer online submission.Online Submission: There are three ways to submit your paper:

(A) (I) First, register yourself using top right corner of Home page then Login. If you are already registered, then login using your username and password.

(II) Choose corresponding Journal.

(III) Click 'Submit Manuscript'. Fill required information and Upload the paper.

(B) If you are using Internet Explorer, then Direct Submission through Homepage is also available.

(C) If these two are not conveninet , and then email the paper directly to dean@globaljournals.org.

Offline Submission: Author can send the typed form of paper by Post. However, online submission should be preferred.

Preferred Author Guidelines

MANUSCRIPT STYLE INSTRUCTION **<u>(Must be strictly followed)</u>**

Page Size: 8.27" X 11'"

- Left Margin: 0.65
- Right Margin: 0.65
- Top Margin: 0.75
- Bottom Margin: 0.75
- Font type of all text should be Swis 721 Lt BT.
- Paper Title should be of Font Size 24 with one Column section.
- Author Name in Font Size of 11 with one column as of Title.
- Abstract Font size of 9 Bold, “Abstract” word in Italic Bold.
- Main Text: Font size 10 with justified two columns section
- Two Column with Equal Column with of 3.38 and Gaping of .2
- First Character must be three lines Drop capped.
- Paragraph before Spacing of 1 pt and After of 0 pt.
- Line Spacing of 1 pt
- Large Images must be in One Column
- Numbering of First Main Headings (Heading 1) must be in Roman Letters, Capital Letter, and Font Size of 10.
- Numbering of Second Main Headings (Heading 2) must be in Alphabets, Italic, and Font Size of 10.

You can use your own standard format also.
Author Guidelines:

1. General,

2. Ethical Guidelines,

3. Submission of Manuscripts,

4. Manuscript’s Category,

5. Structure and Format of Manuscript,

6. After Acceptance.

1. GENERAL

Before submitting your research paper, one is advised to go through the details as mentioned in following heads. It will be beneficial, while peer reviewer justify your paper for publication.

Scope

The Global Journals Inc. (US) welcome the submission of original paper, review paper, survey article relevant to the all the streams of Philosophy and knowledge. The Global Journals Inc. (US) is parental platform for Global Journal of Computer Science and Technology, Researches in Engineering, Medical Research, Science Frontier Research, Human Social Science, Management, and Business organization. The choice of specific field can be done otherwise as following in Abstracting and Indexing Page on this Website. As the all Global

Journals Inc. (US) are being abstracted and indexed (in process) by most of the reputed organizations. Topics of only narrow interest will not be accepted unless they have wider potential or consequences.

2. ETHICAL GUIDELINES

Authors should follow the ethical guidelines as mentioned below for publication of research paper and research activities.

Papers are accepted on strict understanding that the material in whole or in part has not been, nor is being, considered for publication elsewhere. If the paper once accepted by Global Journals Inc. (US) and Editorial Board, will become the copyright of the Global Journals Inc. (US).

Authorship: The authors and coauthors should have active contribution to conception design, analysis and interpretation of findings. They should critically review the contents and drafting of the paper. All should approve the final version of the paper before submission

The Global Journals Inc. (US) follows the definition of authorship set up by the Global Academy of Research and Development. According to the Global Academy of R&D authorship, criteria must be based on:

1) Substantial contributions to conception and acquisition of data, analysis and interpretation of the findings.

2) Drafting the paper and revising it critically regarding important academic content.

3) Final approval of the version of the paper to be published.

All authors should have been credited according to their appropriate contribution in research activity and preparing paper. Contributors who do not match the criteria as authors may be mentioned under Acknowledgement.

Acknowledgements: Contributors to the research other than authors credited should be mentioned under acknowledgement. The specifications of the source of funding for the research if appropriate can be included. Suppliers of resources may be mentioned along with address.

Appeal of Decision: The Editorial Board's decision on publication of the paper is final and cannot be appealed elsewhere.

Permissions: It is the author's responsibility to have prior permission if all or parts of earlier published illustrations are used in this paper.

Please mention proper reference and appropriate acknowledgements wherever expected.

If all or parts of previously published illustrations are used, permission must be taken from the copyright holder concerned. It is the author's responsibility to take these in writing.

Approval for reproduction/modification of any information (including figures and tables) published elsewhere must be obtained by the authors/copyright holders before submission of the manuscript. Contributors (Authors) are responsible for any copyright fee involved.

3. SUBMISSION OF MANUSCRIPTS

Manuscripts should be uploaded via this online submission page. The online submission is most efficient method for submission of papers, as it enables rapid distribution of manuscripts and consequently speeds up the review procedure. It also enables authors to know the status of their own manuscripts by emailing us. Complete instructions for submitting a paper is available below.

Manuscript submission is a systematic procedure and little preparation is required beyond having all parts of your manuscript in a given format and a computer with an Internet connection and a Web browser. Full help and instructions are provided on-screen. As an author, you will be prompted for login and manuscript details as Field of Paper and then to upload your manuscript file(s) according to the instructions.

To avoid postal delays, all transaction is preferred by e-mail. A finished manuscript submission is confirmed by e-mail immediately and your paper enters the editorial process with no postal delays. When a conclusion is made about the publication of your paper by our Editorial Board, revisions can be submitted online with the same procedure, with an occasion to view and respond to all comments.

Complete support for both authors and co-author is provided.

4. MANUSCRIPT'S CATEGORY

Based on potential and nature, the manuscript can be categorized under the following heads:

Original research paper: Such papers are reports of high-level significant original research work.

Review papers: These are concise, significant but helpful and decisive topics for young researchers.

Research articles: These are handled with small investigation and applications

Research letters: The letters are small and concise comments on previously published matters.

5.STRUCTURE AND FORMAT OF MANUSCRIPT

The recommended size of original research paper is less than seven thousand words, review papers fewer than seven thousands words also.Preparation of research paper or how to write research paper, are major hurdle, while writing manuscript. The research articles and research letters should be fewer than three thousand words, the structure original research paper; sometime review paper should be as follows:

Papers: These are reports of significant research (typically less than 7000 words equivalent, including tables, figures, references), and comprise:

(a)Title should be relevant and commensurate with the theme of the paper.

(b) A brief Summary, "Abstract" (less than 150 words) containing the major results and conclusions.

(c) Up to ten keywords, that precisely identifies the paper's subject, purpose, and focus.

(d) An Introduction, giving necessary background excluding subheadings; objectives must be clearly declared.

(e) Resources and techniques with sufficient complete experimental details (wherever possible by reference) to permit repetition; sources of information must be given and numerical methods must be specified by reference, unless non-standard.

(f) Results should be presented concisely, by well-designed tables and/or figures; the same data may not be used in both; suitable statistical data should be given. All data must be obtained with attention to numerical detail in the planning stage. As reproduced design has been recognized to be important to experiments for a considerable time, the Editor has decided that any paper that appears not to have adequate numerical treatments of the data will be returned un-refereed;

(g) Discussion should cover the implications and consequences, not just recapitulating the results; conclusions should be summarizing.

(h) Brief Acknowledgements.

(i) References in the proper form.

Authors should very cautiously consider the preparation of papers to ensure that they communicate efficiently. Papers are much more likely to be accepted, if they are cautiously designed and laid out, contain few or no errors, are summarizing, and be conventional to the approach and instructions. They will in addition, be published with much less delays than those that require much technical and editorial correction.

The Editorial Board reserves the right to make literary corrections and to make suggestions to improve briefness.

It is vital, that authors take care in submitting a manuscript that is written in simple language and adheres to published guidelines.

Format

Language: The language of publication is UK English. Authors, for whom English is a second language, must have their manuscript efficiently edited by an English-speaking person before submission to make sure that, the English is of high excellence. It is preferable, that manuscripts should be professionally edited.

Standard Usage, Abbreviations, and Units: Spelling and hyphenation should be conventional to The Concise Oxford English Dictionary. Statistics and measurements should at all times be given in figures, e.g. 16 min, except for when the number begins a sentence. When the number does not refer to a unit of measurement it should be spelt in full unless, it is 160 or greater.

Abbreviations supposed to be used carefully. The abbreviated name or expression is supposed to be cited in full at first usage, followed by the conventional abbreviation in parentheses.

Metric SI units are supposed to generally be used excluding where they conflict with current practice or are confusing. For illustration, 1.4 l rather than 1.4 × 10-3 m3, or 4 mm somewhat than 4 × 10-3 m. Chemical formula and solutions must identify the form used, e.g. anhydrous or hydrated, and the concentration must be in clearly defined units. Common species names should be followed by underlines at the first mention. For following use the generic name should be constricted to a single letter, if it is clear.

Structure

All manuscripts submitted to Global Journals Inc. (US), ought to include:

Title: The title page must carry an instructive title that reflects the content, a running title (less than 45 characters together with spaces), names of the authors and co-authors, and the place(s) wherever the work was carried out. The full postal address in addition with the e-mail address of related author must be given. Up to eleven keywords or very brief phrases have to be given to help data retrieval, mining and indexing.

Abstract, used in Original Papers and Reviews:

Optimizing Abstract for Search Engines

Many researchers searching for information online will use search engines such as Google, Yahoo or similar. By optimizing your paper for search engines, you will amplify the chance of someone finding it. This in turn will make it more likely to be viewed and/or cited in a further work. Global Journals Inc. (US) have compiled these guidelines to facilitate you to maximize the web-friendliness of the most public part of your paper.

Key Words

A major linchpin in research work for the writing research paper is the keyword search, which one will employ to find both library and Internet resources.

One must be persistent and creative in using keywords. An effective keyword search requires a strategy and planning a list of possible keywords and phrases to try.

Search engines for most searches, use Boolean searching, which is somewhat different from Internet searches. The Boolean search uses "operators," words (and, or, not, and near) that enable you to expand or narrow your affords. Tips for research paper while preparing research paper are very helpful guideline of research paper.

Choice of key words is first tool of tips to write research paper. Research paper writing is an art.A few tips for deciding as strategically as possible about keyword search:

- One should start brainstorming lists of possible keywords before even begin searching. Think about the most important concepts related to research work. Ask, "What words would a source have to include to be truly valuable in research paper?" Then consider synonyms for the important words.
- It may take the discovery of only one relevant paper to let steer in the right keyword direction because in most databases, the keywords under which a research paper is abstracted are listed with the paper.
- One should avoid outdated words.

Keywords are the key that opens a door to research work sources. Keyword searching is an art in which researcher's skills are bound to improve with experience and time.

Numerical Methods: Numerical methods used should be clear and, where appropriate, supported by references.

Acknowledgements: Please make these as concise as possible.

References

References follow the Harvard scheme of referencing. References in the text should cite the authors' names followed by the time of their publication, unless there are three or more authors when simply the first author's name is quoted followed by et al. unpublished work has to only be cited where necessary, and only in the text. Copies of references in press in other journals have to be supplied with submitted typescripts. It is necessary that all citations and references be carefully checked before submission, as mistakes or omissions will cause delays.

References to information on the World Wide Web can be given, but only if the information is available without charge to readers on an official site. Wikipedia and Similar websites are not allowed where anyone can change the information. Authors will be asked to make available electronic copies of the cited information for inclusion on the Global Journals Inc. (US) homepage at the judgment of the Editorial Board.

The Editorial Board and Global Journals Inc. (US) recommend that, citation of online-published papers and other material should be done via a DOI (digital object identifier). If an author cites anything, which does not have a DOI, they run the risk of the cited material not being noticeable.

The Editorial Board and Global Journals Inc. (US) recommend the use of a tool such as Reference Manager for reference management and formatting.

Tables, Figures and Figure Legends

Tables: Tables should be few in number, cautiously designed, uncrowned, and include only essential data. Each must have an Arabic number, e.g. Table 4, a self-explanatory caption and be on a separate sheet. Vertical lines should not be used.

Figures: Figures are supposed to be submitted as separate files. Always take in a citation in the text for each figure using Arabic numbers, e.g. Fig. 4. Artwork must be submitted online in electronic form by e-mailing them.

Preparation of Electronic Figures for Publication

Even though low quality images are sufficient for review purposes, print publication requires high quality images to prevent the final product being blurred or fuzzy. Submit (or e-mail) EPS (line art) or TIFF (halftone/photographs) files only. MS PowerPoint and Word Graphics are unsuitable for printed pictures. Do not use pixel-oriented software. Scans (TIFF only) should have a resolution of at least 350 dpi (halftone) or 700 to 1100 dpi (line drawings) in relation to the imitation size. Please give the data for figures in black and white or submit a Color Work Agreement Form. EPS files must be saved with fonts embedded (and with a TIFF preview, if possible).

For scanned images, the scanning resolution (at final image size) ought to be as follows to ensure good reproduction: line art: >650 dpi; halftones (including gel photographs) : >350 dpi; figures containing both halftone and line images: >650 dpi.

Color Charges: It is the rule of the Global Journals Inc. (US) for authors to pay the full cost for the reproduction of their color artwork. Hence, please note that, if there is color artwork in your manuscript when it is accepted for publication, we would require you to complete and return a color work agreement form before your paper can be published.

Figure Legends: Self-explanatory legends of all figures should be incorporated separately under the heading 'Legends to Figures'. In the full-text online edition of the journal, figure legends may possibly be truncated in abbreviated links to the full screen version. Therefore, the first 100 characters of any legend should notify the reader, about the key aspects of the figure.

6. AFTER ACCEPTANCE

Upon approval of a paper for publication, the manuscript will be forwarded to the dean, who is responsible for the publication of the Global Journals Inc. (US).

6.1 Proof Corrections

The corresponding author will receive an e-mail alert containing a link to a website or will be attached. A working e-mail address must therefore be provided for the related author.

Acrobat Reader will be required in order to read this file. This software can be downloaded

(Free of charge) from the following website:

www.adobe.com/products/acrobat/readstep2.html. This will facilitate the file to be opened, read on screen, and printed out in order for any corrections to be added. Further instructions will be sent with the proof.

Proofs must be returned to the dean at dean@globaljournals.org within three days of receipt.

As changes to proofs are costly, we inquire that you only correct typesetting errors. All illustrations are retained by the publisher. Please note that the authors are responsible for all statements made in their work, including changes made by the copy editor.

6.2 Early View of Global Journals Inc. (US) (Publication Prior to Print)

The Global Journals Inc. (US) are enclosed by our publishing's Early View service. Early View articles are complete full-text articles sent in advance of their publication. Early View articles are absolute and final. They have been completely reviewed, revised and edited for publication, and the authors' final corrections have been incorporated. Because they are in final form, no changes can be made after sending them. The nature of Early View articles means that they do not yet have volume, issue or page numbers, so Early View articles cannot be cited in the conventional way.

6.3 Author Services

Online production tracking is available for your article through Author Services. Author Services enables authors to track their article - once it has been accepted - through the production process to publication online and in print. Authors can check the status of their articles online and choose to receive automated e-mails at key stages of production. The authors will receive an e-mail with a unique link that enables them to register and have their article automatically added to the system. Please ensure that a complete e-mail address is provided when submitting the manuscript.

6.4 Author Material Archive Policy

Please note that if not specifically requested, publisher will dispose off hardcopy & electronic information submitted, after the two months of publication. If you require the return of any information submitted, please inform the Editorial Board or dean as soon as possible.

6.5 Offprint and Extra Copies

A PDF offprint of the online-published article will be provided free of charge to the related author, and may be distributed according to the Publisher's terms and conditions. Additional paper offprint may be ordered by emailing us at: editor@globaljournals.org .

the search? Will I be able to find all information in this field area? If the answer of these types of questions will be "Yes" then you can choose that topic. In most of the cases, you may have to conduct the surveys and have to visit several places because this field is related to Computer Science and Information Technology. Also, you may have to do a lot of work to find all rise and falls regarding the various data of that subject. Sometimes, detailed information plays a vital role, instead of short information.

2. Evaluators are human: First thing to remember that evaluators are also human being. They are not only meant for rejecting a paper. They are here to evaluate your paper. So, present your Best.

3. Think Like Evaluators: If you are in a confusion or getting demotivated that your paper will be accepted by evaluators or not, then think and try to evaluate your paper like an Evaluator. Try to understand that what an evaluator wants in your research paper and automatically you will have your answer.

4. Make blueprints of paper: The outline is the plan or framework that will help you to arrange your thoughts. It will make your paper logical. But remember that all points of your outline must be related to the topic you have chosen.

5. Ask your Guides: If you are having any difficulty in your research, then do not hesitate to share your difficulty to your guide (if you have any). They will surely help you out and resolve your doubts. If you can't clarify what exactly you require for your work then ask the supervisor to help you with the alternative. He might also provide you the list of essential readings.

6. Use of computer is recommended: As you are doing research in the field of Computer Science, then this point is quite obvious.

7. Use right software: Always use good quality software packages. If you are not capable to judge good software then you can lose quality of your paper unknowingly. There are various software programs available to help you, which you can get through Internet.

8. Use the Internet for help: An excellent start for your paper can be by using the Google. It is an excellent search engine, where you can have your doubts resolved. You may also read some answers for the frequent question how to write my research paper or find model research paper. From the internet library you can download books. If you have all required books make important reading selecting and analyzing the specified information. Then put together research paper sketch out.

9. Use and get big pictures: Always use encyclopedias, Wikipedia to get pictures so that you can go into the depth.

10. Bookmarks are useful: When you read any book or magazine, you generally use bookmarks, right! It is a good habit, which helps to not to lose your continuity. You should always use bookmarks while searching on Internet also, which will make your search easier.

11. Revise what you wrote: When you write anything, always read it, summarize it and then finalize it.

12. Make all efforts: Make all efforts to mention what you are going to write in your paper. That means always have a good start. Try to mention everything in introduction, that what is the need of a particular research paper. Polish your work by good skill of writing and always give an evaluator, what he wants.

13. Have backups: When you are going to do any important thing like making research paper, you should always have backup copies of it either in your computer or in paper. This will help you to not to lose any of your important.

14. Produce good diagrams of your own: Always try to include good charts or diagrams in your paper to improve quality. Using several and unnecessary diagrams will degrade the quality of your paper by creating "hotchpotch." So always, try to make and include those diagrams, which are made by your own to improve readability and understandability of your paper.

15. Use of direct quotes: When you do research relevant to literature, history or current affairs then use of quotes become essential but if study is relevant to science then use of quotes is not preferable.

16. Use proper verb tense: Use proper verb tenses in your paper. Use past tense, to present those events that happened. Use present tense to indicate events that are going on. Use future tense to indicate future happening events. Use of improper and wrong tenses will confuse the evaluator. Avoid the sentences that are incomplete.

17. Never use online paper: If you are getting any paper on Internet, then never use it as your research paper because it might be possible that evaluator has already seen it or maybe it is outdated version.

18. **Pick a good study spot:** To do your research studies always try to pick a spot, which is quiet. Every spot is not for studies. Spot that suits you choose it and proceed further.

19. Know what you know: Always try to know, what you know by making objectives. Else, you will be confused and cannot achieve your target.

20. Use good quality grammar: Always use a good quality grammar and use words that will throw positive impact on evaluator. Use of good quality grammar does not mean to use tough words, that for each word the evaluator has to go through dictionary. Do not start sentence with a conjunction. Do not fragment sentences. Eliminate one-word sentences. Ignore passive voice. Do not ever use a big word when a diminutive one would suffice. Verbs have to be in agreement with their subjects. Prepositions are not expressions to finish sentences with. It is incorrect to ever divide an infinitive. Avoid clichés like the disease. Also, always shun irritating alliteration. Use language that is simple and straight forward. put together a neat summary.

21. Arrangement of information: Each section of the main body should start with an opening sentence and there should be a changeover at the end of the section. Give only valid and powerful arguments to your topic. You may also maintain your arguments with records.

22. Never start in last minute: Always start at right time and give enough time to research work. Leaving everything to the last minute will degrade your paper and spoil your work.

23. Multitasking in research is not good: Doing several things at the same time proves bad habit in case of research activity. Research is an area, where everything has a particular time slot. Divide your research work in parts and do particular part in particular time slot.

24. Never copy others' work: Never copy others' work and give it your name because if evaluator has seen it anywhere you will be in trouble.

25. Take proper rest and food: No matter how many hours you spend for your research activity, if you are not taking care of your health then all your efforts will be in vain. For a quality research, study is must, and this can be done by taking proper rest and food.

26. Go for seminars: Attend seminars if the topic is relevant to your research area. Utilize all your resources.

27. Refresh your mind after intervals: Try to give rest to your mind by listening to soft music or by sleeping in intervals. This will also improve your memory.

28. Make colleagues: Always try to make colleagues. No matter how sharper or intelligent you are, if you make colleagues you can have several ideas, which will be helpful for your research.

29. **Think technically:** Always think technically. If anything happens, then search its reasons, its benefits, and demerits.

30. Think and then print: When you will go to print your paper, notice that tables are not be split, headings are not detached from their descriptions, and page sequence is maintained.

31. Adding unnecessary information: Do not add unnecessary information, like, I have used MS Excel to draw graph. Do not add irrelevant and inappropriate material. These all will create superfluous. Foreign terminology and phrases are not apropos. One should NEVER take a broad view. Analogy in script is like feathers on a snake. Not at all use a large word when a very small one would be sufficient. Use words properly, regardless of how others use them. Remove quotations. Puns are for kids, not grunt readers. Amplification is a billion times of inferior quality than sarcasm.

32. Never oversimplify everything: To add material in your research paper, never go for oversimplification. This will definitely irritate the evaluator. Be more or less specific. Also too, by no means, ever use rhythmic redundancies. Contractions aren't essential and shouldn't be there used. Comparisons are as terrible as clichés. Give up ampersands and abbreviations, and so on. Remove commas, that are, not necessary. Parenthetical words however should be together with this in commas. Understatement is all the time the complete best way to put onward earth-shaking thoughts. Give a detailed literary review.

33. Report concluded results: Use concluded results. From raw data, filter the results and then conclude your studies based on measurements and observations taken. Significant figures and appropriate number of decimal places should be used. Parenthetical remarks are prohibitive. Proofread carefully at final stage. In the end give outline to your arguments. Spot out perspectives of further study of this subject. Justify your conclusion by at the bottom of them with sufficient justifications and examples.

34. After conclusion: Once you have concluded your research, the next most important step is to present your findings. Presentation is extremely important as it is the definite medium though which your research is going to be in print to the rest of the crowd. Care should be taken to categorize your thoughts well and present them in a logical and neat manner. A good quality research paper format is essential because it serves to highlight your research paper and bring to light all necessary aspects in your research.

Informal Guidelines of Research Paper Writing

Key points to remember:

- Submit all work in its final form.
- Write your paper in the form, which is presented in the guidelines using the template.
- Please note the criterion for grading the final paper by peer-reviewers.

Final Points:

A purpose of organizing a research paper is to let people to interpret your effort selectively. The journal requires the following sections, submitted in the order listed, each section to start on a new page.

The introduction will be compiled from reference matter and will reflect the design processes or outline of basis that direct you to make study. As you will carry out the process of study, the method and process section will be constructed as like that. The result segment will show related statistics in nearly sequential order and will direct the reviewers next to the similar intellectual paths throughout the data that you took to carry out your study. The discussion section will provide understanding of the data and projections as to the implication of the results. The use of good quality references all through the paper will give the effort trustworthiness by representing an alertness of prior workings.

Writing a research paper is not an easy job no matter how trouble-free the actual research or concept. Practice, excellent preparation, and controlled record keeping are the only means to make straightforward the progression.

General style:

Specific editorial column necessities for compliance of a manuscript will always take over from directions in these general guidelines.

To make a paper clear

· Adhere to recommended page limits

Mistakes to evade

- Insertion a title at the foot of a page with the subsequent text on the next page

- Separating a table/chart or figure - impound each figure/table to a single page
- Submitting a manuscript with pages out of sequence

In every sections of your document

· Use standard writing style including articles ("a", "the," etc.)

· Keep on paying attention on the research topic of the paper

· Use paragraphs to split each significant point (excluding for the abstract)

· Align the primary line of each section

· Present your points in sound order

· Use present tense to report well accepted

· Use past tense to describe specific results

· Shun familiar wording, don't address the reviewer directly, and don't use slang, slang language, or superlatives

· Shun use of extra pictures - include only those figures essential to presenting results

Title Page:

Choose a revealing title. It should be short. It should not have non-standard acronyms or abbreviations. It should not exceed two printed lines. It should include the name(s) and address (es) of all authors.

Abstract:

The summary should be two hundred words or less. It should briefly and clearly explain the key findings reported in the manuscript--must have precise statistics. It should not have abnormal acronyms or abbreviations. It should be logical in itself. Shun citing references at this point.

An abstract is a brief distinct paragraph summary of finished work or work in development. In a minute or less a reviewer can be taught the foundation behind the study, common approach to the problem, relevant results, and significant conclusions or new questions.

Write your summary when your paper is completed because how can you write the summary of anything which is not yet written? Wealth of terminology is very essential in abstract. Yet, use comprehensive sentences and do not let go readability for briefness. You can maintain it succinct by phrasing sentences so that they provide more than lone rationale. The author can at this moment go straight to shortening the outcome. Sum up the study, with the subsequent elements in any summary. Try to maintain the initial two items to no more than one ruling each.

- Reason of the study - theory, overall issue, purpose
- Fundamental goal
- To the point depiction of the research
- Consequences, including definite statistics - if the consequences are quantitative in nature, account quantitative data; results of any numerical analysis should be reported
- Significant conclusions or questions that track from the research(es)

Approach:

- Single section, and succinct
- As a outline of job done, it is always written in past tense
- A conceptual should situate on its own, and not submit to any other part of the paper such as a form or table
- Center on shortening results - bound background information to a verdict or two, if completely necessary
- What you account in an conceptual must be regular with what you reported in the manuscript
- Exact spelling, clearness of sentences and phrases, and appropriate reporting of quantities (proper units, important statistics) are just as significant in an abstract as they are anywhere else

Introduction:

The **Introduction** should "introduce" the manuscript. The reviewer should be presented with sufficient background information to be capable to comprehend and calculate the purpose of your study without having to submit to other works. The basis for the study should be offered. Give most important references but shun difficult to make a comprehensive appraisal of the topic. In the introduction, describe the problem visibly. If the problem is not acknowledged in a logical, reasonable way, the reviewer will have no attention in your result. Speak in common terms about techniques used to explain the problem, if needed, but do not present any particulars about the protocols here. Following approach can create a valuable beginning:

- Explain the value (significance) of the study
- Shield the model - why did you employ this particular system or method? What is its compensation? You strength remark on its appropriateness from a abstract point of vision as well as point out sensible reasons for using it.
- Present a justification. Status your particular theory (es) or aim(s), and describe the logic that led you to choose them.
- Very for a short time explain the tentative propose and how it skilled the declared objectives.

Approach:

- Use past tense except for when referring to recognized facts. After all, the manuscript will be submitted after the entire job is done.
- Sort out your thoughts; manufacture one key point with every section. If you make the four points listed above, you will need a least of four paragraphs.
- Present surroundings information only as desirable in order hold up a situation. The reviewer does not desire to read the whole thing you know about a topic.
- Shape the theory/purpose specifically - do not take a broad view.
- As always, give awareness to spelling, simplicity and correctness of sentences and phrases.

Procedures (Methods and Materials):

This part is supposed to be the easiest to carve if you have good skills. A sound written Procedures segment allows a capable scientist to replacement your results. Present precise information about your supplies. The suppliers and clarity of reagents can be helpful bits of information. Present methods in sequential order but linked methodologies can be grouped as a segment. Be concise when relating the protocols. Attempt for the least amount of information that would permit another capable scientist to spare your outcome but be cautious that vital information is integrated. The use of subheadings is suggested and ought to be synchronized with the results section. When a technique is used that has been well described in another object, mention the specific item describing a way but draw the basic principle while stating the situation. The purpose is to text all particular resources and broad procedures, so that another person may use some or all of the methods in one more study or referee the scientific value of your work. It is not to be a step by step report of the whole thing you did, nor is a methods section a set of orders.

Materials:

- Explain materials individually only if the study is so complex that it saves liberty this way.
- Embrace particular materials, and any tools or provisions that are not frequently found in laboratories.
- Do not take in frequently found.
- If use of a definite type of tools.
- Materials may be reported in a part section or else they may be recognized along with your measures.

Methods:

- Report the method (not particulars of each process that engaged the same methodology)
- Describe the method entirely
- To be succinct, present methods under headings dedicated to specific dealings or groups of measures
- Simplify - details how procedures were completed not how they were exclusively performed on a particular day.
- If well known procedures were used, account the procedure by name, possibly with reference, and that's all.

Approach:

- It is embarrassed or not possible to use vigorous voice when documenting methods with no using first person, which would focus the reviewer's interest on the researcher rather than the job. As a result when script up the methods most authors use third person passive voice.
- Use standard style in this and in every other part of the paper - avoid familiar lists, and use full sentences.

What to keep away from

- Resources and methods are not a set of information.
- Skip all descriptive information and surroundings - save it for the argument.
- Leave out information that is immaterial to a third party.

Results:

The principle of a results segment is to present and demonstrate your conclusion. Create this part a entirely objective details of the outcome, and save all understanding for the discussion.

The page length of this segment is set by the sum and types of data to be reported. Carry on to be to the point, by means of statistics and tables, if suitable, to present consequences most efficiently.You must obviously differentiate material that would usually be incorporated in a study editorial from any unprocessed data or additional appendix matter that would not be available. In fact, such matter should not be submitted at all except requested by the instructor.

Content

- Sum up your conclusion in text and demonstrate them, if suitable, with figures and tables.
- In manuscript, explain each of your consequences, point the reader to remarks that are most appropriate.
- Present a background, such as by describing the question that was addressed by creation an exacting study.
- Explain results of control experiments and comprise remarks that are not accessible in a prescribed figure or table, if appropriate.
- Examine your data, then prepare the analyzed (transformed) data in the form of a figure (graph), table, or in manuscript form.

What to stay away from

- Do not discuss or infer your outcome, report surroundings information, or try to explain anything.
- Not at all, take in raw data or intermediate calculations in a research manuscript.

- Do not present the similar data more than once.
- Manuscript should complement any figures or tables, not duplicate the identical information.
- Never confuse figures with tables - there is a difference.

Approach

- As forever, use past tense when you submit to your results, and put the whole thing in a reasonable order.
- Put figures and tables, appropriately numbered, in order at the end of the report
- If you desire, you may place your figures and tables properly within the text of your results part.

Figures and tables

- If you put figures and tables at the end of the details, make certain that they are visibly distinguished from any attach appendix materials, such as raw facts
- Despite of position, each figure must be numbered one after the other and complete with subtitle
- In spite of position, each table must be titled, numbered one after the other and complete with heading
- All figure and table must be adequately complete that it could situate on its own, divide from text

Discussion:

The Discussion is expected the trickiest segment to write and describe. A lot of papers submitted for journal are discarded based on problems with the Discussion. There is no head of state for how long a argument should be. Position your understanding of the outcome visibly to lead the reviewer through your conclusions, and then finish the paper with a summing up of the implication of the study. The purpose here is to offer an understanding of your results and hold up for all of your conclusions, using facts from your research and generally accepted information, if suitable. The implication of result should be visibly described. Infer your data in the conversation in suitable depth. This means that when you clarify an observable fact you must explain mechanisms that may account for the observation. If your results vary from your prospect, make clear why that may have happened. If your results agree, then explain the theory that the proof supported. It is never suitable to just state that the data approved with prospect, and let it drop at that.

- Make a decision if each premise is supported, discarded, or if you cannot make a conclusion with assurance. Do not just dismiss a study or part of a study as "uncertain."
- Research papers are not acknowledged if the work is imperfect. Draw what conclusions you can based upon the results that you have, and take care of the study as a finished work
- You may propose future guidelines, such as how the experiment might be personalized to accomplish a new idea.
- Give details all of your remarks as much as possible, focus on mechanisms.
- Make a decision if the tentative design sufficiently addressed the theory, and whether or not it was correctly restricted.
- Try to present substitute explanations if sensible alternatives be present.
- One research will not counter an overall question, so maintain the large picture in mind, where do you go next? The best studies unlock new avenues of study. What questions remain?
- Recommendations for detailed papers will offer supplementary suggestions.

Approach:

- When you refer to information, differentiate data generated by your own studies from available information
- Submit to work done by specific persons (including you) in past tense.
- Submit to generally acknowledged facts and main beliefs in present tense.

Administration Rules Listed Before
Submitting Your Research Paper to Global Journals Inc. (US)

Please carefully note down following rules and regulation before submitting your Research Paper to Global Journals Inc. (US):

Segment Draft and Final Research Paper: You have to strictly follow the template of research paper. If it is not done your paper may get rejected.

- The **major constraint** is that you must independently make all content, tables, graphs, and facts that are offered in the paper. You must write each part of the paper wholly on your own. The Peer-reviewers need to identify your own perceptive of the concepts in your own terms. NEVER extract straight from any foundation, and never rephrase someone else's analysis.

- Do not give permission to anyone else to "PROOFREAD" your manuscript.

- Methods to avoid Plagiarism is applied by us on every paper, if found guilty, you will be blacklisted by all of our collaborated research groups, your institution will be informed for this and strict legal actions will be taken immediately.)
- To guard yourself and others from possible illegal use please do not permit anyone right to use to your paper and files.

Criterion for Grading a Research Paper (Compilation) by Global Journals Inc. (US)

Please note that following table is only a Grading of "Paper Compilation" and not on "Performed/Stated Research" whose grading solely depends on Individual Assigned Peer Reviewer and Editorial Board Member. These can be available only on request and after decision of Paper. This report will be the property of Global Journals Inc. (US).

Topics	Grades		
	A-B	**C-D**	**E-F**
Abstract	Clear and concise with appropriate content, Correct format. 200 words or below	Unclear summary and no specific data, Incorrect form Above 200 words	No specific data with ambiguous information Above 250 words
Introduction	Containing all background details with clear goal and appropriate details, flow specification, no grammar and spelling mistake, well organized sentence and paragraph, reference cited	Unclear and confusing data, appropriate format, grammar and spelling errors with unorganized matter	Out of place depth and content, hazy format
Methods and Procedures	Clear and to the point with well arranged paragraph, precision and accuracy of facts and figures, well organized subheads	Difficult to comprehend with embarrassed text, too much explanation but completed	Incorrect and unorganized structure with hazy meaning
Result	Well organized, Clear and specific, Correct units with precision, correct data, well structuring of paragraph, no grammar and spelling mistake	Complete and embarrassed text, difficult to comprehend	Irregular format with wrong facts and figures
Discussion	Well organized, meaningful specification, sound conclusion, logical and concise explanation, highly structured paragraph reference cited	Wordy, unclear conclusion, spurious	Conclusion is not cited, unorganized, difficult to comprehend
References	Complete and correct format, well organized	Beside the point, Incomplete	Wrong format and structuring

INDEX

Q

R

S

T

U

V

W

save our planet

Global Journal of Science Frontier Research

Visit us on the Web at www.GlobalJournals.org | www.JournalofScience.org
or email us at helpdesk@globaljournals.org

ISSN 9755896